Programmable In Situ Amplification for Multiplexed Bioimaging

Thesis by

Harry Ming Tak Choi

In Partial Fulfillment of the Requirements

for the Degree of

Doctor of Philosophy

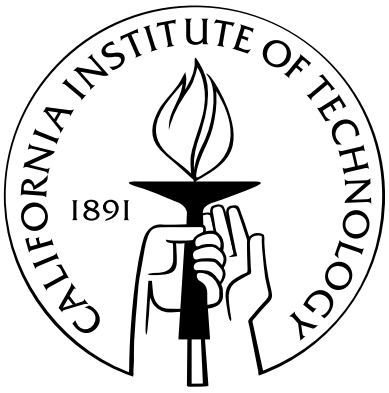

California Institute of Technology

Pasadena, California

2010

(Defended August 3, 2009)

Acknowledgements

First, I would like to thank my advisor, Niles Pierce, for his patience, support, and guidance throughout my graduate life here at Caltech. Without his creativity, enthusiasm, and knowledge, none of the work in this thesis would be possible. I would also want to thank all the past and present lab members for providing a fun and exciting learning environment.

I also want to thank my technician, Joann Chang, my collaborators, Justin Bois, Robert Dirks, Ruobing Zhang, Paul Selvin, Peng Yin, Colby Calvert, Rizal Hariadi, Erik Winfree, Jennifer Padilla, Le Trinh, and Scott Fraser, for their experimental help and insightful discussions.

As well as my best friend and co-worker, Suvir Venkataraman, for many years of support and help both inside and outside the lab. He is also my daily coffee break and swimming buddy. Without him, graduate life would not be as fun as it was.

Finally, I would like to thank my friends Gabriel Kwong and Randy Chen, my girlfriend Ruby Chen, and my family Richard, Angelin, Amy, Franky, Bever, and Tiffany for their patience, support, and encouragement.

Nothing happens unless first a dream.

- Carl Sandburg

Abstract

In situ hybridization methods enable the mapping of mRNA expression within intact biological samples. With current approaches, it is challenging to simultaneously detect multiple target mRNAs in vertebrate embryos and tissue sections – a significant limitation in attempting to study interacting regulatory elements in systems most relevant to human development and disease. This thesis presents a multiplexed fluorescent in situ hybridization method based on orthogonal amplification with hybridization chain reaction (HCR). Using this approach, RNA probes complementary to mRNA targets trigger chain reactions in which fluorophore-labeled RNA hairpins self-assemble into tethered fluorescent amplification polymers. Robust performance and high signal-to-background are achieved when imaging five target mRNAs at the same time in fixed whole-mount zebrafish embryos. The programmability and sequence specificity of these amplification cascades enable all five amplifiers to operate orthogonally at the same time in the same sample. The fact that amplification polymers are triggered to self-assemble in situ results in excellent sample penetration and high signal-to-background. These properties suggest the broad applicability of fluorescent in situ HCR amplification to multiplexed imaging of mRNA expression in normal and pathological cells, embryos, and tissue sections.

Contents

List of Figures

List of Tables

Chapter 1

Introduction

Each cell in a developing embryo contains the same genome, yet the regulatory circuits encoded within this genome implement a developmental program yielding significant spatial heterogeneity and complexity. In situ hybridization (ISH) methods are an essential tool for elucidating these developmental processes, enabling the detailed spatial mapping of mRNA expression in a morphological context from subcellular to organismal levels [1–16]. ISH, introduced in 1969 [17–19], initially used radioisotopes to label RNA probes, providing high sensitivity but limited spatial resolution. The inconvenience of hazardous materials led to the invention of several nonradioactive alternatives. Direct fluorescent detection [3] yields low sensitivity due to difficulties involved in the synthesis and purification of multiply labeled oligonucleotides [10, 15]. Amplification using dendritically branched DNA self-assembly [20, 21] improves sensitivity, but the use of large components is known to reduce sample penetration [22]. Multiple (50–130) singly-labeled short probes [15] can be used to detect single mRNAs in cells, but this approach does not provide the degree of amplification currently required for tissue sections or whole-mount embryo studies. To date, immunological detection equipped with catalyzed reporter deposition (CARD) is the most popular ISH method [8, 10, 11, 23–27]. Commercially available reagents and high sensitivity make CARD attractive, but simultaneous detection of multiple mRNA species is cumbersome and time-consuming [28, 29]. Owing to the lack of compatible orthogonal deposition chemistries, multiple probes must be amplified serially to ensure that each reporter is deposited at only one target species. Due to sample degradation, serial amplification is generally difficult to extend beyond two colors [27–30] in vertebrate embryos and tissue

sections, a signicant limitation in attempting to study interacting regulatory elements in systems most relevant to human development and disease. Here, we overcome this difficulty by programming orthogonal HCR amplifiers [31] that function as independent molecular instruments, simultaneously reading out the expression patterns of five target mRNAs from within a single intact biological sample.

In Chapter 2, it is shown that previous HCR designs are not functional under the stringent buffer conditions of ISH, which are necessary to destabilize non-specific binding in situ [32, 33]. In vitro and in situ calibration experiments are performed to obtain constraints for engineering new HCR systems suitable for ISH applications.

In Chapter 3, newly designed HCR systems are validated for imaging mRNA expression with high signal-to-background. The parallel multiplexing capabilities of in situ HCR amplification are demonstrated by simultaneously imaging five mRNA target species in fixed whole-mount zebrafish embryos.

Appendices A and B provide supplementary information for Chapters 2 and 3 and Appendix C describes an autonomous bipedal walker powered by DNA hybridization.

References

[1] J. B. Lawrence, R. H. Singer and L. M. Marselle. Highly localized tracks of specific transcripts within interphase nuclei visualized by in situ hybridization. *Cell* **57**, 493–502 (1989).

[2] D. Tautz and C. Pfeifle. A non-radioactive in situ hybridization method for the localization of specific RNAs in drosophila embryos reveals translational control of the segmentation gene hunchback. *Chromosoma* **98**, 81–85 (1989).

[3] E. H. Kislauskis, Z. F. Li, R. H. Singer and K. L. Taneja. Isoform-specific 3′-untranslated sequences sort α-cardiac and β-cytoplasmic actin messenger-RNAs to different cytoplasmic compartments. *Journal of Cell Biology* **123**, 165–172 (1993).

[4] J. W. O'Neill and E. Bier. Double-label in situ hybridization using biotin and digoxigenin-tagged RNA probes. *Biotechniques* **17**, 870–875 (1994).

[5] S. C. Hughes and H. M. Krause. Double labeling with fluorescence in situ hybridization in drosophila whole-mount embryos. *Biotechniques* **24**, 530–532 (1998).

[6] A. Femino, F. S. Fay, K. Fogarty and R. H. Singer. Visualization of single RNA transcripts in situ. *Science* **280**, 585–590 (1998).

[7] G. S. Wilkie, A. W. Shermoen, P. H. O'Farrell and I. Davis. Transcribed genes are localized according to chromosomal position within polarized drosophila embryonic nuclei. *Current Biology* **9**, 1263–1266 (1999).

[8] A. U. Zaidi, H. Enomoto, J. Milbrandt and K. A. Roth. Dual fluorescent in situ hybridization and immunohistochemical detection with tyramide signal amplification. *Journal of Histochemistry & Cytochemistry* **48**, 1369–1375 (2000).

[9] J. M. Levsky, S. M. Shenoy, R. C. Pezo and R. H. Singer. Single-cell gene expression profiling. *Science* **297**, 836–840 (2002).

[10] D. Kosman *et al.* Multiplex detection of RNA expression in drosophila embryos. *Science* **305**, 846–846 (2004).

[11] X. Qian, L. Jin and R. V. Lloyd. In situ hybridization: Basic approaches and recent development. *Journal of Histotechnology* **27**, 53–67 (2004).

[12] R. D. Powell *et al.* Metallographic in situ hybridization. *Human Pathology* **38**, 1145–1159 (2007).

[13] M. B. Lambros, R. Natrajan and J. S. Reis-Filho. Chromogenic and fluorescent in situ hybridization in breast cancer. *Human Pathology* **38**, 1105–1122 (2007).

[14] A. P. Silverman and E. T. Kool. Oligonucleotide probes for RNA-targeted fluorescence in situ hybridization. *Advances in Clinical Chemistry* **43**, 79–115 (2007).

[15] A. Raj, P. van den Bogaard, S. A. Rifkin, A. van Oudenaarden and S. Tyagi. Imaging individual mRNA molecules using multiple singly labeled probes. *Nature Methods* **5**, 877–879 (2008).

[16] R. Amann and B. M. Fuchs. Single-cell identification in microbial communities by improved fluorescence in situ hybridization techniques. *Nature Review Microbiology* **6**, 339–348 (2008).

[17] H. A. John, M. L. Birnstiel and K. W. Jones. RNA-DNA hybrids at cytological level. *Nature* **223**, 582–587 (1969).

[18] J. G. Gall and M. L. Pardue. Formation and detection of RNA-DNA hybrid molecules in cytological preparations. *Proceedings of the National Academy of Sciences of the United States of America* **63**, 378–383 (1969).

[19] M. Buongior-Nardelli and F. Amaldi. Autoradiographic detection of molecular hybrids between rRNA and DNA in tissue sections. *Nature* **225**, 946–948 (1970).

[20] M. L. Collins *et al.* A branched DNA signal amplification assay for quantification of nucleic acid targets below 100 molecules/mL. *Nucleic Acids Research* **25**, 2979–2984 (1997).

[21] A. N. Player, L. P. Shen, D. Kenny, V. P. Antao and J. A. Kolberg. Single-copy gene detection using branched DNA (bDNA) in situ hybridization. *Journal of Histochemistry & Cytochemistry* **49**, 603–611 (2001).

[22] D. M. Hougaard, H. Hansen and L. I. Larsson. Non-radioactive in situ hybridization for mrna with emphasis on the use of oligodeoxynucleotide probes. *Histochemistry and Cell Biology* **108**, 335–344 (1997).

[23] R. M. Harland. In situ hybridization - an improved whole-mount method for Xenopus embryos. *Methods in Cell Biology* **36**, 685–695 (1991).

[24] I. Zehbe *et al.* Sensitive in situ hybridization with catalyzed reporter deposition, streptavidin-nanogold, and silver acetate autometallography - Detection of single-copy human papillomavirus. *American Journal of Pathology* **150**, 1553–1561 (1997).

[25] M. P. C. van de Corput *et al.* Sensitive mRNA detection by fluorescence in situ hybridization using horseradish peroxidase-labeled oligodeoxynucleotides and tyramide signal amplification. *Journal of Histochemistry & Cytochemistry* **46**, 1249–1259 (1998).

[26] E. J. Speel, A. H. Hopman and P. Komminoth. Amplification methods to increase the sensitivity of in situ hybridization: Play CARD(s). *Journal of Histochemistry & Cytochemistry* **47**, 281–288 (1999).

[27] P. Barroso-Chinea *et al.* Detection of two different mRNAs in a single section by dual in situ hybridization: A comparison between colorimetric and fluorescent detection. *Journal of Neuroscience Methods* **162**, 119–128 (2007).

[28] B. Thisse *et al.* Spatial and temporal expression of the zebrafish genome by large-scale in situ hybridization screening. *Methods in Cell Biology* **77**, 505–519 (2004).

[29] H. Acloque, D. G. Wilkinson and M. A. Nieto. In situ hybridization analysis of chick embryos in whole-mount and tissue sections. *Methods in Cell Biology* **87**, 169–185 (2008).

[30] H. Clay and L. Ramakrishnan. Multiplex fluorescent in situ hybridization in zebrafish embryos using tyramide signal amplification. *Zebrafish* **2**, 105–111 (2005).

[31] R. M. Dirks and N. A. Pierce. Triggered amplification by hybridization chain reaction. *Proceedings of the National Academy of Sciences of the United States of America* **101**, 15275–15278 (2004).

[32] A. R. Leitch, T. Schwarzacher, D. Jackson and I. J. Leitch. *In Situ Hybridization: A Practical Guide* (BIOS Scientific Publishers, Oxford, 1994).

[33] J. M. Polak and J. O'D. McGee. *In Situ Hybridization: Principles and Practice* (Oxford University Press, Oxford, 1998).

Chapter 2

HCR Design Constraints for In Situ Hybridization Applications

2.1 Introduction

Hybridization chain reaction (HCR) was invented by Dirks and Pierce in 2004 [1]. HCR is an amplification mechanism that exploits the concept of triggered self-assembly [2] to assemble a long polymer from two small monomer species upon detection of a target molecule. Using nucleic acids as a building material, one can design many HCR systems that can simultaneously detect and amplify unique targets without cross-talk. The ability to multiplex makes this mechanism extremely attractive in situations when one wishes to study the relationship between multiple targets, since it facilitates their simultaneous detection in a single sample.

In this chapter, HCR is introduced, and it is shown that the original design is not functional under the stringent ISH conditions required for target specificity. Several calibration experiments are used to measure the free energy requirements for HCR to proceed as intended under ISH conditions. These measurements will be employed in Chapter 3 to build a new HCR amplifier suitable for localizing mRNA targets in fixed zebrafish embryos.

2.2 Hybridization Chain Reaction

An HCR amplifier consists of two nucleic acid hairpin species (H1 and H2 in Figure 2.1a) that are designed to coexist metastably in the absence of a nucleic acid initiator (I). Each HCR hairpin consists of an input domain with an exposed toehold and an output domain

with a toehold sequestered in the hairpin loop (see Figure 2.2 for hairpin nomenclature). Hybridization of the initiator to the input domain of H1 (labeled 'a-b' in Figure 2.1a) opens the hairpin to expose its output domain ('c*-b*'). Hybridization of this output domain to the input domain of H2 ('b-c') opens the hairpin to expose an output domain ('b*-a*') identical in sequence to the initiator. Regeneration of the initiator sequence provides the basis for a chain reaction of alternating H1 and H2 polymerization steps leading to formation of a nicked double-stranded 'polymer'. If the initiator is absent, the hairpins are metastable (i.e., kinetically impeded from polymerizing) due to the sequestration of the output toeholds in hairpin loops. Figure 2.1b demonstrates simultaneous and specific detection of four different DNA targets using four HCR amplification systems in the presence of total RNA extracted from zebrafish embryos.

This mechanism has two conceptual properties that are significant in attempting to achieve simultaneous multiplexed in situ amplification in vertebrate embryos. First, the programmable chemistry of nucleic acid base pairing suggests the feasibility of engineering orthogonal HCR amplifiers that operate independently in the same embryo at the same time. Second, in contrast to molecular self-assembly via traditional annealing protocols in which components interact as soon as they are mixed together [3–5], HCR is an isothermal triggered self-assembly process. Hence, hairpins should penetrate the sample prior to undergoing triggered self-assembly in situ, suggesting the potential for excellent sample penetration and high signal-to-background.

2.3 Testing the Original HCR System for In Situ Hybridization

The original HCR system was designed to function optimally at room temperature in a phosphate buffered sodium solution (1× SPSC: 50 mM Na_2HPO_4, 0.5 M NaCl, pH 6.8) [1]. Under these conditions, the stem of each hairpin remains closed in the absence of an initiator and the two monomers will not interact with each other. When an initiator is introduced to the system, a nucleation event between the toehold of an H1 hairpin and the initiator occurs. This triggers a cascade of branch migration reactions that leads to polymer

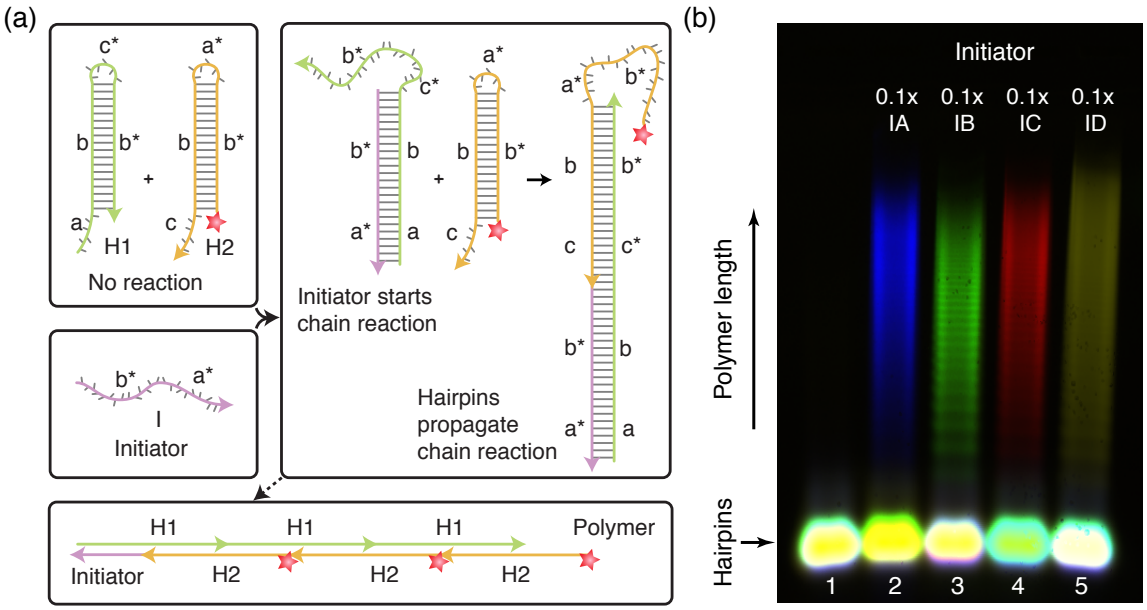

Figure 2.1: Multiplexing amplification with orthogonal hybridization chain reactions. (a) HCR mechanism. Metastable DNA hairpins self-assemble into amplification polymers upon detection of a specific DNA initiator. Initiator I nucleates with hairpin H1 via base-pairing to single-stranded toehold 'a', mediating a brach migration [6] that opens the hairpin to form complex I·H1 containing single-stranded segment 'c*-b*'. This complex nucleates with hairpin H2 via base-pairing to toehold 'c', mediating a brach migration that opens the hairpin to form complex I·H1·H2 containing single-stranded segment 'b*-a*'. Thus, the initiator sequence is regenerated, providing the basis for a chain reaction of alternating H1 and H2 polymerization steps. (b) Four orthogonal HCR amplifiers were used to demonstrate the specific detection of four distinct DNA fragments in the presence of total zebrafish RNA. All lanes in the native agarose gel contained four pairs of hairpin species (HA1 and HA2, HB1 and HB2, HC1 and HC2, and HD1 and HD2) comprising the four independent HCR systems. Hairpins HA2, HB2, HC2, and HD2 were labeled with the organic fluorophores FAM (blue), Cy5 (green), Cy3 (red), and Cy5.5 (yellow), respectively. Lane 1: No amplification in the absence of initiator. Lane 2–5: specific detection of an unique initiator for each HCR system. See Appendix A for sequences and experimental details.

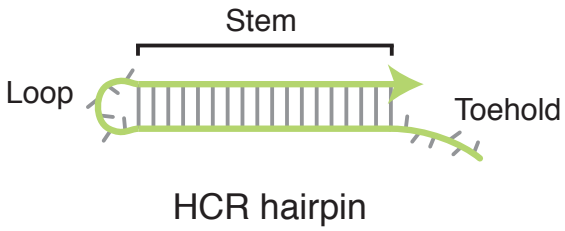

Figure 2.2: HCR hairpin nomenclature.

formation, as shown in Figure 2.1.

ISH uses a solution that contains a high concentration (40–50%) of formamide, a destabilizing agent, which inhibits the formation of nucleic acid duplexes by disrupting their hydrogen bonds [7, 8]. Additionally, ISH is performed under temperature ranges from 45 to 70 °C. These stringent conditions are used to minimize non-specific binding within the sample; however, they are not amenable to proper function of the original HCR system.

Due to the incompatibility between HCR and traditional ISH conditions, we decided to decouple the detection and amplification steps. (1) Detection step: a 78-nucleotide (nt) long probe is hybridized to a target using the traditional stringent ISH protocol. The probe is made up of a 24-nt HCR initiator, a 4 uridine spacer, and a 50-nt target recognition region (Table A.2). Excess probes are removed with a series of stringent washes. (2) Amplification step: HCR hairpins (H1 and fluorescently labeled H2) are introduced in an HCR-friendly buffer (1× SPSC) to the sample. After polymerization, unreacted hairpins are removed with mild washes.

We chose an EGFP transgene, driven by an *flk1* promoter, as the target in fixed 25 hours postfertilization (hpf) zebrafish embryos [9, 10] to test this protocol (Figure 2.3). Fluorescent signal (red) was observed in both the GFP+ and GFP- embryos, which shows that the staining is not triggered by the GFP mRNA and that the hairpin washes were not sufficiently stringent. Additionally, fluorescent signal in the embryo treated with only H2 hairpin further suggests that the staining is an outcome of random aggregation instead of the designed polymerization. After testing HCR in zebrafish embryos under a variety of conditions in situ, we found that it was not possible to adjust the ISH protocol to ensure HCR functionality, therefore we decided to modify the HCR design so that it would be

compatible with stringent ISH conditions.

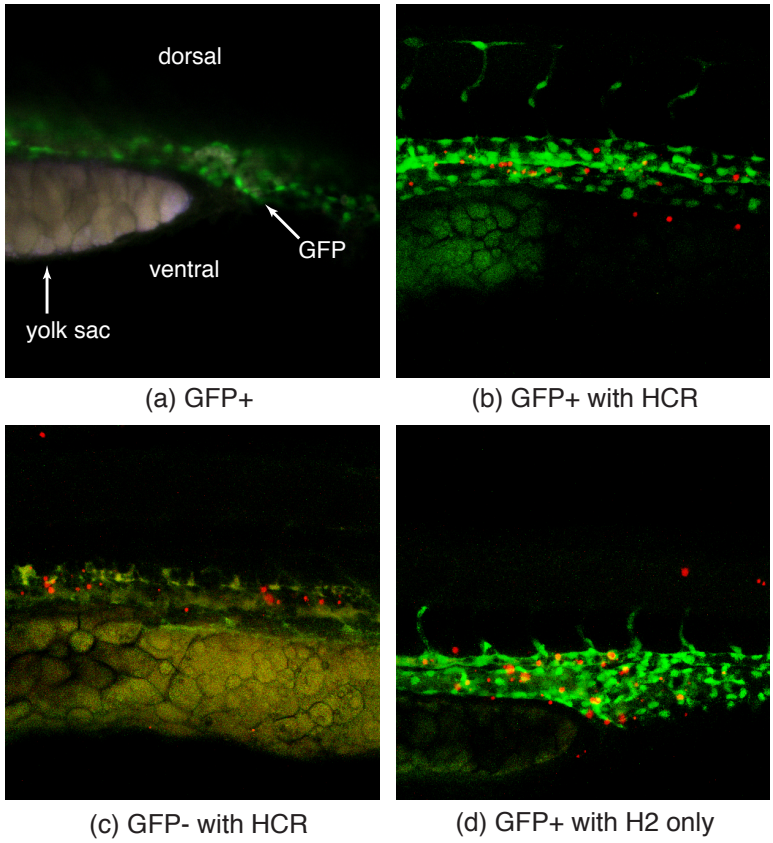

Figure 2.3: In situ hybridization with the original HCR system. (a) Expression pattern of the *flk1::egfp* transgene. The gene is expressed in the endothelial cells of the blood vessels above the yolk sac and under the notochord (shown by the green fluorescence of GFP). (b-c) The experiment was performed in two steps with different hybridization conditions. First, a probe trailing an HCR initiator was incubated with the embryos in stringent hybridization solution at 45 °C for 16 hr. Excess probes were removed with stringent washes as described in Appendix A.1. Then, HCR hairpins were introduced to the embryos in 1× SPSC buffer at room temperature. The embryos were washed with 1× SPSC buffer after 16 hr to remove unbound hairpins. (d) Same experimental procedure as (b-c) but only the H2 hairpin was introduced to the sample. Without stringent hybridization conditions, non-specific staining will be problematic as demonstrated by the red puncta in all three cases. See Appendix A for sequences and experimental details.

2.4 Duplex Calibration

The free energy of each HCR polymerization step arises from the enthalpic benefit of forming additonal stacked base pairs between the toehold in the output domain at the living end of the polmyer and the toehold in the input domain of a newly recruited hairpin, as well as from the entropic benefit of opening the hairpin loop of the recruited hairpin. The original HCR system employed DNA hairpins with 6-nt toeholds/loops and 18-bp stems [1] (resulting in six stacked base pairs plus the opening of a 6-nt hairpin loop per polymerization step). Previous in vitro and in situ studies revealed that this small-loop DNA-HCR system did not polymerize under stringent hybridization conditions due to insufficient free energy per polymerization step. Thus, we confronted the challenge of engineering new HCR hairpins that retain two key properties under these conditions: (1) hairpin metastability in the absence of the initiator, (2) hairpin polymerization in the presence of the initiator. Previous experience told us that these two objectives are at odds. Hairpin metastability is promoted by reducing toehold/loop size; hairpin polymerization is promoted by increasing toehold/loop size. Hence, it was unclear a priori whether HCR hairpins could be re-dimensioned for use in stringent hybridization conditions.

Secondary structure free energy parameters [11, 12] have not been measured for stringent hybridization conditions (e.g., 50% formamide), so we could not re-dimension components based on computational simulation [2, 13]. Instead, we employed test tube and in situ control experiments to measure the minimum number of base pairs required for two monomers to hybridize stably under stringent conditions by using an RNA probe of fixed length while varying the length (L = 10, 12, 18, 24, 30) of an RNA target strand with roughly 50% GC content (Table A.3). Figure 2.4 shows the binding assay, performed using a native polyacrylamide gel, and its quantification, for an RNA target strand of length 12. Similar experiments were performed for all other lengths (data not shown). We found that 12 RNA base pairs provide the minimum free energy gain required for two strands to form a stable duplex in hybridization solution at 45 °C. A similar binding assay performed in situ with fixed zebrafish embryos reached the same conclusion (Figure 2.5).

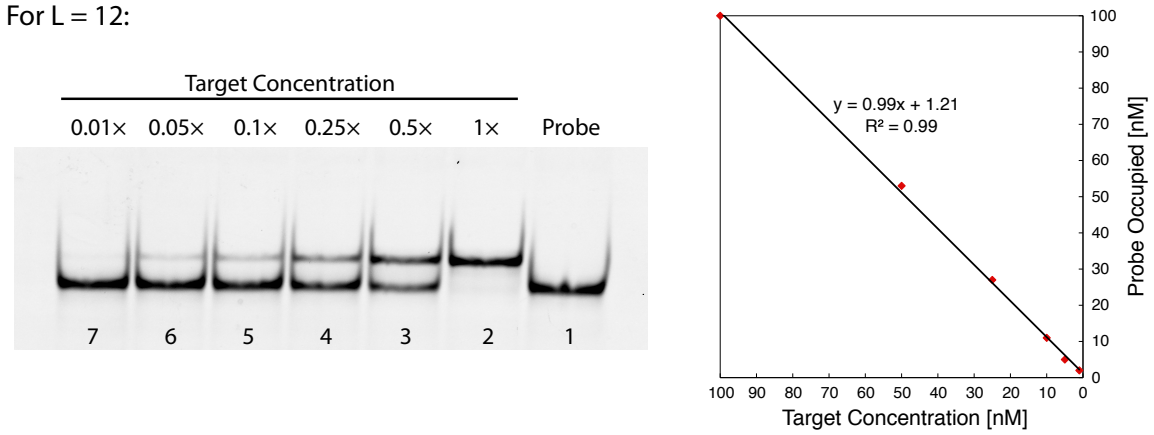

Figure 2.4: In vitro RNA duplex binding assay. This assay helped us to determine the minimum number of base pairs required for two complementary strands to form a stable duplex in stringent hybridization solution (50% formamide, 2× SSC, 0.1% Tween 20, 9 mM citric acid, 500 μg/mL tRNA, 0.02% BSA, 0.2% fish powder) at 45 °C. The concentration of the FAM-labeled probe was fixed at 100 nM for all lanes. We varied the target concentration (lane 2–7) and quantified the target-probe duplex (upper band) to determine the extent of hybridization. The slope of the fitted line suggests that 99% of the targets were bound to a probe when the duplex length was 12 base pairs long. See Appendix A for experimental details.

2.5 Hairpin Calibration

To favor metastability of the HCR hairpins, it is preferable to use a smaller loop and correspondingly shorter toehold. Since additional free energy can be gained from the increase in entropy due to opening of the hairpin loop, we repeated the in vitro binding assay described above, this time substituting a hairpin for the target. In this study, we varied the length of the hairpin toehold (L = 8, 10, 12 nt) with roughly 30% GC content. Figure 2.6 shows the binding assay and its quantification for a hairpin with toehold of length 10. Similar experiments were performed for all other toehold lengths (data not shown). From these data, we conclude that L $\geq$ 10 is required to provide stable binding between the hairpin and the initiator. This in vitro result guides the design of new HCR systems for in situ applications in Chapter 3.

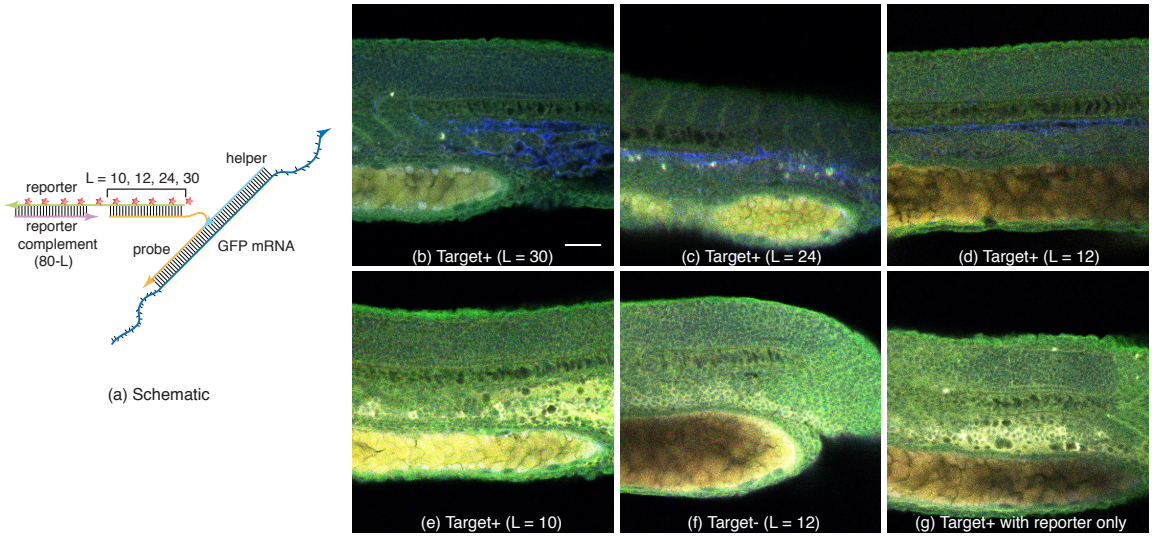

Figure 2.5: In situ duplex binding assay. (a) Schematic of the binding assay. A 50-nt RNA probe (orange strand) for GFP mRNA has a single-stranded region of length L that is complementary to the overhang of the reporter complex. The reporter (green) was labeled with multiple Alexa 647 fluorophores. The reporter complement strand (purple) was used to prevent any non-specific base pairing of the reporter strand to other DNA or RNA in the zebrafish and the 50-nt helper strand (cyan) was there to block undesired hybridization between the overhang of the probe to the proximal mRNA sequence. (b-f) The assay was performed over a two-day period. On the first day, the GFP probe and helper strand were hybridized to the fish for 16 hr in hybridization solution. Excess probes and helper strands were eliminated with stringent washes as described in Appendix A.1.6. The reporter complex, labeled with Alexa 647, was then introduced to start the second day of hybridization. Finally, the embryos were washed again to remove unbound reporters. (g) Same experimental procedure as (b-f) but only the helper strand (no probe) was introduced on the first day. The occurrence of staining (blue), only in the GFP positive embryos, demonstrated that $L \geq 12$ is sufficient for the reporter to hybridize stably and specifically to the probe. The morphology of the fish is shown in green, using autofluorescence from an image acquired with a 488 nm laser and a 515 ± 15 nm bandpass filter. Scale bar, 50 μm, is applicable to all images.

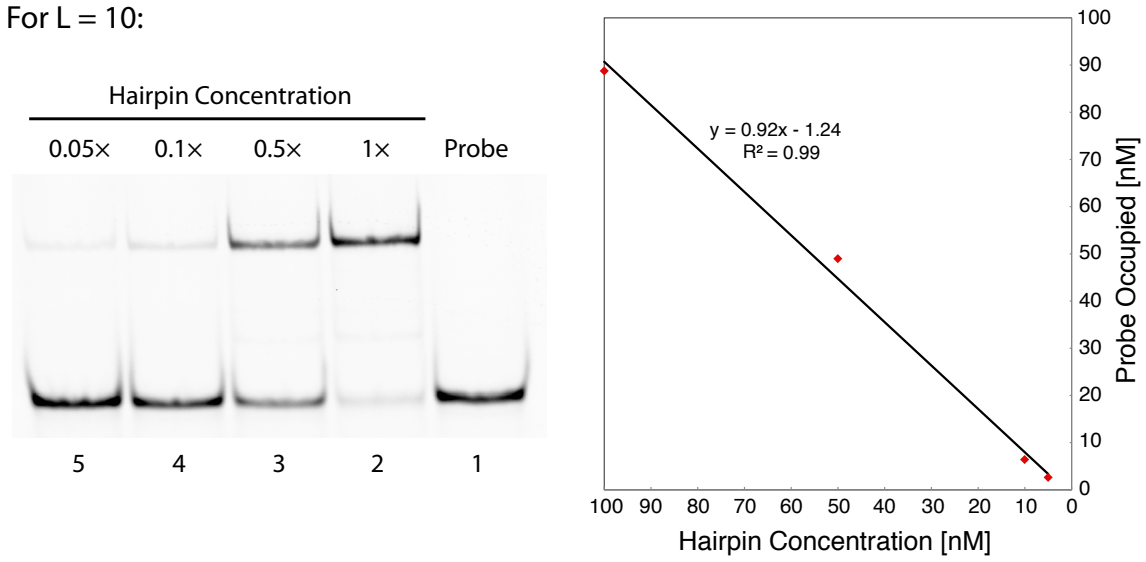

Figure 2.6: In vitro RNA hairpin binding assay. This assay allows us to determine the minimum number of base pairs required for adding a hairpin monomer to an HCR polymer in stringent hybridization solution (50% formamide, 2× SSC, 0.1% Tween 20, 9 mM citric acid, 500 μg/mL tRNA, 0.02% BSA, 0.2% fish powder) at 45 °C. The concentration of the FAM-labeled probe (HCR initiator) was fixed at 100 nM for all lanes. We varied the hairpin concentrations (lane 2–5) and quantified the hairpin-probe duplex band (upper band) to determine the amount of probe hybridized to a hairpin. From the plot, we conclude that a hairpin toehold length of 10 RNA bases is sufficient for the initiator to hybridize stably. See Appendix A for experimental details.

2.6 Conclusion

The original HCR system is not functional under stringent ISH conditions due to insufficient free energy gain from nucleation between the hairpin and the initiator. However, we have demonstrated that relaxing the ISH conditions to ensure HCR functionality is not viable because stringency during hybridization is crucial to avoid non-specific staining in the sample. Therefore, we attempted to modify the dimensions of the HCR hairpins to make them functional under stringent ISH conditions.

By performing duplex and hairpin calibration experiments both in vitro and in situ, we have successfully determined the minimum number of base pairs necessary for two RNA strands to hybridize stably and specifically in stringent conditions. We conclude that a minimum of 12 RNA base pairs with 58% GC content provide the minimum free energy gain required for two single-stranded RNA sequences to form a stable duplex in hybridization

solution at 45 °C. For the hairpin construct, a toehold at least 10 RNA bases long with 30% GC content will ensure stable binding between the hairpin and the initiator. In the next chapter, the results drawn from these extensive studies will lead us to a new HCR system that is functional in stringent ISH conditions.

Please refer to Appendix A for supplementary information pertaining to this chapter.

References

[1] R. M. Dirks and N. A. Pierce. Triggered amplification by hybridization chain reaction. *Proceedings of the National Academy of Sciences of the United States of America* **101**, 15275–15278 (2004).

[2] P. Yin, H. M. T. Choi, C. R. Calvert and N. A. Pierce. Programming biomolecular self-assembly pathways. *Nature* **451**, 318–322 (2008).

[3] E. Winfree, F. R. Liu, L. A. Wenzler and N. C. Seeman. Design and self-assembly of two-dimensional DNA crystals. *Nature* **394**, 539–544 (1998).

[4] W. M. Shih, J. D. Quispe and G. F. Joyce. A 1.7-kilobase single-stranded DNA that folds into a nanoscale octahedron. *Nature* **427**, 618–621 (2004).

[5] P. W. K. Rothemund. Folding DNA to create nanoscale shapes and patterns. *Nature* **440**, 297–302 (2006).

[6] B. Yurke, A. J. Turberfield, J. Mills, F. C. Simmel and J. L. Neumann. A DNA-fuelled molecular machine made of DNA. *Nature* **406**, 605–608 (2000).

[7] A. R. Leitch, T. Schwarzacher, D. Jackson and I. J. Leitch. *In Situ Hybridization: A Practical Guide* (BIOS Scientific Publishers, Oxford, 1994).

[8] J. M. Polak and J. O'D. McGee. *In Situ Hybridization: Principles and Practice* (Oxford University Press, Oxford, 1998).

[9] C. B. Kimmel, W. W. Ballard, S. R. Kimmel, B. Ullmann and T. F. Schilling. Stages of embryonic development of the zebrafish. *Developmental Dynamics* **203**, 253–310 (1995).

[10] S. Isogai, M. Horiguchi and B. M. Weinstein. The vascular anatomy of the developing zebrafish: An atlas of embryonic and early larval development. *Developmental Biology* **230**, 278–301 (2001).

[11] J. SantaLucia. A unified view of polymer, dumbbell, and oligonucleotide DNA nearest-neighbor thermodynamics. *Proceedings of the National Academy of Sciences of the United States of America* **95**, 1460–1465 (1998).

[12] D. H. Mathews, J. Sabina, M. Zuker and D. H. Turner. Expanded sequence dependence of thermodynamic parameters improves prediction of RNA secondary structure. *Journal of Molelcular Biology* **288**, 911–940 (1999).

[13] R. M. Dirks, J. S. Bois, J. M. Schaeffer, E. Winfree and N. A. Pierce. Thermodynamic analysis of interacting nucleic acid strands. *SIAM Review* **49**, 65–88 (2007).

Chapter 3

Multiplexed In Situ Amplification via Fluorescent Hybridization Chain Reactions

The work presented here is heavily based on the following manuscript in preparation:
H. M. T. Choi, J. Y. Chang, L. A. Trinh, J. E. Padilla, S. E. Fraser and N. A. Pierce. Programmable in situ amplification for multiplexed bioimaging.

3.1 Introduction

Based on the free energy design constraints obtained in Chapter 2, here we develop a new HCR-based ISH method to achieve multiplexed ISH with high signal-to-background. This method will offer biologists, medical researchers, and doctors new possibilities for observing, elucidating, and diagnosing the regulatory circuits encoded in our genes.

3.2 Redesigning HCR for ISH Applications

The results from Chapter 2 showed that a gain of 10 RNA base pairs with 30% GC content is sufficient to achieve stable hybridization between a hairpin and its target in stringent ISH conditions. Imposing this design constraint to promote hairpin polymerization did not prevent us from retaining hairpin metastability under the same conditions. Therefore, we designed four new HCR systems, each consisting of RNA hairpins with 10-nt toeholds and loops targeting four unique RNA initiators. The test tube study of Figure 3.1b illustrates

four HCR amplifiers operating simultaneously and orthogonally in a background of zebrafish total RNA under stringent hybridization conditions. The hairpins exhibit metastability in the absence of initiators; the introduction of a single initiator species selectively triggers the cognate polymerization reaction. The designed sequence independence between amplifiers ensures that multiple targets can be amplified in parallel without cross-talk. These results suggest that the ability to generate orthogonal amplifiers (i.e., the numbers of mRNAs that can be detected simultaneously) will not be a limiting factor because the design space for nucleic acid sequences is large.

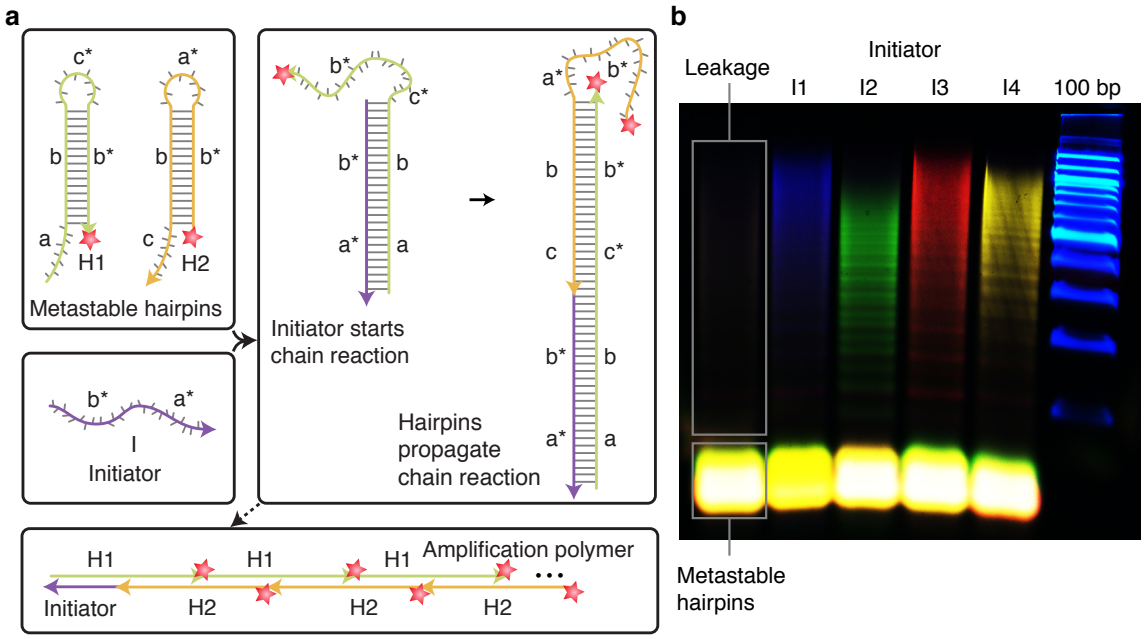

Figure 3.1: Multiplexed amplification with orthogonal HCR amplifiers. (a) Mechanism. Metastable fluorescent RNA hairpins self-assemble into a polydisperse population of fluorescent amplification polymers upon detection of specific RNA initiators. (b) Validation in a test tube. Agarose gel demonstrating orthogonal amplification in a reaction volume containing four HCR amplifiers and zebrafish total RNA. Minimal leakage from metastable states is observed in the absence of initiators.

3.3 Multiplexed In Situ Hybridization using In Situ HCR Amplification

We perform in situ hybridization in two stages independent of the number of target mRNAs (Figure 3.2). In the detection stage, all target mRNAs are detected simultaneously via in situ hybridization of complementary RNA probes; unused probes are washed from the sample. Each target mRNA is addressed by a probe set comprising one or more RNA probe species carrying identical initiators; different targets are addressed by probe sets carrying orthogonal initiators. In the amplification stage, optical readouts are generated for all target mRNAs simultaneously using fluorescent in situ HCR. Orthogonal initiators trigger orthogonal hybridization chain reactions in which metastable RNA hairpins self-assemble into tethered amplification polymers labeled with spectrally distinct fluorophores; unused hairpins are washed from the sample prior to imaging.

3.4 Validation of In Situ HCR Amplification

To validate in situ HCR amplification in fixed whole-mount zebrafish embryos, we first targeted a transgenic mRNA, observing bright staining with the expected expression pattern (Figure 3.3a). Wildtype embryos (lacking the target) show minimal staining (Figure 3.3b), comparable to the autofluorescence observed in the absence of probes and hairpins (Figure 3.3c). As expected, amplification is not observed if the probe or either of the two hairpin species is omitted (Figure 3.3d-f). To verify that the staining in Figure 3.3a results from the intended polymerization mechanism rather than from aggregation of closed hairpins, alteration of one or both hairpin stem sequences yields the expected loss (Figure 3.3g and 3.3i) and recovery (Figure 3.3h) of signal.

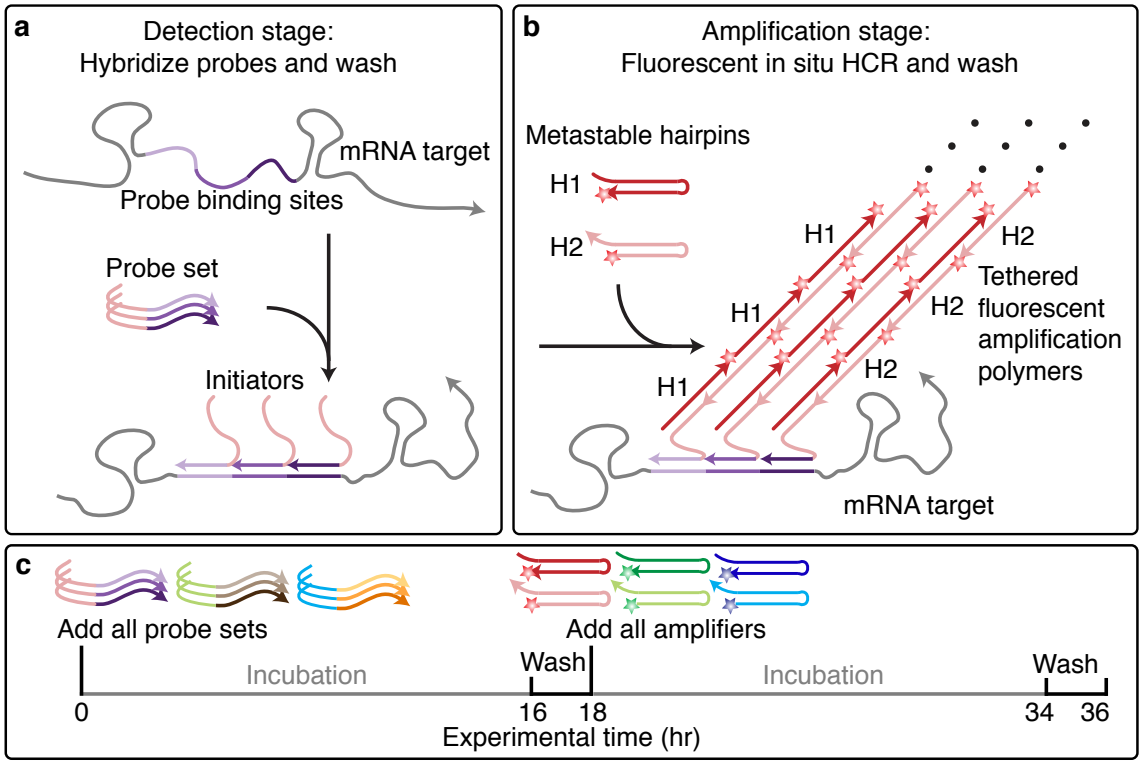

Figure 3.2: In situ hybridization using fluorescent in situ HCR amplification. (a) Detection stage. Probe sets are hybridized to mRNA targets prior to washing unused probes from the sample. (b) Amplification stage. Initiators trigger self-assembly of tethered fluorescent amplification polymers prior to washing unused hairpins from the sample. (c) Experimental timeline. The same two-stage protocol is used independent of the number of target mRNAs. For multiplexed experiments (3-color example depicted), probe sets for different target mRNAs carry orthogonal initiators that trigger orthogonal HCR amplification cascades labeled by spectrally distinct fluorophores.

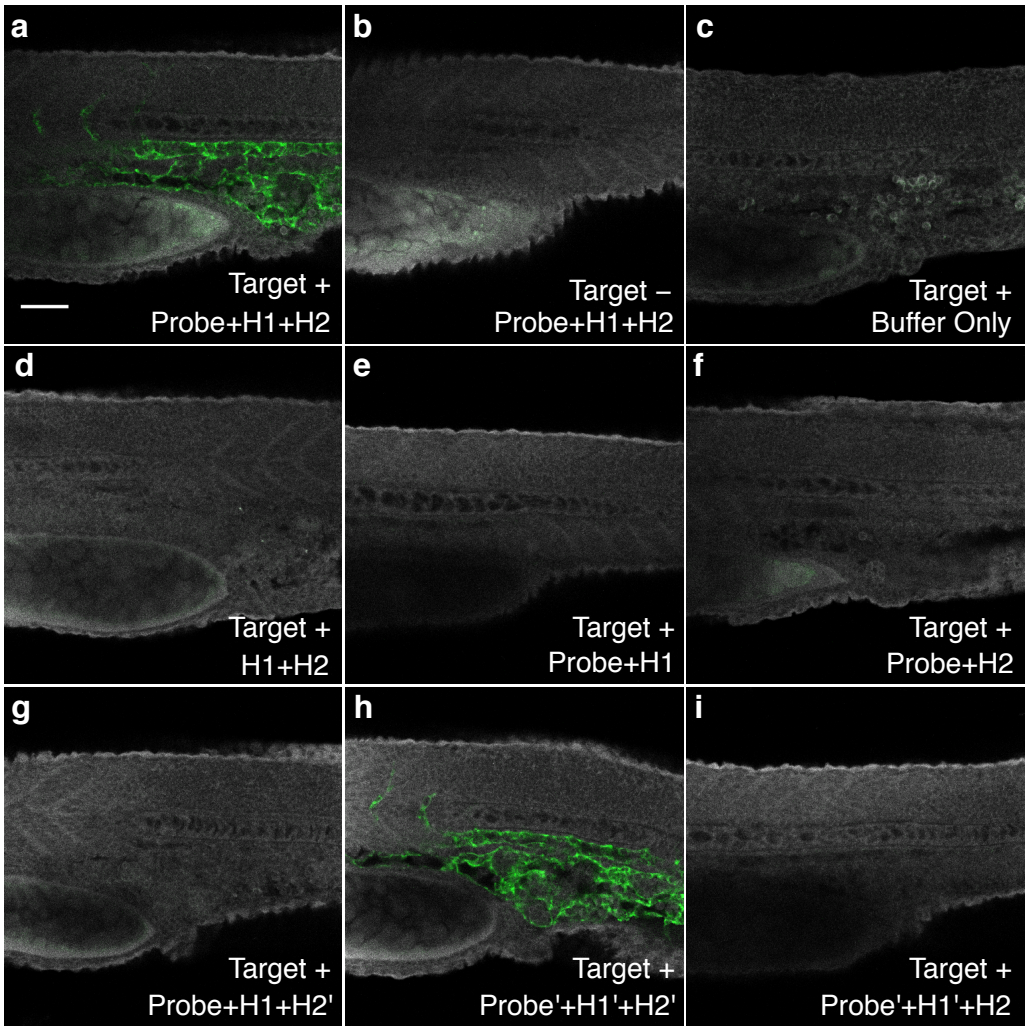

Figure 3.3: Validation of fluorescent in situ HCR amplification in fixed whole-mount zebrafish embryos. Embryo morphology is depicted by autofluorescence in the gray channel. The target is the transgenic transcript *Tg*(*flk1:egfp*), expressed below the notochord and between the somites (see the expression atlas of Figure 3.5a). Fluorescent staining (green channel) using in situ HCR in Target+ (a) and Target- (b) embryos compared to (green channel) autofluorescence in the absence of probes and hairpins (c). No amplification in the absence of probes (d) or of one hairpin species (e, f). Modification of hairpin stem sequences (H1′, H2′) disrupts (g, i) and restores (h) toehold-mediated branch migration, confirming that staining arises from triggered polymerization rather than from random aggregation of hairpins. Typical for zebrafish, the yolk sack (bottom left of each panel) often exhibits autofluorescence. Embryos fixed 25 hpf. Probe set: 1 RNA probe. Scale bar: 50 μm.

3.5 Sample Penetration with Small Components and Triggered Self-Assembly

Detection and amplification components must successfully penetrate an embryo in order to generate signal at the site of an mRNA target. HCR is a triggered self-assembly mechanism, offering the conceptual benefit that small RNA probes and hairpins penetrate the embryo prior to generating larger, less-mobile amplification polymers at the site of mRNA targets. To assess the practical significance of these properties, we imaged an endogenous mRNA with a superficial expression pattern, comparing in situ HCR to the ex situ HCR alternative in which amplification polymers are pre-assembled prior to penetrating the sample. The images of Figure 3.4a and pixel intensity histograms of Figure 3.4b demonstrate dramatic signal loss using ex situ HCR, confirming that it is desirable to penetrate the sample with small components that self-assemble in a triggered fashion at the site of mRNA targets.

3.6 High Signal-to-Background

In situ amplification is intended to generate high signal-to-background to enable accurate mapping of mRNA expression patterns. With our approach, signal is produced when specifically hybridized probes initiate specific HCR amplification to yield fluorescent polymers tethered to cognate mRNA targets. Background can arise from three sources: non-specific detection (probes that bind non-specifically and are subsequently amplified), non-specific amplification (hairpins and polymers that are not hybridized to cognate initiators), and autofluorescence (inherent fluorescence of the fixed embryo). To characterize the relative magnitudes of these effects, we imaged an mRNA target with a sharply defined region of expression and plotted histograms of pixel intensity within a rectangle that crosses the boundary of this expression region. The pixel intensity histograms of Figure 3.4b reveal that autofluorescence is the primary source of background, that non-specific detection contributes a small amount of additional background, and that non-specific amplification contributes negligibly to background. By comparison, the signal generated using in situ HCR amplification yields pixel intensities that are significantly higher than background.

The observation that autofluorescence is the dominant source of background suggests that addressing each target mRNA with a probe set comprising multiple probes [1–3] would further increase the signal-to-background ratio. Subsequent in situ HCR amplification would then decorate each target with an array of amplification polymers. Figure 3.4c demonstrates that the ratio of signal to autofluorescence increases with the number of probes per target. Notably, using in situ HCR, the pixel intensity distribution is bimodal using either 3 or 9 probes per target, with a peak at low intensity corresponding to background (from the portion of the rectangle outside the expression region) and a broad distribution at higher intensities corresponding to signal (from the portion of the rectangle within the expression region).

3.7 Simultaneous Mapping of Five Target mRNAs in a Fixed Whole-Mount Zebrafish Embryo

The fundamental benefit of using orthogonal HCR amplifiers is the ability to perform simultaneous in situ amplification for multiple target mRNAs, enabling straightforward multiplexed imaging. Figure 3.5 demonstrates simultaneous imaging of five target mRNAs in a fixed whole-mount zebrafish embryo. Targets were detected using five probe sets carrying five orthogonal initiators and amplification was performed using five orthogonal HCR amplifiers carrying five spectrally distinct fluorophores.

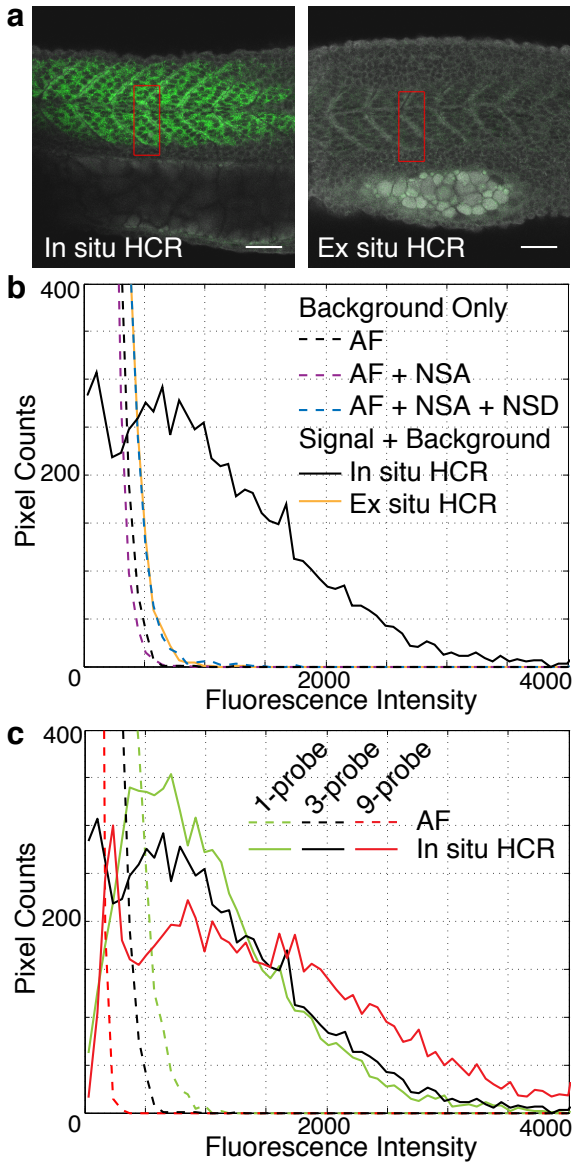

Figure 3.4: Characterizing signal-to-background for fluorescent in situ HCR amplification. The target is a muscle gene transcript (*desm*) expressed in the somites. Embryos fixed 25 hpf. (a) Sample penetration with small components. In situ HCR: probes and hairpins penetrate the sample prior to executing triggered self-assembly of tethered amplification polymers in situ. Ex situ HCR: probes trigger self-assembly of amplification polymers prior to penetrating the sample. Probe set: 3 RNA probes. Scale bar: 50 μm. (b) Background and signal contributions. Histograms of pixel intensity are plotted for a rectangle partially within the expression region and partially outside the expression region (e.g., see panel (a)). Background arises from three sources: autofluorescence (AF; buffer only), non-specific amplification (NSA; hairpins only); non-specific detection (NSD; in situ HCR amplification following detection of absent target *Tg(flk1:egfp)*). Probe set: 3 RNA probes. NSD studies employ a probe set of three RNA probes targeting transgenic transcript *Tg(flk1:egfp)*, which is absent from the WT embryo. (c) Multiple probes per mRNA target. Comparison of autofluorescence and in situ HCR using probe sets with 1, 3, or 9 RNA probes (compare curves of the same color). The microscope PMT gain was decreased as the size of the probe set increased to avoid saturating pixels in the images employing in situ HCR amplification (this accounts for the reduction in AF intensity as the size of the probe set increases).

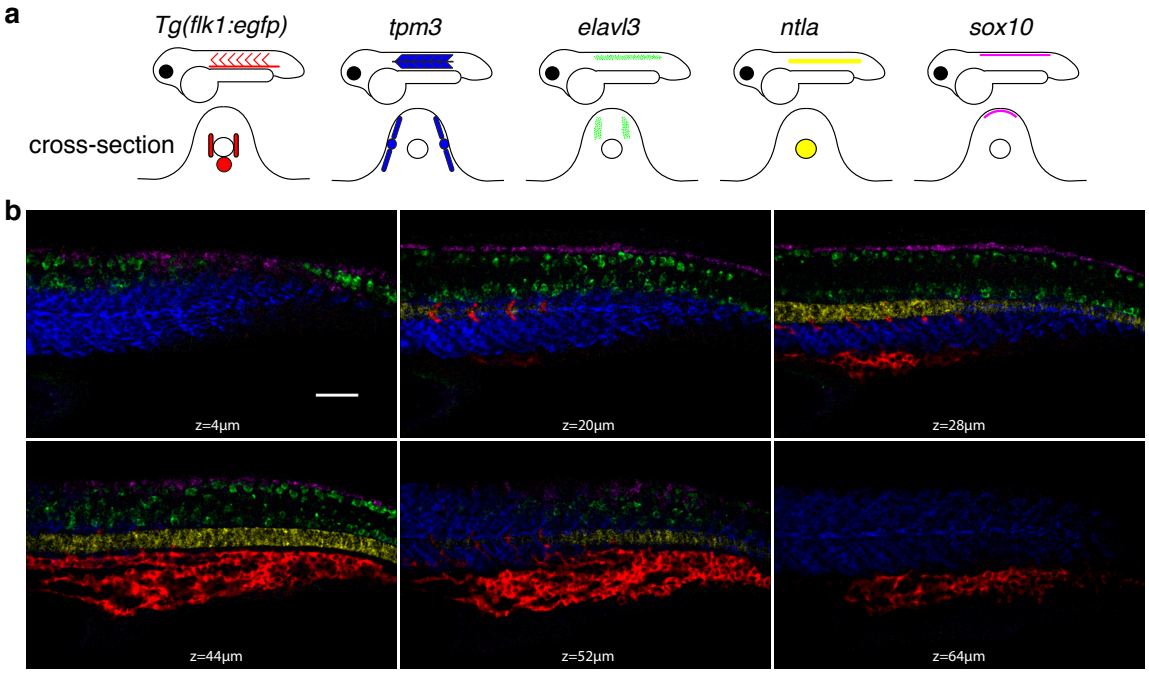

Figure 3.5: Multiplexed imaging in fixed whole-mount zebrafish embryos. (a) Expression atlas for five target mRNAs (*Tg(flk1:egfp)*, *tpm3*, *elavl3*, *ntla*, *sox10*). (b) mRNA expression in six lateral slices within an embryo using confocal microscopy. This type of multiplexed experiment can be routinely performed using the same two-stage protocol that we employ for single-color experiments (summarized in Figure 3.2). Detection is performed using five probe sets carrying orthogonal initiators. The probe sets have different numbers of RNA probes (10, 7, 18, 30, 20) based on the strength of expression of each mRNA target and the strength of the autofluorescence in each channel. Amplification is performed using five orthogonal HCR amplifiers carrying spectrally distinct fluorophores. Embryos fixed 27 hpf. Scale bar: 50 μm.

3.8 Conclusion

The sequencing of numerous genomes has launched a new era in biology, enabling powerful comparative approaches, and revealing the nucleotide sequences that contribute to the differences between species, between individuals of the same species, and between cells within an individual. However, knowledge of these sequences is not sufficient to reveal the architecture and function of the biological circuits that account for these differences. Much work remains to elucidate both the details and the principles of the molecular circuits that regulate development, maintenance, repair, and disease within living organisms.

Over four decades [4], in situ hybridization methods have become an indispensible tool for the study of genetic regulation in a morphological context. Current methods-of-choice for performing in situ amplification in vertebrate embryos and tissue sections require serial amplification for multiplexed studies [5–7]. This shortcoming is a major impediment to the study of interacting regulatory elements in situ.

In recent years, biomolecular engineers have made significant progress in designing nucleic acid molecules that interact and change conformation to execute diverse dynamic functions [8–15]. Here, we exploit design principles drawn from this experience to engineer RNA molecules that interact and change conformation to amplify the expression patterns of multiple target mRNAs in parallel within intact vertebrate embryos. The resulting programmable molecular technology addresses a longstanding challenge in the biological sciences.

Fluorescent in situ HCR is conceptually suited for use in a variety of biological contexts including fixed cells, embryos, tissue sections, and microbial populations. By coupling HCR initiators to aptamer or antibody probes, the approach is also suitable for extension to multiplexed imaging of small molecules and proteins. The HCR amplifiers presented here are suitable for use with diverse mRNA targets because the initiator sequences (and consequently the HCR hairpins) are independent of the mRNA target sequences. Imaging a new target mRNA requires only a new probe set with each probe carrying an HCR initiator.

Please refer to Appendix B for supplementary information pertaining to this work.

References

[1] A. Femino, F. S. Fay, K. Fogarty and R. H. Singer. Visualization of single RNA transcripts in situ. *Science* **280**, 585–590 (1998).

[2] J. M. Levsky, S. M. Shenoy, R. C. Pezo and R. H. Singer. Single-cell gene expression profiling. *Science* **297**, 836–840 (2002).

[3] A. Raj, P. van den Bogaard, S. A. Rifkin, A. van Oudenaarden and S. Tyagi. Imaging individual mRNA molecules using multiple singly labeled probes. *Nature Methods* **5**, 877–879 (2008).

[4] J. G. Gall and M. L. Pardue. Formation and detection of RNA-DNA hybrid molecules in cytological preparations. *Proceedings of the National Academy of Sciences of the United States of America* **63**, 378–383 (1969).

[5] P. Barroso-Chinea *et al.* Detection of two different mRNAs in a single section by dual in situ hybridization: A comparison between colorimetric and fluorescent detection. *Journal of Neuroscience Methods* **162**, 119–128 (2007).

[6] B. Thisse *et al.* Spatial and temporal expression of the zebrafish genome by large-scale in situ hybridization screening. *Methods in Cell Biology* **77**, 505–519 (2004).

[7] H. Acloque, D. G. Wilkinson and M. A. Nieto. In situ hybridization analysis of chick embryos in whole-mount and tissue sections. *Methods in Cell Biology* **87**, 169–185 (2008).

[8] B. Yurke, A. J. Turberfield, J. Mills, F. C. Simmel and J. L. Neumann. A DNA-fuelled molecular machine made of DNA. *Nature* **406**, 605–608 (2000).

[9] A. J. Turberfield *et al.* DNA fuel for free-running nanomachines. *Phys. Rev. Lett.* **90**, 118102 (2003).

[10] R. M. Dirks and N. A. Pierce. Triggered amplification by hybridization chain reaction. *Proceedings of the National Academy of Sciences of the United States of America* **101**, 15275–15278 (2004).

[11] G. Seelig, D. Soloveichik, D. Y. Zhang and E. Winfree. Enzyme-free nucleic acid logic circuits. *Science* **314**, 1585–1588 (2006).

[12] S. Venkataraman, R. M. Dirks, P. W. K. Rothemund, E. Winfree and N. A. Pierce. An autonomous polymerization motor powered by DNA hybridization. *Naure Nanotechnology* **2**, 490–494 (2007).

[13] D. Y. Zhang, A. J. Turberfield, B. Yurke and E. Winfree. Engineering entropy-driven reactions and networks catalyzed by DNA. *Science* **318**, 1121–1125 (2007).

[14] P. Yin, H. M. T. Choi, C. R. Calvert and N. A. Pierce. Programming biomolecular self-assembly pathways. *Nature* **451**, 318–322 (2008).

[15] T. Omabegho, R. Sha and N. C. Seeman. A bipedal DNA brownian motor with coordinated legs. *Science* **324**, 67–71 (2009).

Appendix A

Supplementary Information for Chapter 2

A.1 Methods

A.1.1 DNA and RNA Synthesis

DNA/RNA sequences were synthesized and HPLC purified by Integrated DNA Technologies (IDT). The purified DNA strands were resuspended in ultrapure water (resistance of 18 MΩ cm). The concentrations of the DNA/RNA solutions were determined by the measurement of UV absorption at 260 nm. Each RNA hairpin for the hairpin calibration experiment was synthesized as two pieces which were then ligated to produce the full hairpin (see Table A.5 for the ligation site). The ligation was performed using T4 RNA ligase (New England Biolabs) at 16 °C overnight. Ligated strands were then purified using a 15% denaturing gel. The bands corresponding to the RNA strands of expected sizes were visualized by UV shadowing and excised from the gel. The RNA hairpins were then eluted, and recovered by ethanol precipitation.

A.1.2 Probes and Reporter Synthesis for ISH

RNA probes were synthesized using in vitro transcription. The DNA templates were generated by PCR from a plasmid containing the EGFP gene. RNA probes were then transcribed using a template and an AmpliScribe T7 or T3 high yield transcription kit (Epicentre Biotechnologies). The probes were purified using an RNeasy mini kit (Qiagen).

A.1.3 HCR Reaction Buffer and Hairpin Preparation

The reaction buffer used in the multiplexed HCR gel (Figure 2.1) and the second step of the first in situ HCR experiment (Figure 2.3) was 1× SPSC buffer (50 mM Na_2HPO_4, 0.5 M NaCl, pH 6.8). Hairpins were prepared as monomers in the reaction buffer using a snap cooling procedure: heat at 95 °C for 90 sec and allow to equilibrate at room temperature for 30 min before use.

A.1.4 Gel Electrophoresis

For the multiplexed HCR gel (Figure 2.1), the concentration of each hairpin is 0.5 μM and the concentration of each initiator is 50 nM. Each lane contains 16 ng/μL of zebrafish total RNA. Samples were loaded with 10% glycerol into a 1% native agarose gel, prepared with 1x LB buffer (Faster Better Media). The gel was run at 250V for 30 min at room temperature and imaged using an FLA-5100 fluorescent scanner (Fujifilm Life Science). The laser excitation sources and the emission filters used were a 473 nm laser and a 530 ± 10 nm bandpass filter for FAM, a 532 nm laser and a 570 ± 10 nm bandpass filter for Cy3, a 635 nm laser and a 665 nm longpass filter for Cy5 and a 670 nm laser and a 705 nm longpass filter for Cy5.5.

For the duplex (Figure 2.4) and hairpin (Figure 2.6) studies, the concentrations of the probes were fixed at 100 nM. Samples were loaded with 10% glycerol into a 12% native polyacrylamide gel, prepared with 1x TBE buffer. The gel was imaged using the fluorescent scanner with a 473 nm laser excitation source and a 530 ± 10 nm bandpass filter.

A.1.5 Preparation of Zebrafish Embryos

Embryos (25 hpf) were fixed in 4% paraformaldehyde (PFA) for 24 hr at 4 °C. Fixation was stopped by washing the embryos 3 × 5 min with phosphate-buffered saline (PBS). Embryos were then dehydrated with 5 methanol (MeOH) washes for a total of 1.5 hr and rehydrated with a series of graded MeOH/PBST (PBS with 0.1% Tween 20) washes (75% MeOH / 25% PBST, 50% MeOH / 50% PBST, 25% MeOH / 75% PBST; 5 min each). Embryos were then washed 5 × 5 min in 100% PBST.

A.1.6 In Situ Hybridization

The probe hybridization of the first in situ HCR experiment (Figure 2.3) and the in situ duplex binding assay (Figure 2.5) used the protocol described here. Embryos were first exchanged into the hybridization solution (50% HB: 50% formamide, 2× saline sodium citrate (SSC), 0.1% Tween 20, 9 mM citric acid (pH 6.0), 500 μg tRNA, 0.02% BSA, 0.2% fish powder) and incubated at 45 °C for 1 hr. Probe solution was prepared by diluting 6 pmol of probe into 200μL of 50% HB and heating to 45 °C. After 16 hr of incubation with the embryos, excess probes were washed away with a series of graded 50% HB / 2× SSC washes (75% of HB / 25% of SSC, 50% of HB / 50% of SSC, 25% of HB / 75% of SSC; 15 min each) at 45 °C. Embryos were further washed with a 15 min 2× SSC wash at 45 °C and a 30 min 2× SSC wash at 45 °C. Finally, the embryos were washed with a series of graded 2× SSC / PBST washes (75% 2× SSC / 25% PBST, 50% 2× SSC / 50% PBST, 25% 2× SSC / 75% PBST, 100% PBST; 10 min each) at room temperature.

In Figure 2.3, the polymerization step used 20 pmol of each hairpin in 200 μL of 1× SPSC buffer. The embryos were washed with 1× SPSC buffer before imaging. In Figure 2.5, hybridization of the reporter followed the same procedures as the probe hybridization with the probe substituted with the Alexa 647 labeled reporter complex.

A.1.7 Fluoresecence Microscopy

For Figure 2.3 and Figure 2.5, a Zeiss 510 upright confocal microscope with a LD LCI Plan-Apochromat 25× / 0.8 Imm Corr DIC objective was used to acquire the images. The channel used to show the morphology and the GFP expression of the embryos was obtained using a 488 nm Ar laser for excitation and a 515 ± 15 nm bandpass filter for emission. The Alexa 647 channel was acquired by exciting the fluorophores with a 633 nm HeNe laser and collecting fluorescence with a 650 nm long pass filter.

A.2 DNA and RNA Sequences

A.2.1 DNA Sequences of Four Original HCR Systems

HCR #1	**Sequence**
Initiator (IA)	AACCACCACCAACCACCCAACATC
Hairpin 1 (HA1)	GATGTTGGGTGGTTGGTGGTGGTTCTCACAAACCACCACCAACCACCC
Hairpin 2 (HA2)	/FAM/ *TT* AACCACCACCAACCACCCAACATCGGGTGGTTGGTGGTGGT TTGTGAG

HCR # 2	**Sequence**
Initiator (IB)	ACAACACACACAAACCACGCACTA
Hairpin 1 (HB1)	TAGTGCGTGGTTTGTGTGTGTTGTGAAGAAACAACACACACAAACCAC
Hairpin 2 (HB2)	/Cy5/ *TT* ACAACACACACAAACCACGCACTAGTGGTTTGTGTGTGTTG TTTCTTC

HCR # 3	**Sequence**
Initiator (IC)	ATCCTTCCCTTCCTCTCCTCCAAT
Hairpin 1 (HC1)	ATTGGAGGAGAGGAAGGGAAGGATTCTGTCATCCTTCCCTTCCTCTCC
Hairpin 2 (HC2)	/Cy3/ *TT* ATCCTTCCCTTCCTCTCCTCCAATGGAGAGGAAGGGAAGGA TGACAGA

HCR # 4	**Sequence**
Initiator (ID)	TCTCTTCTTCTCTTCTTCACTCAT
Hairpin 1 (HD1)	ATGAGTGAAGAAGAGAAGAAGAGATCGTGTTCTCTTCTTCTCTTCTTC
Hairpin 2 (HD2)	/Cy5.5/ *TT* TCTCTTCTTCTCTTCTTCACTCATGAAGAAGAGAAGAAGA GAACACGA

Table A.1: DNA sequences of the four orthogonal HCR systems. Note the TT-spacer (italicized) in between the fluorophore and the hairpin sequence that is employed to reduce the influence of the dye on the kinetic and thermodynamic properties of the hairpins.

A.2.2 DNA Sequences for the First In Situ HCR Experiment

Strand	**Sequence**
Probe	CTTAGTTTCATTCAGTACGTCCAA *TTTT* GTTCTTCTGCTTGTCGGCCATGATATAGACGTTGTGGCTGTTGTAGTTGT
Hairpin 1	TTGGACGTACTGAATGAAACTAAGCTCGATCTTAGTTTCATTCAGTAC
Hairpin 2	/Cy3/ CTTAGTTTCATTCAGTACGTCCAAGTACTGAATGAAACTAAGATCGAG

Table A.2: Probe and hairpin sequences of the first in situ HCR system.

A.2.3 RNA Sequences for Calibration Experiments

Strand	Sequence
Probe	/FAM/ UUUGAGACUGGACGGAUAGAGCGAAUGAUGAG
Target-30	CUCAUCAUUCGCUCUAUCCGUCCAGUCUCA
Target-24	AUUCGCUCUAUCCGUCCAGUCUCA
Target-18	UCUAUCCGUCCAGUCUCA
Target-12	CGUCCAGUCUCA
Target-10	UCCAGUCUCA

Table A.3: RNA sequences for the in vitro duplex study.

Strand	Sequence
Probe-30	CUCAUCAUUCGCUCUAUCCGUCCAGUCUCA *AAAAA* **GUUCUUCUGC UUGUCGGCCAUGAUAUAGACGUUGUGGCUGUUGUAGUUGU**
Probe-24	AUUCGCUCUAUCCGUCCAGUCUCA *AAAAA* **GUUCUUCUGCUUGUC GGCCAUGAUAUAGACGUUGUGGCUGUUGUAGUUGU**
Probe-18	UCUAUCCGUCCAGUCUCA *AAAAA* **GUUCUUCUGCUUGUCGGCCA UGAUAUAGACGUUGUGGCUGUUGUAGUUGU**
Probe-12	CGUCCAGUCUCA *AAAAA* **GUUCUUCUGCUUGUCGGCCAUGAUA UAGACGUUGUGGCUGUUGUAGUUGU**
Probe-10	UCCAGUCUCA *AAAAA* **GUUCUUCUGCUUGUCGGCCAUGAUAU AGACGUUGUGGCUGUUGUAGUUGU**
Reporter	UGAGACUGGACGGAUAGAGCGAAUGAUGAG *UUACU* CGUCUUCUAU GUCUAGCUACUUGUAUCUUGUUAUGUACUUGACUAUUGUG
Complement-30	CACAATAGTCAAGTACATAACAAGATACAAGTAGCTAGACATAGAAGA CG
Complement-24	CACAATAGTCAAGTACATAACAAGATACAAGTAGCTAGACATAGAAGA CGAGTAAC
Complement-18	CACAATAGTCAAGTACATAACAAGATACAAGTAGCTAGACATAGAAGA CGAGTAACTCATCA
Complement-12	CACAATAGTCAAGTACATAACAAGATACAAGTAGCTAGACATAGAAGA CGAGTAACTCATCATTCGCT
Complement-10	CACAATAGTCAAGTACATAACAAGATACAAGTAGCTAGACATAGAAGA CGAGTAACTCATCATTCGCTCT

Table A.4: RNA sequences for the in situ duplex study. Bases are truncated from the 5′ end to obtain various probe lengths. Note the 5-nt spacers (italicized) in the probes and the reporter strand. The last 50 bases (bold) of each probe correspond to the EGFP mRNA binding region.

Strand	Sequence
Probe-12	/FAM/ *UU* ACUCCGUUACCUCGCCAUUAUCUGUGUC
Hairpin-12	GACACAGAUAAUGGCGAGGU–AACGGAGUGACUACUCCCGAACUCCGUUAC CUCGCC
Probe-10	/FAM/ *UU* ACUCCGUUACCUCGCCAUUAUCUGUG
Hairpin-10	CACAGAUAAUGGCGAGGU–AACGGAGUGCUACUCCCGACUCCGUUACCUCG CC
Probe-8	/FAM/ *UU* ACUCCGUUACCUCGCCAUUAUCUG
Hairpin-8	CAGAUAAUGGCGAGGUAACGGAGUCUACUCCCACUCCGUUACCUCGCC

Table A.5: RNA sequences of in vitro hairpin study. The number on the name specified the length of the hairpin sticky end. In the probe, the dye (FAM) is separated from the sequence by a UU-spacer (italicized). The dash "–" indicates the ligation point used for hairpin synthesis (see Section A.1 for details).

Appendix B

Supplementary Information for Chapter 3

B.1 Methods

B.1.1 Probe Synthesis

RNA probes are 81-nt long (26-nt initiator, 5-nt spacer, 50-nt mRNA recognition sequence). mRNAs are addressed by probe sets containing one or more probes that hybridize adjacently at 50-nt binding sites. Probe sequences are displayed in Section B.8.1. RNA probes were synthesized by in vitro transcription. The coding strand for each probe contained three random nucleotides and a 19-nt SP6 promoter sequence upstream of the 81-nt initiator-linker-probe sequence. Complementary DNA coding and template strands were ordered as DNA ultramers (unpurified) from Integrated DNA Technologies (IDT). Strands were resuspended in ultrapure water (resistance of 18 MΩ cm) and concentrations were determined by measuring absorption at 260 nm using a NanoDrop 8000 (Thermo Scientific). The double-stranded template was formed by annealing the two strands (heat at 95 °C for 5 min, cool 1 °C/min to room temperature) in 1× SPSC buffer (0.4 M NaCl, 50 mM Na_2HPO_4, pH 7.5). RNA probes were transcribed overnight at 37 °C using an AmpliScribe SP6 high yield transcription kit (Epicentre Biotechnologies) with four unmodified ribonucleotide triphosphates. Probes were purified using an RNeasy mini kit (Qiagen) and concentrations were determined by measuring absorbance at 260 nm.

B.1.2 Hairpin Design, Synthesis, and Preparation

B.1.2.1 HCR Hairpin Design

RNA HCR hairpins are 52-nt long (10-nt toehold, 16-bp stem, 10-nt loop). Hairpin dimensioning was performed based on in vitro and in situ binding studies performed in Chapter 2. HCR hairpin sequences were designed by considering a set of target secondary structures involving different subsets of the strands (I, H1, H2, I·H1 and I·H1·H2, each as depicted in Figure 3.1). Sequence optimization was performed by calculating the average number of incorrectly paired nucleotides at equilibrium [1] for each set of strands and corresponding target structure, and mutating the sequences to minimize the sum of this quantity over all the target structures [2]. Multiple HCR amplifiers were designed independently and then sequence orthogonality was checked using NUPACK (www.nupack.org) to simulate the equilibrium species concentrations and base-pairing properties for a test tube [3] containing different subsets of strands. This approach was used to check for off-target interactions between each of the five initiators and the other four hairpin sets, as well as between the 10-nt toehold and loop segments of each hairpin set and the 10-nt toehold and loop segments of the other four hairpin sets. The sequences are shown in Section B.8.7.

B.1.2.2 HCR Hairpin Synthesis

Each HCR hairpin was synthesized by IDT as two segments with one segment end-labeled with an amine (3′-end for H1 and 5′-end for H2) to permit subsequent coupling to a fluorophore. The strand with a 5′-end at the ligation site was ordered with a 5′-phosphate to permit ligation. Ligation of the two segments produced the full 52-nt hairpin. The ligation was performed using T4 RNA ligase 2 (New England Biolabs) at 16 °C for a minimum of 8 hr. The ligated strands were purified using a 15% denaturing polyacrylamide gel. The bands corresponding to the expected sizes of the ligated products were visualized by UV shadowing and excised from the gel. The RNA strands were then eluted by soaking in 0.3 M NaCl overnight and recovered by ethanol precipitation. The pellet was dried and resuspended in ultrapure water and quantified by measuring absorbance at 260 nm. The dye coupling reaction was performed by mixing an amine-labeled hairpin with an Alexa Fluor

succinimidyl ester (Invitrogen) and incubating in the dark for 3 hr. Alexa-labeled hairpins were separated from unincorporated dyes by repeating the denaturing PAGE purification described above.

B.1.2.3 HCR Hairpin Preparation

To ensure hairpins were formed properly, as monomers, each hairpin was snap cooled in 1× SPSC buffer (see section B.2.3) by heating at 95 °C for 90 sec and allowed to cool to room temperature on the benchtop for 30 min before use. In the in vitro multiplexing gel (Figure 3.1), 3 pmol of each hairpin was snap cooled at 3 μM (total 1 μL). In the validation experiment (Figure 3.3), 10 pmol of each hairpin was snap cooled at 2 μM (total 5 μL). For the signal-to-background (Figure 3.4) and multiplexing (Figure 3.5) experiments, 30 pmol of each hairpin is used due to the increased number of probes for each target. Each hairpin was snap cooled at 3 μM (total 10 μL).

B.1.3 Multiplexed Gel Electrophoresis

Reactions for Figure 1b were performed in 40% hybridization buffer without blocking agents (40% formamide, 2× SSC, 9 mM citric acid (pH 6.0), 0.1% Tween 20) with 0.1 μg/μL of total RNA extracted from zebrafish using TRIzol (Invitrogen). Each of the eight hairpin species (two for each of the four HCR amplifiers) was snap cooled at 3 μM in 1× SPSC buffer. The RNA initiator for each HCR system was diluted to 0.3 μM in ultrapure water. Each lane was prepared by mixing 12 μL of formamide, 6 μL of 5× HB supplements without blocking agents (10× SSC, 45 mM citric acid (pH 6.0), 0.5% Tween 20), 1.76 μL of 1.7 μg/μL extracted zebrafish total RNA, and 1 μL of each of the eight hairpins. When an initiator was absent (lane 1), 2.24 μL of ultrapure water was added to bring the reaction volume to 30 μL. For lanes 2 to 5, 1 μL of 0.3 μM initiator for one HCR amplifier and 1.24 μL of ultrapure water were added. The reactions were incubated at 45 °C for 1.5 hr. The samples were supplemented with 7.5 μL of 50% glycerol and loaded into a native 2% agarose gel, prepared with 1× LB buffer (Faster Better Media). The gel was run at 150 V for 90 min at room temperature and imaged using an FLA-5100 fluorescent scanner (Fujifilm

Life Science). The 4 HCR systems were labeled and imaged as follows:

HCR #	Dye	Excitation	Filters
3	Alexa 488	473 nm	BP 530 ± 10 nm
5	Alexa 546	532 nm	BP 570 ± 10 nm
1	Alexa 647	635 nm	LP 665 nm
4	Alexa 700	670 nm	LP 705 nm

Table B.1: Excitation lasers and emission filters used for multiplexed gel electrophoresis.

For the gel in Figure B.3, the reaction conditions were the same as those of Figure 3.1. Only two hairpins of each HCR system were used in each lane. The five HCR systems (see Section B.8.7) were labeled with Alexa 647. The samples were supplemented with 7.5 μL of 50% glycerol and loaded into a 2% native agarose gel. The gels were run at 150 V for 90 min and imaged with a 635 nm laser and a 665 longpass filter. The 100 bp DNA ladder was pre-stained with SYBR Gold (Invitrogen) and imaged using a 488 nm laser and a 575 nm long pass filter.

B.1.4 In Situ Hybridization Studies

Embryos were fixed and permeablized using the protocol of Section B.2.1. For the transgenic samples, GFP+ embryos were identified using a Leica MZ16 FA fluorescence stereomicroscope. In situ hybridization experiments for Figures 3.3-3.5 were performed using the protocol of Section B.2.2. Overnight incubations were performed for 16 hr. For Figure 3.3, probe solution was prepared by introducing 6 pmol of each probe (1-3 μL depending on the stock solution) into 300 μL of 50% HB at 55 °C. Hairpin solution was prepared by introducing 10 pmol of each hairpin (snap cooled in 5 μL) into 300 μL of 40% HB at 45 °C. Figure 3.4 experiments were performed using WT embryos. A probe set with three probes (1 pmol of each probe) was used for Figures 3.4a and 3.4b; probe sets with 1, 3, or 9 probes (1 pmol of each probe) were used for Figure 3.4c. The standard in situ protocol was used for both the (AF + NSA) sample (with probes excluded) and for the AF sample (with probes and hairpins excluded). For the (AF + NSA + NSD) sample, *desm* probes were replaced with *egfp* probes carrying the same initiator sequence as the *desm* probes. For the ex situ HCR study of Figures 3.4a and 3.4b, snap-cooled hairpins (30 pmol of each hairpin) and probes

(1 pmol of each probe) were added to 300 μL of 40% HB and incubated at 45 °C for 16 hr while the embryos were incubated without probes in 50% HB at 55 °C. For consistency, these embryos were subjected to the standard probe washes and the standard amplification protocol (substituting the pre-assembled polymer solution for the hairpin solution).

B.1.5 Confocal Microscopy

A chamber for mounting the embryo was made by aligning 2 stacks of Scotch tape (8 pieces per stack) 1 cm apart on a 25 mm × 75 mm glass slide (VWR). Approximately 200 μL of 3% methyl cellulose mounting medium was added between the tape stacks on the slide and embryos were placed on the medium oriented for lateral imaging. A 22 mm × 22 mm No. 1 coverslip (VWR) was placed on top of the stacks to close the chamber. A Zeiss 510 upright confocal microscope with an LD LCI Plan-Apochromat 25× / 0.8 Imm Corr DIC objective was used to acquire the images for Figures 3.3 and 3.4. The excitation laser sources and emissions filters were: 488 nm Ar laser excitation source and a 520 ± 10 nm bandpass filter (gray; autofluorescence), 633 nm HeNe laser and a 650 nm long pass filter (green; Alexa 647). A Leica TCS SP5 inverted confocal microscope with an HCX PL APO 20× / 0.7 Imm objective was used to acquire the 5-color image stack of Figure 3.5b. Excitation laser sources and tuned emissions bandpass filters were as follows: 488 nm / 500-540 nm (Alexa 488), 514 nm / 550-565 nm (Alexa 514), 543 nm / 550-605 nm (Alexa 546), 594 nm / 605-640 nm (Alexa 594), 633 nm / 655-720 nm (Alexa 647). Cluster analysis (Leica) was performed to enhance dye separation. All images are presented without background subtraction.

B.2 Protocols

B.2.1 Preparation of Fixed Whole-Mount Zebrafish Embryos

1. Collect embryos and incubate at 28 °C in a petri dish with egg H_2O until they reach 20 hr post-fertilization (20 hpf).
2. Dechorinate using two pairs of sharp tweezers under a dissecting scope.
3. Transfer ∼80 embryos (25 hpf) to a 2 mL eppendorf tube and remove excess egg H_2O.
4. Fix embryos in 1 mL of 4% paraformaldehyde (PFA)* for 24 hr at 4 °C .
5. Wash embryos 3 × 5 min with 1 mL of phosphate-buffered saline (PBS) to stop the fixation. Fixed embryos can be stored at 4 °C at this point.
6. Dehydrate and permeabilize with a series of methanol (MeOH) washes (1 mL each):
   (a) 100% MeOH for 4 × 10 min
   (b) 100% MeOH for 1 × 50 min.
7. Rehydrate with a series of graded 1 mL MeOH/PBST washes for 5 min each:
   (a) 75% MeOH / 25% PBST
   (b) 50% MeOH / 50% PBST
   (c) 25% MeOH / 75% PBST
   (d) 5 × 100% PBST.
8. Store embryos at 4 °C before use.†

*Use fresh PFA and cool to 4 °C before use to avoid increased autofluorescence.
†Prepare embryos every two weeks to avoid increased autofluorescence.

B.2.2 Two-Stage Multiplexed In Situ Hybridization using HCR

Detection Stage

1. For each sample, move 8 embryos to a 1.5 mL eppendorf tube.
2. Pre-hybridize with 300 μL of 50% hybridization buffer (50% HB) for 30 min at 55 °C.
3. Prepare probe solution by adding 6 pmol of each probe (1-3 μL per probe depending on the stock) to HB reagents at 55 °C to yield probes in 500 μL of 50% HB.
4. Remove the pre-hybridization solution and add the 500 μL of probe solution.
5. Incubate the embryos overnight (12-16 hr) at 55 °C.
6. Remove excess probes by washing at 55 °C with 500 μL of:
   (a) 75% of 50% HB / 25% 2× SSC for 15 min
   (b) 50% of 50% HB / 50% 2× SSC for 15 min
   (c) 25% of 50% HB / 75% 2× SSC for 15 min
   (d) 100% 2× SSC for 15 min
   (e) 100% 2× SSC for 30 min.

   Wash solutions should be pre-heated to 55 °C before use.
7. Wash at room temperature for 10 min each with 500 μL of:
   (a) 75% 2× SSC / 25% PBST
   (b) 50% 2× SSC / 50% PBST
   (c) 25% 2× SSC / 75% PBST
   (d) 100% PBST.

Amplification Stage

1. Prepare 30 pmol of each fluorescently labeled hairpin by snap cooling in 10 μL of 1× SPSC buffer (heat at 95 °C for 90 sec and cool to room temperature on the benchtop for 30 min).
2. Pre-hybridize embryos with 300 μL of 40% HB for 30 min at 45 °C.
3. Prepare hairpin solution by adding all snap-cooled hairpins to HB reagents at 45 °C to yield hairpins in 500 μL of 40% HB.
4. Remove the pre-hybridization solution and add the 500 μL of hairpin solution.
5. Incubate the embryos overnight (12-16 hr) at 45 °C.
6. Repeat step 6 above using 40% HB at 45 °C (instead of 50% HB at 55 °C).
7. Repeat step 7 above.

B.2.3 Buffer Recipes

50% Hybridization Buffer (50% HB)	For 40 mL of solution
50% Formamide	20 mL formamide
2× Sodium Chloride Sodium Citrate (SSC)	4 mL of 20× SSC
9 mM Citric Acid (pH 6.0)	360 μL 1 M Citric Acid, pH 6.0
0.1% Tween 20	400 μL of 10% Tween 20
500 μg/mL tRNA	200 μL of 100 mg/mL tRNA
50 μg/mL Heparin	200 μL of 10 mg/mL Heparin
	fill up to 40 mL with ultrapure H_2O

40% Hybridization Buffer (40% HB)	For 40 mL of solution
40% Formamide	16 mL formamide
2× Sodium Chloride Sodium Citrate (SSC)	4 mL of 20× SSC
9 mM Citric Acid (pH 6.0)	360 μL 1 M Citric Acid, pH 6.0
0.1% Tween 20	400 μL of 10% Tween 20
500 μg/mL tRNA	200 μL of 100 mg/mL tRNA
50 μg/mL Heparin	200 μL of 10 mg/mL Heparin
	fill up to 40 mL with ultrapure H_2O

5× HB Supplements	For 40 mL of solution
10× Sodium Chloride Sodium Citrate (SSC)	20 mL of 20× SSC
45 mM Citric Acid (pH 6.0)	1.8 mL 1 M Citric Acid, pH 6.0
0.5% Tween 20	2 mL of 10% Tween 20
2.5 mg/mL tRNA	1 mL of 100 mg/mL tRNA
250 μg/mL Heparin	1 mL of 10 mg/mL Heparin
	fill up to 40 mL with ultrapure H_2O

5× HB Supplements without Blocking Agents	For 40 mL of solution
10× Sodium Chloride Sodium Citrate (SSC)	20 mL of 20× SSC
45 mM Citric Acid (pH 6.0)	1.8 mL 1 M Citric Acid, pH 6.0
0.5% Tween 20	2 mL of 10% Tween 20
	fill up to 40 mL with ultrapure H_2O

10× PBS[‡]	For 1 L of solution
1.37 M NaCl	80 g NaCl
27 mM KCl	2 g KCl
100 mM Na_2HPO_4	14.2 g Na_2HPO_4 anhydrous
20 mM KH_2PO_4	2.7 g KH_2PO_4 anhydrous
pH 7.4	Adjust pH to 7.4 with HCl
	fill up to 1 L with ultrapure H_2O

PBST	For 50 mL of solution
1× PBS	5 mL of 10× PBS
0.1% Tween 20	500 μL of 10% Tween 20
	fill up to 50 mL with ultrapure H_2O

5× Sodium Phosphate Sodium Chloride (SPSC)	For 50 mL of solution
2 M NaCl	25 mL of 4 M NaCl
250 mM Na_2HPO_4	12.5 mL of 1 M Na_2HPO_4
	12.5 mL of ultrapure H_2O

[‡]Avoid using calcium chloride and magnesium chloride in PBS as this leads to increased autofluorescence in the embryos.

B.2.4 Reagents and Supplies

SP6 Transcription Kit (Epicentre cat. # AS3106)
RNeasy Mini Kit (Qiagen cat. # 74104)
T4 RNA Ligase II (NEB cat. # M0239L)
Alexa Fluor 488 carboxylic Acid, 2,3,5,6-tetraFluorophenyl ester (Molecular Probes cat. # A30005)
Alexa Fluor 514 carboxylic acid, succinimidyl ester (Molecular Probes cat. # A30002)
Alexa Fluor 546 carboxylic acid, succinimidyl ester (Molecular Probes cat. # A20002)
Alexa Fluor 594 carboxylic acid, succinimidyl ester (Molecular Probes cat. # A20004)
Alexa Fluor 647 carboxylic acid, succinimidyl ester (Molecular Probes cat. # A20006)
Alexa Fluor 700 carboxylic acid, succinimidyl ester (Molecular Probes cat. # A20010)
Dimethyl Sulfoxide (DMSO) (Sigma cat. # 276855)
Paraformaldehyde (PFA) (Sigma cat. # P6148)
Formamide (EMD cat. # FX0420-6)
20× Sodium Chloride Sodium Citrate (SSC) (Invitrogen cat. # 15557044)
Tween 20 (Sigma cat. # P1379)
tRNA from baker's yeast (Roche cat. # 109495)
Heparin (Sigma cat. # 3393)
SYBR Gold Nucleic Acid Gel Stain (Invitrogen cat. # S-11494)
25 mm × 75 mm glass slide (VWR cat. # 48300-025)
22 mm × 22 mm No. 1 coverslip (VWR cat. # 48366-067)

B.3 Gels for In Vitro Validation of HCR Amplifiers

Figure B.1 demonstrates the triggered polymerization properties of each of the five HCR amplifiers used in Figure 3.5. The hairpins for each HCR amplifier exhibit metastability in the absence of initiator and undergo triggered polymerization upon the introduction of initiator. Previous control experiments (data not shown) show that the H1 and H2 hairpins migrate as separate bands. The hairpins for amplifier HCR4 exist metastably as both monomers and as putative dimers; introduction of initiators triggers polymerization from either metastable state.

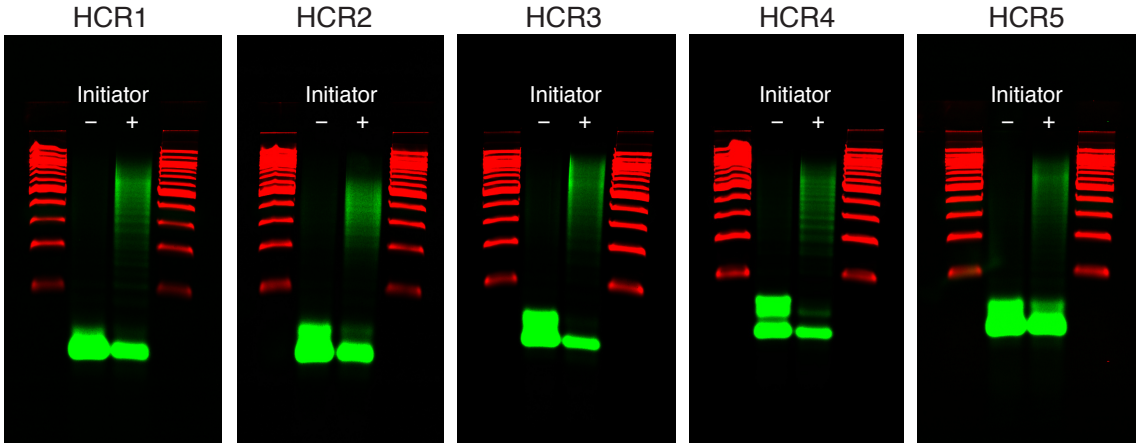

Figure B.1: Agarose gel electrophoresis for five HCR amplifiers. The reaction conditions were the same as for Figure1b. Each gel tests the hairpins for one HCR amplifier. All hairpins were labeled with Alexa 647. Native 2% agarose gels were run at 150 V for 90 min and imaged with a 635 nm laser and a 665 longpass filter. The 100 bp DNA ladders (red) were pre-stained with SYBR Gold (Invitrogen) and imaged using a 488 nm laser and a 575 nm long pass filter.

B.4 Single-Channel Images for In Situ Validation of HCR Amplifiers

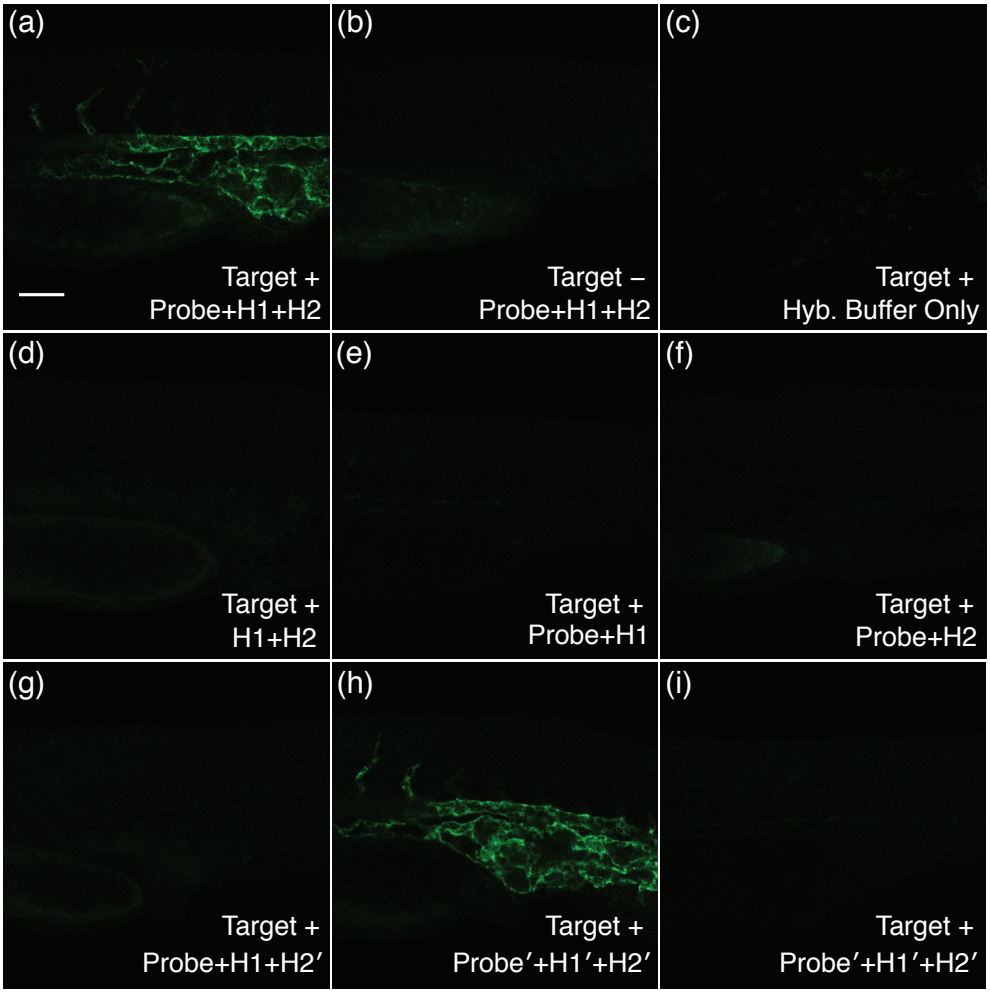

Figure B.2: Single-channel version of Figure 3.3. Turning off the gray autofluorescence channel emphasizes the minimal degree of background staining. Scale bar: 50 μm.

B.5 Images for Signal-to-Background Studies

The pixel intensity histograms of Figures 3.4b and 3.4c are calculated within the rectangles depicted in Figures B.3 and B.4. These rectangles are positioned so that they encompass both a region with high target expression (to characterize signal) and a region with no target expression (to characterize background). The conclusions are insensitive to the precise positioning of the rectangles (data not shown).

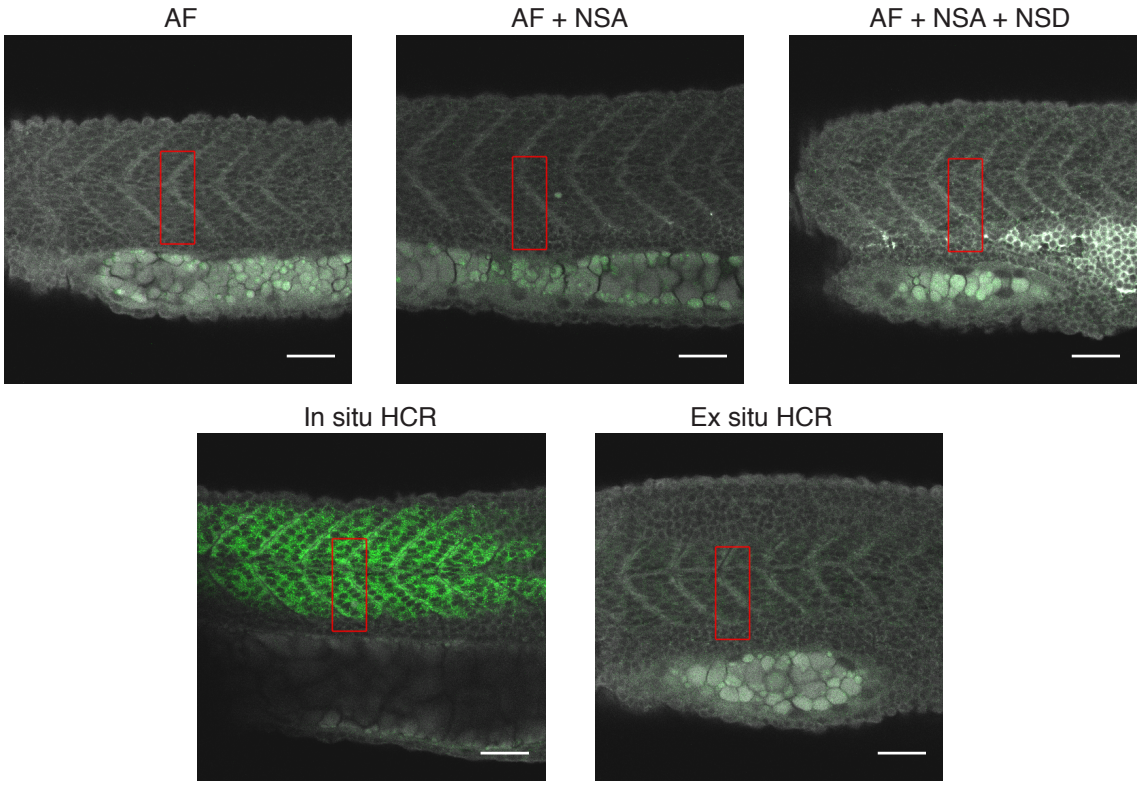

Figure B.3: Images and rectangle placements for the pixel intensity histograms of Figure 3.4b. Scale bar: 50 μm.

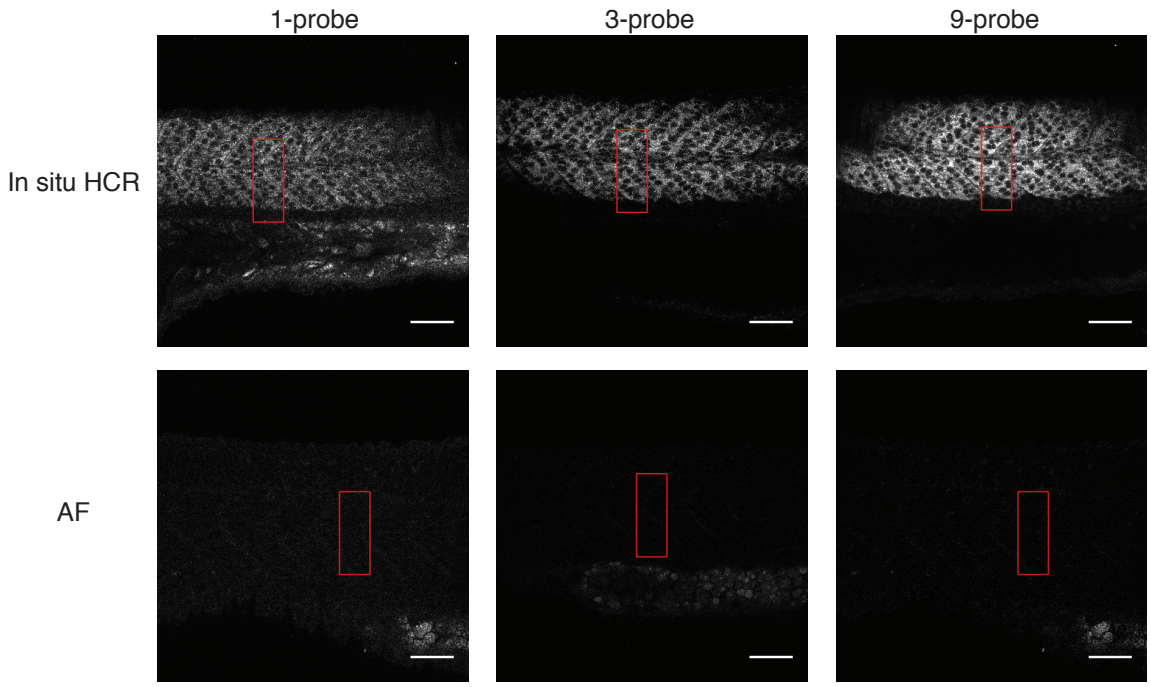

Figure B.4: Images and rectangle placements for the pixel intensity histograms of Figure 3.4c. The microscope PMT gain was optimized for each probe set (1, 3, or 9 probes) to avoid saturating pixels using HCR amplification. The two images in each column were obtained using the same microscope settings. Scale bar: 50 μm.

B.6 Expression Patterns for Target mRNAs

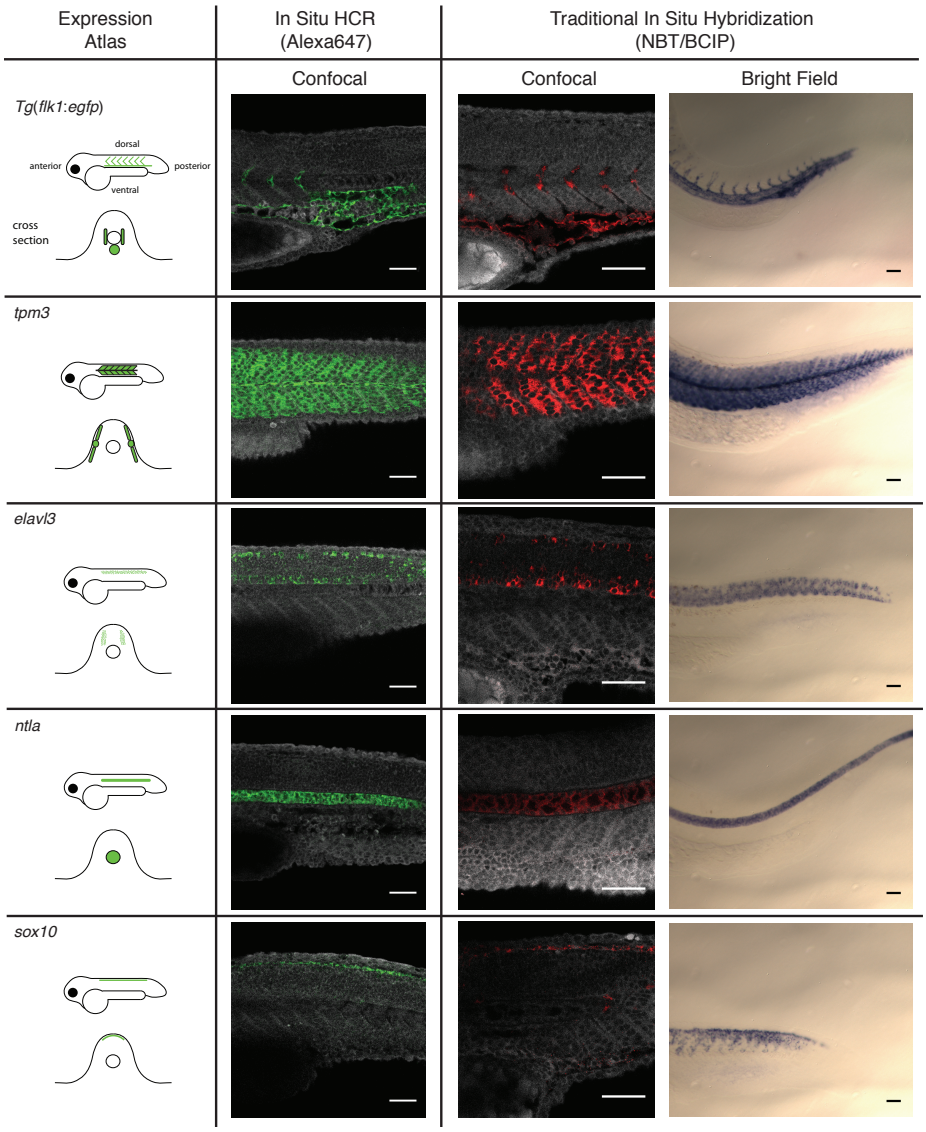

Figure B.5: Comparison of mRNA expression patterns observed using fluorescent in situ HCR and traditional in situ hybridization for the five targets of Figure 3.5. Traditional in situ hybridization experiments were performed using digoxigenin (DIG) labeled probes as described by Alexander and co-workers [4]. Embryo fixed 25 hpf. Scale bars: 50 μm.

B.7 Image Stack for Five-Color Fixed Whole-Mount Zebrafish Embryo

The full image stack for the embryo depicted in Figure 3.5b is available as a Supplementary Movie. For each frame in the movie, a 3×3 median filter was applied to each channel and the dimensions were reduced by a factor of two. Each plane in the stack is separated by 4 μm.

B.8 Sequences

B.8.1 Probe Sets

Sequences for the six target mRNAs used in this paper were obtained from the Zebrafish Information Network (ZFIN) [5].

B.8.2 SP6 Transcription Construct

To enable in vitro transcription, a 19-nt SP6 promoter sequence was placed in front of the initiator sequence of the probe. Three additional random nucleotides were added before the promoter to increase the yield for these short probe syntheses. Depending on the initiator sequence, the transcribed probes vary in length from 81-83 nt based on the properties of SP6 (Epicentre Biotechnologies). The construct is:

5′-Three Random Nucleotides - SP6 Promoter - HCR Initiator - Spacer - Probe Sequence-3′

Three Random Nucleotides: `CAg`
SP6 Promoter: `ATTTAggTgACACTATAgA`

B.8.3 RNA Probe Sequences for Figure 3.3

A single probe was used to detect the *egfp* target mRNA and trigger polymerization of HCR1 (Figures 3.3a-f). Figures 3.3g-i also employ a probe with a modified initiator (Probe′) and amplification hairpins with modified stem sequences (HCR1′). The 26-nt initiator and 5-nt spacer sequences prepended to the 5′-end of the probes are specified for each HCR amplifer below.

Target mRNA: **enhanced green fluorescent protein (*egfp*)**
Amplifier: **HCR1**
Fluorophore: **Alexa Fluor 647**
Initiator – Spacer: `gACCCUAAgCAUACAUCgUCCUUCAU - UUUUU`

Probe #	Probe Sequence
1	`gUUCUUCUgCUUgUCggCCAUgAUAUAgACgUUgUggCUgUUgUAgUUgU`

Target mRNA: **enhanced green fluorescent protein (*egfp*)**
Amplifier: **HCR1′**
Fluorophore: **Alexa Fluor 647**
Initiator – Spacer: `CCAgUUAUCAgUAgUCCgUCCUUCAU - UUUUU`

Probe #	Probe Sequence
1	`gUUCUUCUgCUUgUCggCCAUgAU-AUAgACgUUgUggCUgUUgUAgUUgU`

B.8.4 RNA Probe Sequences for Figure 3.4a and 3.4b

Three adjacent *desm* probes, three adjacent *egfp* probes, and amplifier HCR3 were used for the penetration study. All probes have identical initiator and spacer sequences.

Target mRNA: **desmin (*desm*)**
Amplifier: **HCR3**
Fluorophore: **Alexa Fluor 647**
Initiator – Spacer: `UACgCCCUAAgAAUCCgAACCCUAUg - AAAUA`

Probe #	Probe Sequence
1	CUUCgUgAAgACCCUCgAUACgUCUUUCCAggUCCAgCCUggCCAgAgUg
2	gCAgCAUCgACAUCAgCUCUgAAAgCAgAAAggUUgUUUUCAgCUUCCUC
3	CUCACUCAUUUgCCUCCUCAgAgACUCAUUggUgCCCUUgAgAgAgUCAA

Target mRNA: **enhanced green fluorescent protein (*egfp*)**
Amplifier: **HCR3**
Fluorophore: **Alexa Fluor 647**
Initiator – Spacer: `UACgCCCUAAgAAUCCgAACCCUAUg - AAAUA`

Probe #	Probe Sequence
1	gUUCUUCUgCUUgUCggCCAUgAUAUAgACgUUgUggCUgUUgUAgUUgU
2	ACUCCAgCUUgUgCCCCAggAUgUUgCCgUCCUCCUUgAAgUCgAUgCCC
3	UUCAgCUCgAUgCggUUCACCAgggUgUCgCCCUCgAACUUCACCUCggC

B.8.5 RNA Probe Sequences for Figure 3.4c

Probe sets with 1, 3, or 9 adjacent probes were used to address each mRNA target. HCR3 was used for all probe sets. Probe set 1: probe # 1. Probe set 3: probes # 1-3. Probe set 9: probes # 1-9.

Target mRNA: **desmin (*desm*)**
Amplifier: **HCR3**
Fluorophore: **Alexa Fluor 647**
Initiator – Spacer: `UACgCCCUAAgAAUCCgAACCCUAUg - AAAUA`

Probe #	Probe Sequence
1	CUCACUCAUUUgCCUCCUCAgAgACUCAUUggUgCCCUUgAgAgAgUCAA
2	gCAgCAUCgACAUCAgCUCUgAAAgCAgAAAggUUgUUUUCAgCUUCCUC
3	CUUCgUgAAgACCCUCgAUACgUCUUUCCAggUCCAgCCUggCCAgAgUg
4	CUgCAgCUCACggAUCUCCUCCUCAUgAAUCUUCCUgAggAAUgCAAUCU
5	ggUUUggACAUgUCCAUUUggAUCUgCACCUgACUCUCCUgCAUCUggUU
6	CgAUAgCCUCgUACUgCAggCgAAUgUCUCUgAgggCCgCAgUCAggUCU
7	UgAAACCUUAgACUUAUACCAgUCCUCggCCUCgCUgAUAUUCUUggCAg
8	UCUCgCAggUgUAggACUggAgCUggUgACggAACUgCAUggUCUCCUgC
9	UUggCUUCUCUgAgAgCCUCgUUAUUCUUgUUCACUgCCUggUUCAAAUC

B.8.6 RNA Probe Sequences for Figure 3.5

The probe sets for each target mRNA contain different numbers of probes as described below. All probes in a given probe set contain the same initiator and are amplified using the same HCR hairpins. The 26-nt initiator and 5-nt spacer sequences prepended to the 5′-end of the probes are also specified below.

Target mRNA: **enhanced green fluorescent protein (*egfp*)**
Amplifier: **HCR3**
Fluorophore: **Alexa Fluor 488**
Initiator and spacer: `UACgCCCUAAgAAUCCgAACCCUAUg - AAAUA`

Probe #	Probe Sequence
1	gUUCUUCUgCUUgUCggCCAUgAUAUAgACgUUgUggCUgUUgUAgUUgU
2	ACUCCAgCUUgUgCCCCAggAUgUUgCCgUCCUCCUUgAAgUCgAUgCCC
3	UUCAgCUCgAUgCggUUCACCAgggUgUCgCCCUCgAACUUCACCUCggC
4	ACgCUgCCgUCCUCgAUgUUgUggCggAUCUUgAAgUUCACCUUgAUgCC
5	CggggCCgUCgCCgAUgggggUgUUCUgCUggUAgUggUCggCgAgCUgC
6	UUUgCUCAgggCggACUgggUgCUCAggUAgUggUUgUCgggCAgCAgCA
7	gCgggUCUUgUAgUUgCCgUCgUCCUUgAAgAAgAUggUgCgCUCCUggA
8	CgUAgCCUUCgggCAUggCggACUUgAAgAAgUCgUgCUgCUUCAUgUgg
9	UCggggUAgCggCUgAAgCACUgCACgCCgUAggUCAgggUggUCACgAg
10	ggUgggCCAgggCACgggCAgCUUgCCggUggUgCAgAUgAACUUCAggg

Target mRNA: **tropomyosin 3 (*tpm3*)**
Amplifier: **HCR2**
Fluorophore: **Alexa Fluor 514**
Initiator and spacer: `CCgAAUACAAAgCAUCAACgACUAgA - AAAAA`

Probe #	Probe Sequence
1	UCCUCAACCAgCUggAUACgCCUgUUCAgAgAAgCCACCUCUgCCUCAgC
2	CCAgCUUUUgCAgggCUgUggCCAgUCUCUCCUgAgCACgAUCCAACUCC
3	AAUCACCUUCAUCCCUCUCUCgCUCUCAUCUgCggCCUUCUCggCUUCCU
4	UggAUCUCCUgCAgCUCCAUCUUCUCCUCAUCCUUCAgAgCCCUgUUCUC
5	CUUCAUAUUUgCggUCAgCCUCCUCAgCAAUgUgCUUggCCUCCUUAAgC
6	CUCUgUACgCUCCAACUCUCCCUCAACgAUCACCAgCUUACgAgCCACCU
7	UggUUUUCUCCAgUUUggCCACAgACCUCUCAgCAAACUCUgCACgggUC

Target mRNA: **ELAV (Embryonic Lethal, Abnormal Vision, Drosophila)-like 3 (Hu antigen C) (*elavl3*)**
Amplifier: **HCR4**
Fluorophore: **Alexa Fluor 546**
Initiator and spacer: gACUACUgAUAACUggAUUgCCUUAg - AAUUU

Probe #	Probe Sequence
1	CCUUgUCggCgUCgUUgggAUCCACAUAgUUUACAAAgCCAUAUCCCAAg
2	CACCUUgAUUgUUUUggUCUgCAgUUUgAgACCgUUgAgCgUgUUgAUAg
3	ACAUACAggUUggCAUCgCggAUggAAgCUgAgCUgggCCUggCgUAAgA
4	AAAACAACUgCUCCAUgUCUUUCUgACUCAUggUUUUgggCAggCCgCUC
5	UgUgACCUggUUUACCAggAUgCgUgAggUgAUgAUCCUUCCAUACUggg
6	gCUUCgUUCCgUUUgUCgAACCgAAUgAAACCUACCCCgCgCgAUAUACC
7	CAgCUgCUCCUAgUggCUUCUgACCgUUCAggCCCUUgAUggCCUCCUCU
8	CUgUCCUgUCUUCUgACUggggUUgUUggCgAACUUUACggUgAUgggCU
9	gggCCAgUgUAgCggCgAgCggCUgUCUggUAgAgCUgggUCAgCAgAgC
10	UgUCAAUggUUAUgggggAgAAUCUgAAgCgCUgggUCUggUggUgCAgA
11	gCCggCUCCAgUgggCCCggUCAggUUgACCCCggCAAgACUAgUCAUgC
12	AggACACUUUCgUCAgCUUCCggggACAggUUgUAgACgAAgAUgCACCA
13	ggAUgACCUUgACgUUUgUgACggCgCCAAAAggCCCgAAgAgCUgCCAC
14	ggUCAUggUgACgAAgCCAAAgCCCUUACAUUUgUUggUggUgAAgUCAC
15	AggCggUAgCCAUUCAgACUggCgAUAgCCAUggCUgCCUCgUCgUAgUU
16	CUCUggCCUgUgAUCUUgUCUCUgACCAAUUUgCAggACUCgAUUUCCCC
17	gAUgCUgCCAAAgAggCUCUUgAACUCUUCCUgggUCAUgUUCUgAggCA
18	ggUAgUUgACgAUCAggUUAgUUUUgCUgUCAUCUgUggCgCCgUUAgUg

Target mRNA: **no tail a (*ntla*)**
Amplifier: **HCR1**
Fluorophore: **Alexa Fluor 594**
Initiator and spacer: `gACCCUAAgCAUACAUCgUCCUUCAU - UUUUU`

Probe #	**Probe Sequence**
1	gCAgCUCUgUggUUCCUCAAgCUggAgUAUCUCUCACAgUACgAACCCgA
2	UgUAgUUAUUggUggUAgUgCUgCggUgggAgUAAUggCUgggAUAUggA
3	CAgggCUgACCAgCUgUCAUgAgACgCAAgACUUCCggAAgAgUUgUCCA
4	gUgUUUgUggUgUgggCCAgggUUCCCAUCCCgCUggAgUUggggAUCUg
5	UCgUCCCUgCAACUgACCACAgACUUgggUACUgACUggUgUUggAggUA
6	UgUCAggCCACCUgUAAUggAgCCCgAUgCUgAgCCUgAUggggUgAgAg
7	gAggAggUCAgACCCgAgUAggACAUCgAAgAACCgCgUAggAACUgAgA
8	CCUCgCUUAggCCUggAUCgUACAUUgAggAgggAgAggACACAggCAgC
9	UgCUgUgAgCCgggCgAUggAgCUCUCgAACUgggCAUCUCCAACgCCAA
10	UCCUUAAAUgUgAAgCgAUCUCAgUAgCUCUgAgCCACAggCgCCCAUgA
11	UUCUAgAUUUCCUCCUgAAgCCAAgAUCAAgUCCAUAACUgCAgCAUCAg
12	gACUUUUAUAgUAAAUCAACCCgUUUUCUgAUUgUCAAAUCAAgAAgCUC
13	ggAgUgAACAggggCCCCAUUgAACUgAggAgggCUgCUgCUggggCCCA
14	UggggCCgUUACUgggCAggAACCAgCCACCgAgUUgUgAAUAUCCAgAU
15	UgCUggUUgUCAgUgCUgUggUCUgggACUUCCUUgUggUCACUUCUCUC
16	UUUggCAUCgAggAAAgCUUUggCAAAAggAUUgUgUUUgAUUUUCAgAg
17	CggUAAUCUCUUCAUUCUgAUAUgCUgUgACUgCAAUAAACUgUgUCUCA
18	ggAAAAgACUgACUgCUgAUCAUUUUCUgAAUCCCACCgACUUUCACgAU
19	gUgUAUCCUgggUUCgUAUUUgUgCAAUgAgUUUAACAUAAUCUgUCCUC
20	CUCCgUUgAgUUUAUUggAgAgUUUgACUUUgCUgAAAgAUACgggUgCU
21	UUCAUCCAgUgCgCgCCgAAgUUgggUgAgUCCgggUggAUgUAgACgCA
22	gCUCgggCUUUggggUUCgggUUUCCCACCgggCACCCAUUCACCgUUCA
23	CgUAUUUCCACCgAUUAUUAUCggCCgCCACAAAAUCCAgCAggACCgAg
24	UACAUUgCAUUAgggUCgAgACCggUgACACUggCUCUgAgCACgggAAA
25	CAUUCgUCUCCCAgUCUUggUgACAAUCAUUUCAUUggUgAgCUCUUUAA
26	AUUUggUCCACAACUCCgCgUCUUCAAgCgAAAgUUUAAUAUCCCgCUCg
27	gACgCgUCCCCUUUCUCgCUgCCCUUCUgAAAUUCgCUCUCCACggCgCU
28	AAggAgAUgAUCCAggCgCUggUCgggACUUgAggCAgACAUAUUUCCgA
29	UCAAAUAAAgCUUgAgAUAAgUCCgACgAUCCUACUAAAUCCCgUUggAU
30	UAAAUgAUgUCAAAAUUUUCUUUUUUgCAAgAACUAACCCUUUAAUUgAU

Target mRNA: **SRY-box containing gene 10 (*sox10*)**
Amplifier: **HCR5**
Fluorophore: **Alexa Fluor 647**
Initiator and spacer: gCAUUACAgUCCUCAUAAgUAUCUCg - UUUUU

Probe #	**Probe Sequence**
1	AUAAACggCCgCUUAUCCgUCUCgUUCAgCAgUCUCCACAgCUUCCCCAg
2	ACUCgggAUAAUCUUUCUUAUgCUgCUUCCUCAAgCgCUCggCCUCCUCg
3	UCUgAgCUggAACCCggUUUgCCgUUCUUgCgUCgACgUggCUggUACUU
4	gUgCgCCACCUCCAggUgCAggCUCUUgUAAUgCgAUUggCUgUggCUgA
5	UgUgACUCUgACCUgUAgCgUgAgggUggUgUCCAUCACCCAAUggUgAC
6	CCAgUCCACUCCgAgAggCUCCgCCCUCACgCUUgCCCUCgCCUgAUUUU
7	UCCACgUUACCgAAgUCgAUgUgCggUUUCCCgCUggCAgACgAUgAggC
8	CgUCgAACggCUCCAUgUUggCCAUCACgUCAUggCUgAUUUCgCCAAUg
9	ggACgCCUgCgggUggCCAUUgggUgggAgAUACUggUCgAACUCgUUCA
10	AgUggCCACUAgCggCCgCUAgCgCgCUggAgAUgCCgUAUgUAUACgAU
11	UCUgCgUUUUCCCgCCAUCUgCgCCCAAAUgCUgCUgggACggCAgUUgC
12	gUgUgAACCgCUCgCCgCUgUAUCCCCAgggAAgUgUgUUUCACUCUUUA
13	gAggggAAggCggAgCUgUAgUgCggCAgUgUUAgCggCgUgUAUgUgAC
14	UAgUAggAUCCCgAggCCUggUgCUCggCgUAUUCggCgAAUUgUgCgCg
15	AgUgUggUgUAUACgggCUgCUCCCAAUgCgUAgggCUgUgUgACUgCgg
16	UUggACCUUUAgUgACUggUCAUCUUggUAgAgUgUgUCACggUCgAgAC
17	UgCAggCgAgUgUUUCgAUgAUUUUUAgCACACACACACACACCUUACgg
18	ACACACACACACACACUCgUUUCUCAgAUCUCAgUUUgUgUCgAUUgUgg
19	UCUggACggUggUCgUCUgAggCACgUgAgAAUAUUUCCCUgCAgAUCUC
20	CgUCUUUUUCgAAAAUACUACUggUgUCAAAUUggCgUUgAgggAgCAgg

B.8.6.1 RNA Probe Sequences for Figure B.5

The following probes were used to perform the traditional in situs of Figure B.5.

Target mRNA: ***egfp***
Probe Sequence: gACgUAAACggCCACAAgUUCAgCgUgUCCggCgAgggCgAgggCgAUgCCACCUACggCAAgCUgACCCUgAA
gUUCAUCUgCACCACCggCAAgCUgCCCgUgCCCUggCCCACCCUCgUgACCACCUUCggCUACggCCUgAUgUgCUUCgCCCgCUACCCCg
ACCACAUgAAgCAgCACgACUUCUUCAAgUCCgCCAUgCCCgAAggCUACgUCCAggAgCgCACCAUCUUCUUCAAggACgACggCAACUAC
AAgACCCgCgCCgAggUgAAgUUCgAgggCgACACCCUggUgAACCgCAUCgAgCUgAAgggCAUCgACUUCAAggAggACggCAACAUCCU
ggggCACAAgCUggAgUACAACUACAACAgCCACAACgUCUAUAUCAUggCCgACAAgCAgAAgAACggCAUCAAggUgAACUUCAAgAUCC
gCCACAACAUCgAggACggCAgCgUgCAgCUCgCCgACCACUACCAgCAgAACACCCCCAUCggCgACggCCCCgUgCUgCUgCCCgACAAC
CACUACCUgAgCUACCAgUCCgCCCUgAgCAAAgACCCCAACgAgAAgCgCgAUCACAUggUCCUgCUggAgUUC

Target mRNA: ***tpm3***
Probe sequence: UgUACAAgACCggUCCUUCAAACAUUgggCUACAgUAUUCCCAgAAggAggACAAgUAUgAggAAgAAAUCAAg
AUCCUCACUgAUAAgCUgAAggAggCUgAgACCCgUgCAgAgUUUgCUgAgAggUCUgUggCCAAACUggAgAAAACCAUUgAUgAUUUggA
AgAUgAgCUUUAUgCUCAgAAACUCAAgUAUAAggCCAUUAgUgAggAgUUggAUCAUgCUCUCAACgACAUgACCUCUAUAUAAAgAgUUU
CUggACUgUUCUgUggCUgACUgUgACUUCAAgAAAUgCUUCCUCgUCUUCUCUgACUgUCCAUAUUUgUUgCUUUUUUUCUUCUUUgUACA
CUUCCUgUUUUgUgUgUUUUUCCgUgUACUCAUgUCUgUAgUgCCAgUUUCUUUAUUCUgUUUCUgCUUCUgUUUUUUAgAUAUUCAUUAUC
UgCCCCAACAUCUUCCUCUUAUCAggAUCUgUUgUUCUUAUgUCCCUgCUCUUgCUCUUCUgUgACCUUUUgCUgUAUUUUUCAUgCCUUgC
gUCCAUgUUUAUUgAAgggAggAgAAAAAACggCUCUgCUCUCUUUUgAAUgUCUgCUUgUCUCUCUUUAUUgCAAUggACUggUgUUgggC
AACCAAgCAUUUACCCAUCUUCAAUUgCACAUgUAUUAUAUCUCAUggUUgAAAgAUAAAAggCUUgAUUAAAUUCUCCgUCACUAAUUgUg
AUUAAAAUCgAAUUCCCgCggCCgCCAUggCggCCggAg

Target mRNA: ***elavl3***
Probe sequence: ggAUAUggCUUUgUAAACUAUgUggAUCCCAACgACgCCgACAAggCUAUCAACACgCUCAACggUCUCAAACU
gCAgACCAAAACAAUCAAggUgUCUUACgCCAggCCCAgCUCAgCUUCCAUCCgCgAUgCCAACCUgUAUgUgAgCggCCUgCCCAAAACCA
UgAgUCAgAAAgACAUggAgCAgUUgUUUUCCCAgUAUggAAggAUCAUCACCUCACgCAUCCUggUAgACCAggUCACAgCAggUAUAUCg
CgCggggUAggUUUCAUUCggUUCgACAAACggAACgAAgCAgAggAggCCAUCAAgggCCUgAACggUCAgAAgCCACUAggAgCAgCUgA
gCCCAUCACCgUAAAgUUCgCCAACAACCCCAgUCAgAAgACAggACAggCUCUgCUgACCCAgCUCUACCAgACAgCCgCUCgCCgCUACA
CUggCCCUCUgCACCACCAgACCCAgCgCUUCAgACUCgACAAUUUACUAAACgCCAgCUACggAgUCAAgAgAUUCUCCCCCAUAACCAUU
gACAgCAUgACUAgUCUUgCCggggUCAACCUgACCgggCCCACUggAgCCggCUggUgCAUCUUCgUCUACAACCUgUCCCCggAAgCUgA
CgAAAgUgUCCUgUggCAgCUCUUCgggCCUUUUggCgCCgUCACAAACgUCAAggUCAUCCgUgACUUCACCACCAACAAAUgUAAgggCU
UUggCUUCgUCACCAUgACCAACUACgACgAggCAgCCAUggCUAUCgCCAgUCUgAAUggCUACCgCCUgggCgACCgCgUgCUgCAggUC
UCgUUCAAgACCAgCAAgCAgCACAAggCUUgAAggAAggCCUAgUCACUAUUgCUCUUUAACAUgCAgggggAgCUACUgAgCUCCCUgUA
CAUUCACUCUACAUgggCCUggACUgAgUCUCUCUCUAACAUACAUUCgACACACACACA

Target mRNA: ***ntla***
Probe sequence: gAAUUCCCgCUgUCAAAgCAACAgUAUCCAACgggAUUUAgUAggAUCgUCggACUUAUCUCAAgCUUUAUUUg
AUCggAAAUAUgUCUgCCUCAAgUCCCgACCAgCgCCUggAUCAUCUCCUUAgCgCCgUggAgAgCgAAUUUCAgAAgggCAgCgAgAAAgg
ggACgCgUCCgAgCgggAUAUUAAACUUUCgCUUgAAgACgCggAgUUgUggACCAAAUUUAAAgAgCUCACCAAUgAAAUgAUUgUCACCA
AgACUgggAgACgAAUgUUUCCCgUgCUCAgAgCCAgUgUCACCggUCUCgACCCUAAUgCAAUgUACUCggUCCUgCUggAUUUUgUggCg
gCCgAUAAUAAUCggUggAAAUACgUgAACggUgAAUgggUgCCCggUgggAAACCCgAACCCCAAAgCCCgAgCUgCgUCUACAUCCACCC
ggACUCACCCAACUUCggCgCgCACUggAUgAAAgCACCCgUAUCUUUCAgCAAAgUCAAACUCUCCAAUAAACUCAACggAggAggACAgA
UUAUgUUAAACUCAUUgCACAAAUACgAACCCAggAUACACAUCgUgAAAgUCggUgggAUUCAgAAAAUgAUCAgCAgUCAgUCUUUUCCU

gAgACACAgUUUAUUgCAgUCACAgCAUAUCAgAAUgAAgAgAUUACCgCUCUgAAAAUCAAACACAAUCCUUUUgCCAAAgCUUUCCUCgA
UgCCAAAgAgAgAAgUgACCACAAggAAgUCCCAgACCACAgCACUgACAACCAgCAAUCUggAUAUUCACAACUCggUggCUggUUCCUgC
CCAgUAACggCCCCAUgggCCCCAgCAgCAgCCCUCCUCAgUUCAAUggggCCCCUgUUCACUCCUCgggUUCgUACUgUgAgAgAUACUCC
AgCUUgAggAACCACAgAgCUgCUCCAUAUCCCAgCCAUUACUCCCACCgCAgCACUACCACCAAUAACUACAUggACAACUCUUCCggAAg
UCUUgCgUCUCAUgACAgCUggUCAgCCCUgCAgAUCCCCAACUCCAgCgggAUgggAACCCUggCCCACACCACAAACACUACCUCCAACA
CCAgUCAgUACCCAAgUCUgUggUCAgUUgCAgggACgACUCUCACCCCAUCAggCUCAgCAUCgggCUCCAUUACAggUggCCUgACAUCU
CAgUUCCUACgCggUUCUUCgAUgUCCUACUCgggUCUgACCUCCUCgCUgCCUgUgUCCUCUCCCUCCUCAAUgUACgAUCCAggCCUAAg
CgAggUUggCgUUggAgAUgCCCAgUUCgAgAgCUCCAUCgCCCggCUCACAgCAUCAUgggCgCCUgUggCUCAgAgCUACUgAgAUCgCU
UCACAUUUAAggACUgAUgCUgCAgUUAUggACUUgAUCUUggCUUCAggAggAAAUCUAgAAgAgCUUCUUgAUUUgACAAUCAgAAAACg
ggUUgAUUUACUAUAAAAgUCACAUCUgUAUCAUACCgAggCAUACgUAUUUACAAUCAAgAUgAgAgACAAUCAAUUAAAgggUUAgUUCU
UgCAAAAAAgAAAAUUUUgACAUCAUUUACUCACCUUUgUUUUAAACAUUgUUAAgUUUUUAUUCUgUUAAACACAAAAgAAgAUAUUUUgA
AgAAUgUUCAAAACUggUAACCAUUgCAUAgAAgCUgUUUUACUUAUggAAgUAAAUggUUACAggUUAUCAgCAUUUUUUUAAAUAUAUUU
UUUAgUUCAACAgAAgAAAgAAACUCUUUAAAgUUUggAACAACUUgAgggUgAgUAAAUUgAgUAAAAgUACgUUUUUgggUUAACUAUCC
CUUUAACUAUCAgAUUUUAgCCAUACAUUUUggggCAAUUAUAgUgUUUAUUCUUgAUAAUAUUAUCUAAAAgAUUAAUAAAAAUCAAAAUUg
UgCUgUUgACUCACUAAAAgUgUAUAUgUgUgUAAAUAAAUAgAAAUUAACgUCCggUUUCAUUgUAUCACAgAAgAAUgUAACAgUCUUAC
AUgUgCUUUCUgUAgAACgAgAgAAAgACAgACUUUgCUgUUUCgUUUgAgAAAgUgAAUACgCUUUgAAAAgUgACCgUAUAgUUUUgUCU
gCUAUUCgUCCUAUAgAgAAACCAUUUgUACAUAUCUAUCUAUUUgUAUUUgUUgggCUCUUUgAgUUUUAUUUAUgUCAUUUUAAUAAUAA
AUUAAAUUUCUUUUUUUUUUCUgUCAAAAAAAAggAgUUCCggAAUUC

Target mRNA: ***sox10***

Probe sequence: gUCgACgCAAgAACggCAAACCgggUUCCAgCUCAgAggCCgACgCCCACUCUgAgggCgAggUCAgCCACAgC
CAAUCgCAUUACAAgAgCCUgCACCUggAggUggCgCACggCggggCUgCAgggUCACCAUUgggUgAUggACACCACCCUCACgCUACAgg
UCAgAgUCACAgCCCUCCAACgCCCCCUACCACCCCCAAgACggAACUgCAgggAggAAAAUCAggCgAgggCAAgCgUgAgggCggAgCCU
CUCggAgUggACUgggggUgggAgCAgAUggAAgCUCCgCCUCAUCgUCUgCCAgCgggAAACCgCACAUCgACUUCggUAACgUggACAUU
ggCgAAAUCAgCCAUgACgUgAUggCCAACAUggAgCCgUUCgACgUgAACgAgUUCgACCAgUAUCUCCCACCCAAUggCCACCCgCAggC
gUCCgCCACUgCCAgCgCAggAUCUgCAgCgCCAUCgUAUACAUACggCAUCUCCAgCgCgCUAgCggCCgCUAgUggCCACUCCACCgCAU
ggCUgUCCAAgCAgCAACUgCCgUCCCAgCAgCAUUUgggCgCAgAUggCggAAAAACgCAgAUAAAgAgUgAAACACACUUCCCCggggAU
ACAgCggCgAgCggUUCACACgUCACAUACACgCCgCUAACACUgCCgCACUACAgCUCCgCCUUCCCCUCgCUggCgUCCCgCgCACAgUU
CgCCgAAUACgCCgAgCACCAggCCUCgggAUCCUACUACgCCCACUCCAgCCAgACCUCAggCCUCUACUCCgCCUUCUCCUACAUgggCC
CCUCACAgCggCCCCUgUACACCgCCAUUCCggAUCCgggAUCCgUgCCgCAgUCgCACAgCCCCACgCACUgggAgCAgCCCgUAUACACC
ACACUgUCUCgACCgUgACACACUCUACCAAgAUgACCAgUCACggAAggUCCAACCgUAAAgUgUgUgUgUgUgUgUgUgCUAAAAAUC
AUCgAAACACUCgCCUgCACCACAAUCgA

B.8.7 HCR Hairpins

RNA initiator and hairpin sequences for the six HCR amplifiers used in this paper. Each amplifier has an initiator (I) and two hairpins (H1 and H2).

– :	Hairpin ligation site
/5′-dye-C12/:	5′ Alexa Fluor modification with a C12 spacer
/C9-dye-3′/:	3′ Alexa Fluor modification with a C9 spacer

HCR1

I	gACCCUAAgCAUACAUCgUCCUUCAU
H1	AUgAAggACgAUgUAUgCUUAgggUCgACUUCCAUAgACCCU-AAgCAUACAU /C9-dye-3'/
H2	/5'-dye-C12/ gACCCUAAgC-AUACAUCgUCCUUCAUAUgUAUgCUUAgggUCUAUggAAgUC

HCR1′

I′	CCAgUUAUCAgUAgUCCgUCCUUCAU
H1′	AUgAAggACggACUACUgAUAACUgggACUUCCAUACCAgU-UAUCAgUAgUC /C9-dye-3'/
H2′	/5'-dye-C12/ CCAgUUAUCAgUAgUCCgUCCUUCAUgACUAC-UgAUAACUggUAUggAAgUC

HCR2

I	CCgAAUACAAAgCAUCAACgACUAgA
H1	UCUAgUCgUUgAUgCUUUgU-AUUCggCgACAgAUAACCgAAUACAAAgCAUC /C9-dye-3'/
H2	/5'-dye-C12/ CCgAAUACAAAg-CAUCAACgACUAgAgAUgCUUUgUAUUCggUUAUCUgUCg

HCR3

I	UACgCCCUAAgAAUCCgAACCCUAUg
H1	CAUAgggUUCggAUUCUUAgggCgUAgCAgCAUCAAUACgC-CCUAAgAAUCC /C9-dye-3'/
H2	/5'-dye-C12/ UACgCCCUAAgAAUCCgAACCCUAUgggAUUC-UUAgggCgUAUUgAUgCUgC

HCR4

I	gACUACUgAUAACUggAUUgCCUUAg
H1	CUAAggCAAUCCAgUUAUCAgUAgUCUgACACgACUgACUAC-UgAUAACUgg /C9-dye-3'/
H2	/5'-dye-C12/ gACUACUgAUA-ACUggAUUgCCUUAgCCAgUUAUCAgUAgUCAgUCgUgUCA

HCR5

I	gCAUUACAgUCCUCAUAAgUAUCUCg
H1	CgAgAUACUUAUgAggACUgUAAUgCAAgUCgUUCAgCAUU-ACAgUCCUCAU /C9-dye-3'/
H2	/5'-dye-C12/ gCAUUACAgUC-CUCAUAAgUAUCUCgAUgAggACUgUAAUgCUgAACgACUU

References

[1] R. M. Dirks, M. Lin, E. Winfree and N. A. Pierce. Paradigms for computational nucleic acid design. *Nucleic Acids Research* **32**, 1392–1403 (2004).

[2] J. N. Zadeh, R. M. Dirks and N. A. Pierce. Sequence design for nucleic acid structural engineering (*in preparation*).

[3] R. M. Dirks, J. S. Bois, J. M. Schaeffer, E. Winfree and N. A. Pierce. Thermodynamic analysis of interacting nucleic acid strands. *SIAM Review* **49**, 65–88 (2007).

[4] J. Alexander, D. Y. R. Stainier and D. Yelon. Screening mosaic F1 females for mutations affecting zebrafish heart induction and patterning. *Developmental Genetics* **22**, 288–299 (1998).

[5] J. Sprague *et al.* The zebrafish information network: The zebrafish model organism database. *Nucleic Acids Res* **34**, D581–D585 (2006).

Appendix C

An Autonomous Bipedal Walker Powered by DNA Hybridization

This work presented here is heavily based on the following paper:
P. Yin, H. M. T. Choi, C. R. Calvert, and N. A. Pierce. Programming biomolecular self-assembly pathways. *Nature* **451**(7176), pp. 318–322 (2008).

C.1 Introduction

The challenge of engineering molecular machines capable of autonomous locomotion has attracted significant interest in recent years [1–5]. Inspired by the bipedal motor protein, kinesin, which hauls intracellular cargo by striding along microtubules [6], we have developed an autonomous enzyme-free bipedal DNA walker capable of stochastic locomotion along a DNA track. In contrast to previous autonomous DNA-based systems, which have employed ribozymes, DNAzymes, [2, 4, 7] or protein enzymes, [1, 3] our enzyme-free walker is powered solely by the free energy of hybridization.

C.2 Fuel System

The bipedal walker is fueled by two DNA hairpins A and B, which are metastable in the absence of a catalyst I. When the catalyst is present, hairpins A and B can be catalyzed to form a duplex A·B. Figure C.1 depicts the mechanism and an agarose gel validating these properties. In the absence of an initiator (lane 7), minimal leakage (formation of A·B in the

absence of I) is observed. When the catalyst is present (lanes 3-6), the formation of duplex A·B is dramatically accelerated. The designed release of I from the waste product (A·B) enables catalytic turnover as indicated by the nearly complete consumption of hairpins at sub-stoichiometric catalyst concentrations (lanes 4-6).

Strand	**Sequence**
A	5′ AAGTAGTGATTGAGCGTGATGAATGTCACTACTTCAACTCGCATTCATCACGCTCAATC 3′
B	5′ TGATGAATGCGAGTTGAAGTAGTGACATTCATCACGCTCAATCACTACTTCAACTCGCA 3′
I	5′ GACATTCATCACGCTCAATCACTACTT 3′

Table C.1: DNA Sequences of the Fuel System.

In addition to the use of sub-stoichiometric catalyst concentrations in the gel, catalyst recovery is further investigated using a fluorescence quenching experiment (Figure C.2a). In this experiment, the catalyst is 3′-labeled with a fluorophore, FAM (6-carboxyfluorescein), and its fluorescence is observed with a spectrofluorometer. The fluorescence baseline of FAM is first recorded before the addition of hairpin A. Then, introduction of hairpin A allows I-FAM to hybridize with A and results in quenching of the FAM fluorescence signal. This quenching effect is due to hybridization-induced proximity of FAM to the guanine base near the 5′ end of hairpin A [8]. Addition of hairpin B releases I-FAM from A and the fluorescence signal recovers (Figure C.2b). The observed recovery of the fluorescence signal (after correcting for dilution effects) confirms that nearly all of the catalysts are released from the A·B duplexes. This catalytic fuel system is employed to power the locomotion of a bipedal DNA walker.

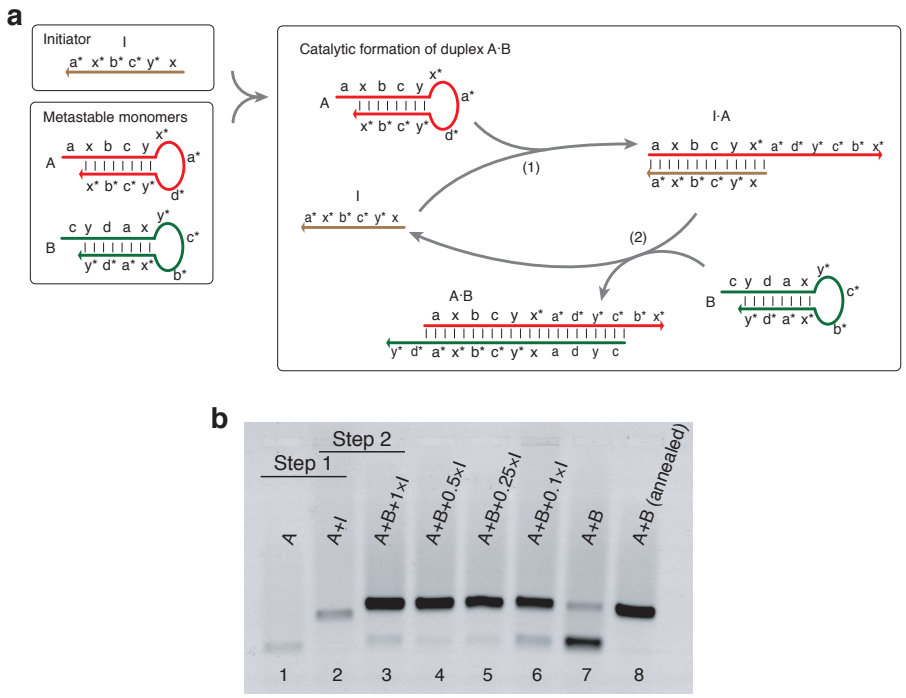

Figure C.1: Catalytic Fuel System. (a) Reaction schematic. Hairpins A and B coexist metastably in the absence of catalyst I. Catalyst I catalyzes the reaction of A and B to form duplex A·B. Step 1: Toehold a* of I nucleates at the toehold a of A, resulting in the opening of hairpin A and the formation of product I·A. Step 2: With newly exposed c*, I·A can now open hairpin B and B will subsequently displace I from A. This sequence of reactions produces the waste product A·B. (b) Native 2% agarose gel electrophoresis demonstrates the catalytic formation of the DNA duplex. The hairpins were snap cooled in reaction buffer before use. Lanes 1-3: A gel shifting assay validated each reaction step depicted in panel (a). Lanes 3-7: Effects of different concentrations of I (1×, 0.5×, 0.25×, 0.1×, and 0×) on the formation of A·B. Reactants were incubated at 1 μM at room temperature for 2 hours before loading on the gel. Lane 8: A·B duplexes were formed by annealing 1 μM of each hairpin over the course of 2.5 hours. A 2% agarose gel was used in this assay.

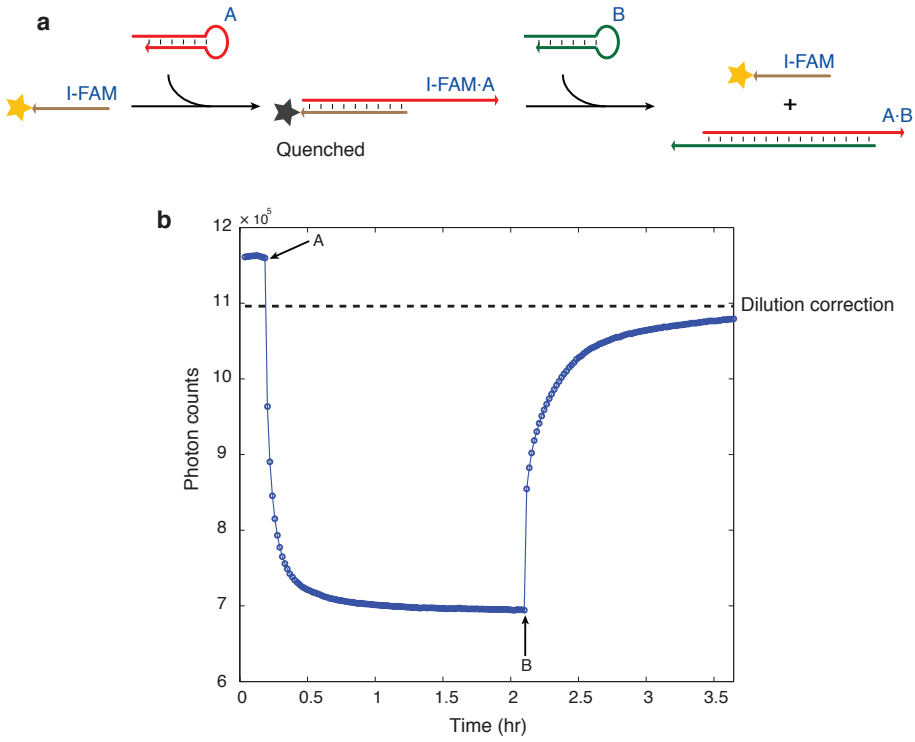

Figure C.2: Fluorescence quenching experiment demonstrating catalyst recovery. (a) Experimental design. (b) Fluorescence data. Hairpin species A and B were snap cooled separately in reaction buffer. The reaction concentrations of I-FAM (I labeled with a fluorophore FAM) and A were at 20 nM and that of B was at 40 nM. After recording the baseline signal produced by the catalyst, I-FAM, hairpin A was introduced and fluorescence signal quenching was observed. After the signal plateaued, hairpin B was introduced and the fluorescence signal recovered to its initial baseline level (after correcting for dilution).

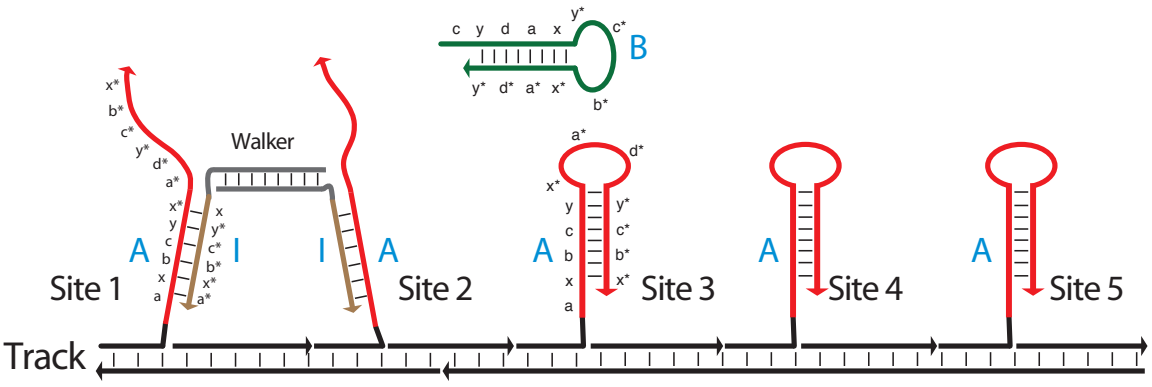

Figure C.3: Secondary structure of the autonomous walker

C.3 Walker Design and Mechanism

Figure C.3 depicts the designed secondary structures of the bipedal walker and the track it will stride on. Joined by a duplex torso, each of the two identical walker legs, I, is capable of catalyzing the formation of waste duplex A·B from metastable fuel hairpins A and B via the reaction pathway described above. The track consists of five A hairpins arranged linearly at regular intervals along a nicked DNA duplex and the walker is initialized with its two legs hybridized to sites 1 and 2. In the absence of hairpin B, the walker will stay bound to the first two anchorages on the track. When hairpin B is introduced to the system, locomotion begins and a subpopulation of walkers is expected to move unidirectionally along the track by sequentially catalyzing the formation of A·B. Due to the one-dimensional arrangement of anchor sites, this processive motion occurs only for those walkers that exhibit a foot-over-foot gait by stochastically lifting the back foot at each step. Figures C.4 and C.5 show all possible processive and non-processive movements of the walker when hairpin B is added to initiate the walker's locomotion.

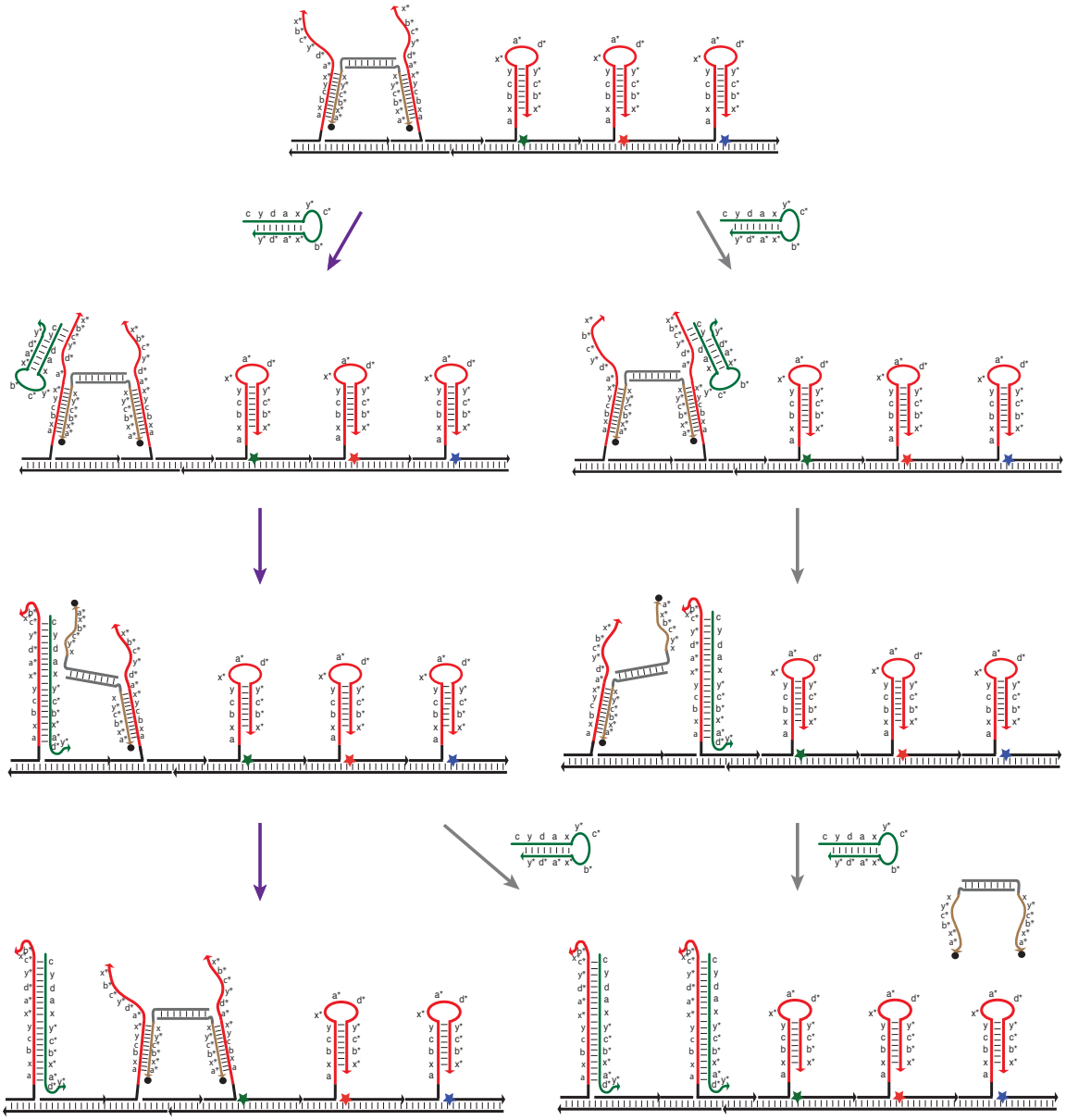

Figure C.4: Detailed secondary structure schematic for the first walker step. Reaction arrows corresponding to the processive subpopulation of walkers are shown in purple. Gray arrows represent the non-processive subpopulation of walkers.

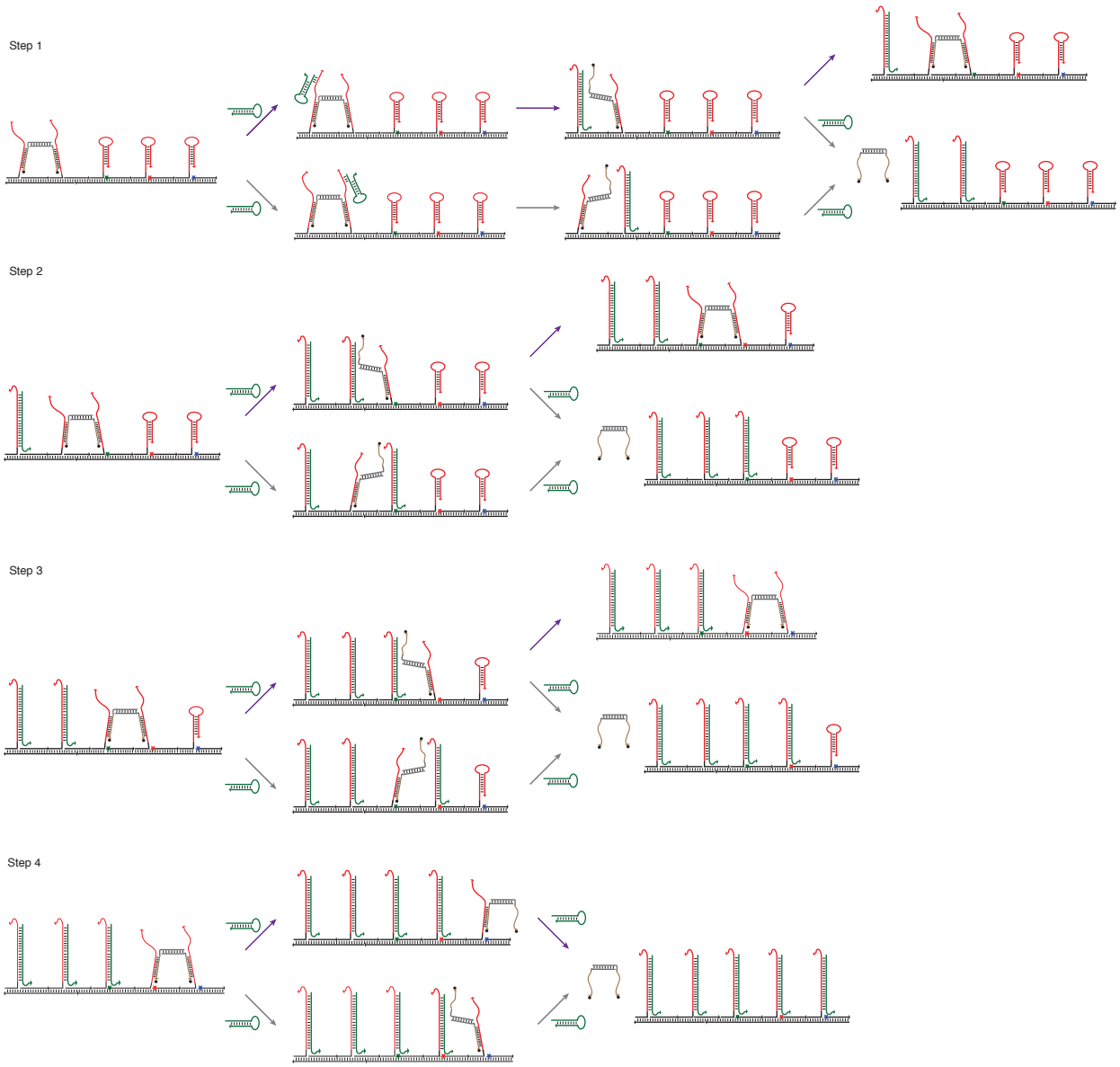

Figure C.5: Step-by-step secondary structure schematic for the autonomous walker. Reaction arrows corresponding to the processive subpopulation of walkers are shown in purple. Gray arrows represent the non-processive population of walkers. A walker will visit positions 3, 4, and 5 in that order if it starts at positions 1 and 2 and follows the purple arrows from step 1 to step 3.

C.4 Results and Discussion

Walker locomotion is investigated using a bulk fluorescence assay that tests whether there is a subpopulation of walkers that locomotes processively through positions 3, 4, and 5, starting from an initial condition with legs anchored at positions 1 and 2 (Figure C.6a). Quenchers are attached to the walker's legs and spectrally distinct fluorophores are positioned proximally to anchorages 3, 4, and 5. The fluorescence signals of the three fluorophores are monitored with a spectrofluorometer.

Consistent with processivity, the anticipated sequential transient quenching of the fluorophores at positions 3, 4, and 5 is observed (Figure C.6b). To rule out the possibility that this signal arises from non-processive walker diffusion through the bulk solution from one position to the next, the experiments were repeated using monopedal walkers (two separate legs) that lack a mechanism for achieving processivity. In this case, the sequential transient quenching no longer matches the ordering of the fluorophores along the track (Figure C.6c). Six independent experiments were performed for both the bipedal and monopedal walkers (Figure C.8) and a statistical analysis of the experiments (Section C.5.4) supports the interpretation that the observed minima are sampled from a distribution in which the ordering of the minima matches the physical ordering of the fluorophores along the track.

Overlaying all 36 traces (18 traces per walker type: three fluorophores, six experiments), it is apparent that the time scale for visiting any one of the three anchorages with the monopedal walker is longer than the time scale to visit all three anchorages for the bipedal system (Figure C.6d). Additional control experiments (Figures C.12 and C.13) show that this difference in time scales cannot be explained by the relative rates with which freely diffusing bipedal and monopedal walkers land on the track. As a further test of processivity for the bipedal walker, reordering the fluorophores along the track leads to the expected change in the ordering of the transient quenching (Figures C.6e and C.9). These experiments confirm the presence of a subpopulation of processive bipedal walkers.

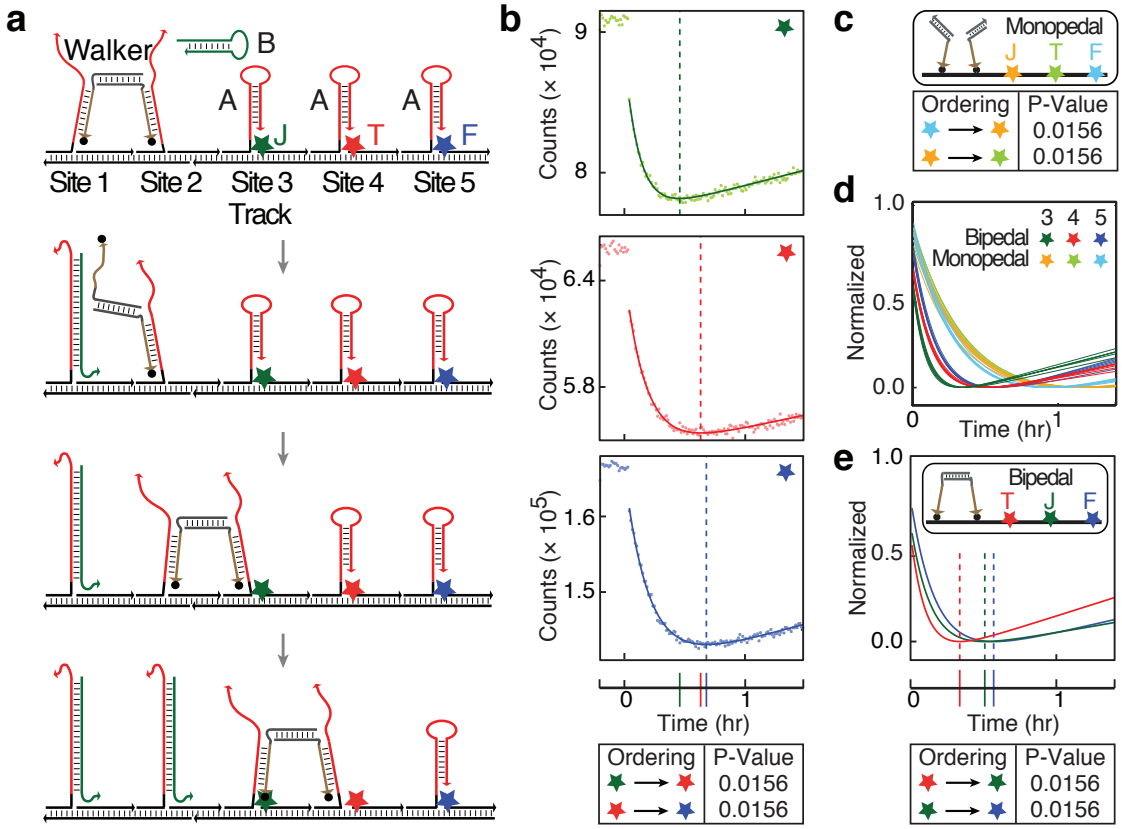

Figure C.6: Summarized results for autonomous locomotion: stochastic movement of a bipedal walker. (a) Secondary structure mechanism depicting processive locomotion. (b-e) Fluorescence quenching experiments measuring the proximity of the quenchers (black dots) on the walker feet to the fluorophores (colored stars) decorating the track. Fitted curves (solid) are used to determine the time at which the minimum fluorescence (maximum quenching) was observed (dashed vertical line) for each fluorophore. (b) Bipedal walker with track labeled JOE (green star) → TAMRA (red) → FAM (blue) as in panel (a). For each pair of consecutive minima (JOE → TAMRA and TAMRA → FAM), we test the null hypothesis that the median time difference between the minima is zero against the alternative hypothesis that the time difference is positive. Based on a statistical analysis of six independent experiments (Section C.5.4), the null hypothesis can be rejected for both time differences with the same P-value of 0.0156, supporting the interpretation that the observed minima are sampled from a distribution in which the ordering of the minima matches the physical ordering of the fluorophores along the track. Similar interpretations apply to the ordering of minima for panels (c) and (e). (c) Monopedal walkers on the same track (JOE (yellow star) → TAMRA (pale green) → FAM (pale blue)). (d) Comparison of time scales for bipedal and monopedal walkers (18 traces per walker type: three fluorophores, six experiments). (e) Bipedal walker with track labeled TAMRA (red star) → JOE (green) → FAM (blue).

C.5 Supplementary Information

C.5.1 Methods

C.5.1.1 DNA and Hairpin Synthesis

DNA was synthesized and purified by Integrated DNA Technologies (IDT). The purified DNA strands were reconstituted in ultrapure water. The concentrations of the DNA solutions were determined by the measurement of UV absorption at 260 nm. Each hairpin was synthesized as two pieces which were then ligated to produce the full hairpin (see C.5.7 for the ligation site). The ligation was performed using T4 DNA ligase (New England Biolabs) at 16 °C overnight. Ligated strands were then purified using a 15% denaturing PAGE gel. The bands corresponding to the DNA strands of expected sizes were visualized by UV shadowing and excised from the gel. The DNA strands were then eluted, and recovered by ethanol precipitation.

C.5.1.2 Reaction Buffer, Snap Cooling, and Annealing

The reaction buffer (4 mM $MgCl_2$, 15 mM KCl, and 10 mM Tris-HCl, pH = 8.0) was used in all the walker experiments described above. Hairpins were prepared as monomers in the reaction buffer using a snap cooling procedure: heating at 90 °C for 5 minutes and cooling on ice for 1 minute. The hairpins were then allowed to equilibrate at room temperature for 30 minutes before use. Annealing for the formation of the A·B duplex for the agarose gel and the walker track for the fluorescence experiments was done by heating the sample at 95 °C for 5 minutes and allowing it to cool at 1 °C per minute to room temperature.

C.5.1.3 Gel Electrophoresis

In the gel electrophoresis, agarose gel was prepared in 1× LB buffer (Faster Better Media, LLC). Samples were loaded with 2× SYBR Gold stain (Invitrogen) and 10% glycerol. The gel used to demonstrate the catalytic mechanism of the fuel system was run at 350 V for 10 minutes at room temperature and the gel used to validate the walker assembly was run at 200 V for 40 minutes at room temperature. Both gels were visualized using an FLA-5100

imaging system (Fuji Photo Film).

C.5.1.4 Fluorescence Experiments

In the catalyst recovery fluorescence experiment, data were acquired using a spectrofluorometer from Photon Technology International (PTI) equipped with a temperature controller set at 21 °C. A 1.7 mL QS quartz cuvette (Hellma GmbH & Co. KG) was used. Excitation and emission wavelengths were set at 492 and 517 nm, respectively. All bandwidths were set at 4 nm.

In the fluorescence quenching experiments used to validate walker locomotion, two 3.5 mL QS quartz cuvettes (Hellma) were used in each set of experiments. Excitation and emission wavelengths were set to 492 and 517 nm (for FAM), 527 and 551 nm (for JOE), and 558 and 578 nm (for TAMRA), respectively, with 4 nm bandwidths. The assembly of the walker system is described in Section C.5.2. Hairpin B was snap cooled in the reaction buffer before use. The system was assembled using 4 nM track and 3.5 nM bipedal walker. A sub-stoichiometric amount of walker was used to ensure that no free-floating walker would bind to hairpin A on the track. For the same reason, sub-stoichiometric monopedal walker (7 nM) was used in the diffusion experiments. The final concentration of hairpin B was 20 nM, which was equimolar with the five A hairpins on the track (5×4 nM = 20 nM). The assembled track was first introduced to record the fluorescence baselines for FAM, JOE, and TAMRA. Hairpin B was then introduced and mixed 100 times by rapid pipetting to start the walker locomotion.

C.5.2 Assembly of the Walker System

The walker system is assembled in four steps (Figure C.7a).

- Step 0. The walker (W) was assembled by annealing strands W1-BHQ1 and W2-BHQ1 as follows: heat the mixture at 95 °C for 5 minutes and slowly cool to room temperature at 1 °C/min.
- Step 1. Hairpins S1 and S4 were mixed with track strands S2, S3, and S5, then annealed to produce Track 1 (T1) as above.
- Step 2. T1 and the pre-assembled walker (W) were incubated at room temperature for 2 hours to produce T1+W.
- Step 3. Hairpins S6, S9, and S11 were mixed with track strands S7, S8, S10, and S12, then annealed to produce Track 2 (T2). For the bipedal and monopedal landing control experiments (Figure C.13), the S7 track strand is replaced by S7 truncated (see Figure C.14b) so that T1 and T2 remain disjoint.
- Step 4. T2 and T1+W were incubated at room temperature for 3 hours to produce the final system, T1+W+T2.

Native agarose gel electrophoresis demonstrates a band shifting pattern that confirms on a step-by-step basis the correct assembly of the walker system. (Figure C.7b).

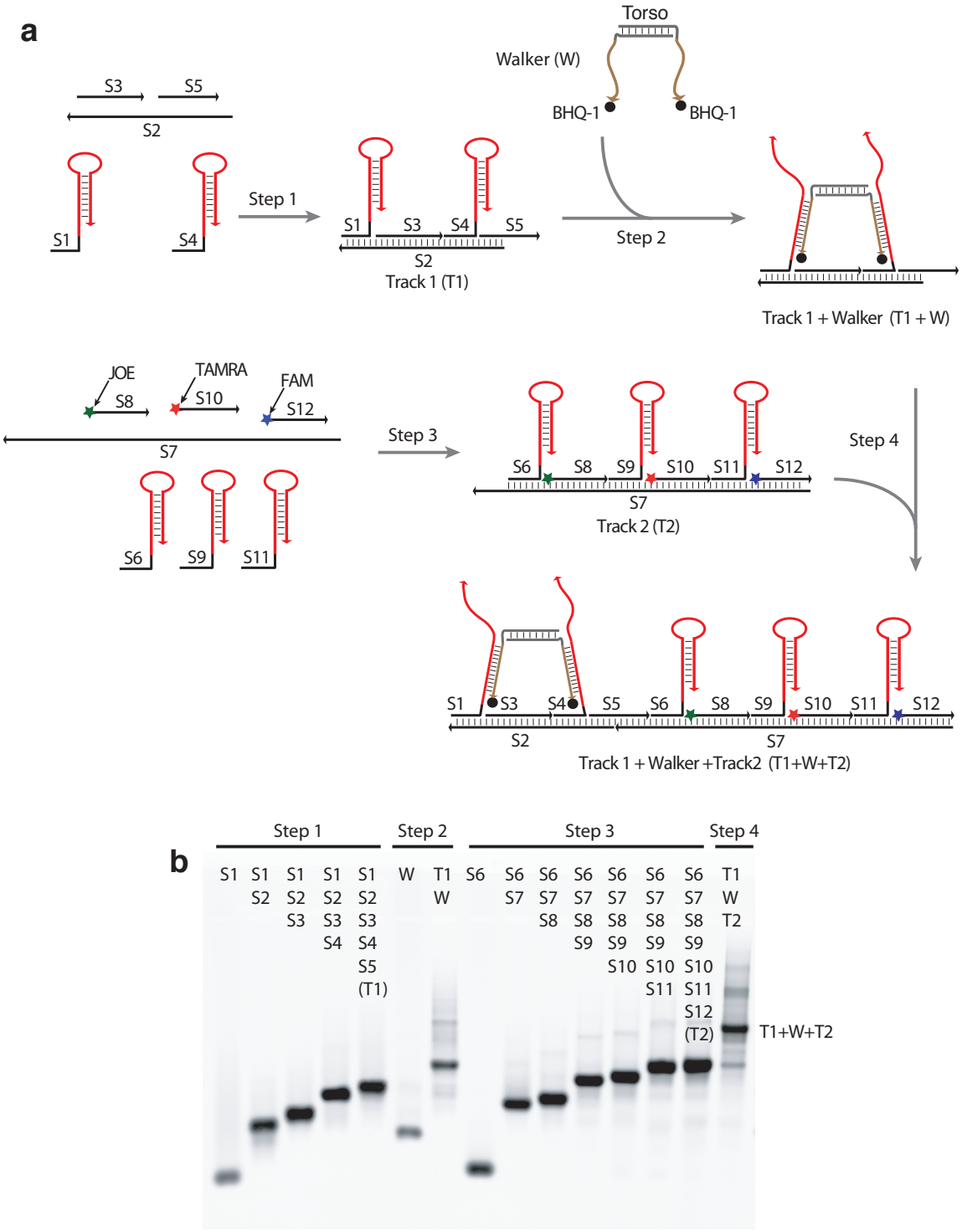

Figure C.7: Assembly of the walker system. (a) Step-by-step assembly procedure. (b) Native 3% agarose gel electrophoresis demonstrating the expected assembly of the system. Samples were annealed and assembled in reaction buffer with all species at 0.5 μM.

C.5.3 Raw Data of the Fluorescence Quenching Experiments

Figures C.8 and C.9 present the raw data and curve fitting results for the fluorescence quenching experiments measuring the proximity of the quenchers (black dots) on the walker feet to the fluorophores (colored stars) decorating the track. In Figure C.8, the walker track is decorated with fluorophores JOE → TAMRA → FAM; in Figure C.9, the walker track is decorated with fluorophores TAMRA → JOE → FAM. For each dye ordering, six pairs of experiments were performed. Each box contains data for one bipedal and one monopedal experiment that were performed simultaneously in separate cuvettes.

Since the walkers' motion is not synchronized, the time scale associated with the quenching of a given dye is characterized by approximating the minimum of the corresponding bulk fluorescence signal. To mitigate the effect of noise on estimating the location of the minimum, fitted double exponential curves (solid) were used to determine the time at which the minimum fluorescence (i.e., maximum quenching) was observed (dashed vertical line) for each fluorophore. For each curve fit, the data points of the initial baseline and those after the point of inflection are excluded (as depicted). The same time window was used for fitting all data for each pair of boxed experiments (i.e., for all six traces: 3 bipedal and 3 monopedal). All curve fits have an R^2 of 0.94 or better.

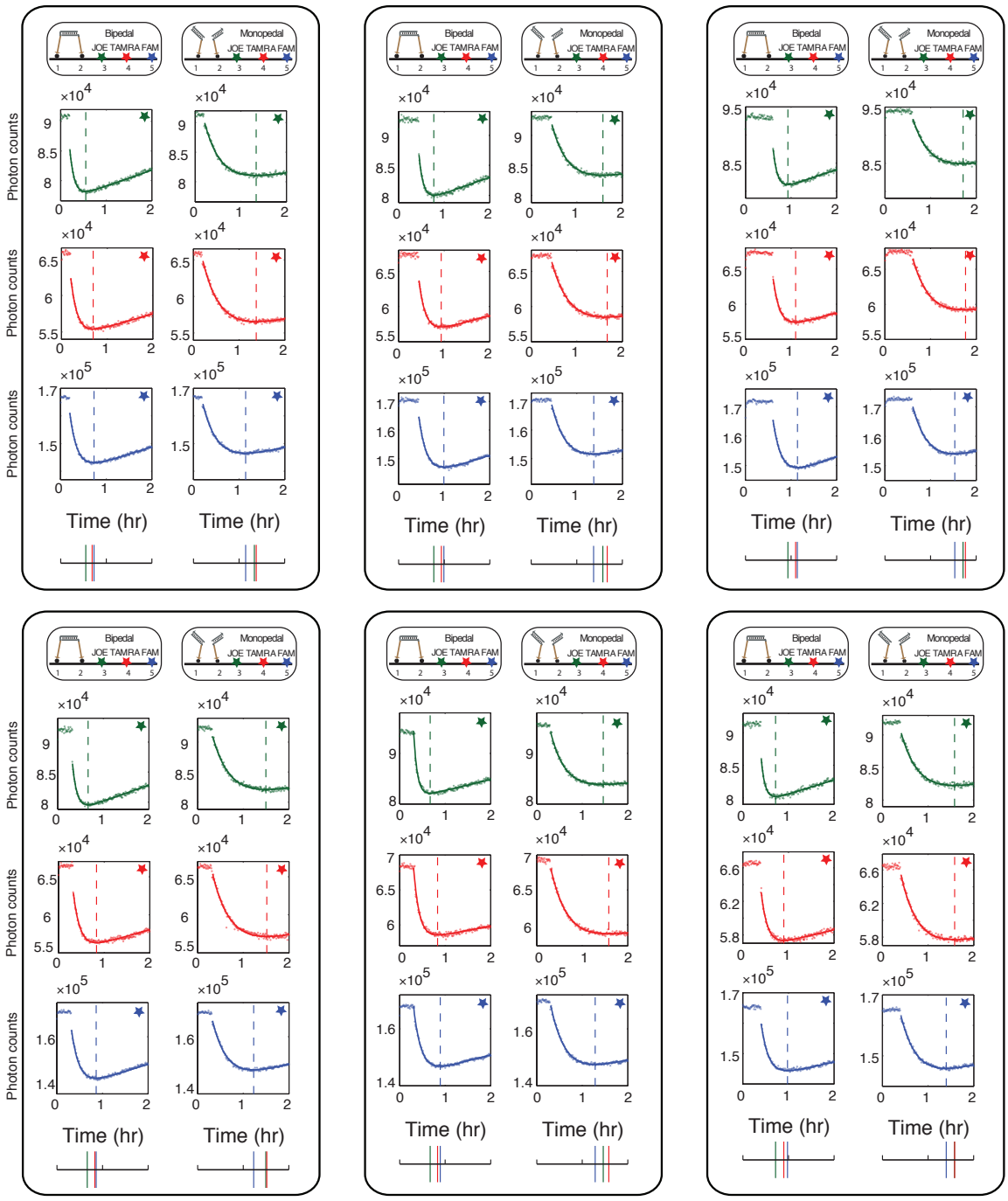

Figure C.8: Fluorescence data for track with fluorophores JOE → TAMRA → FAM.

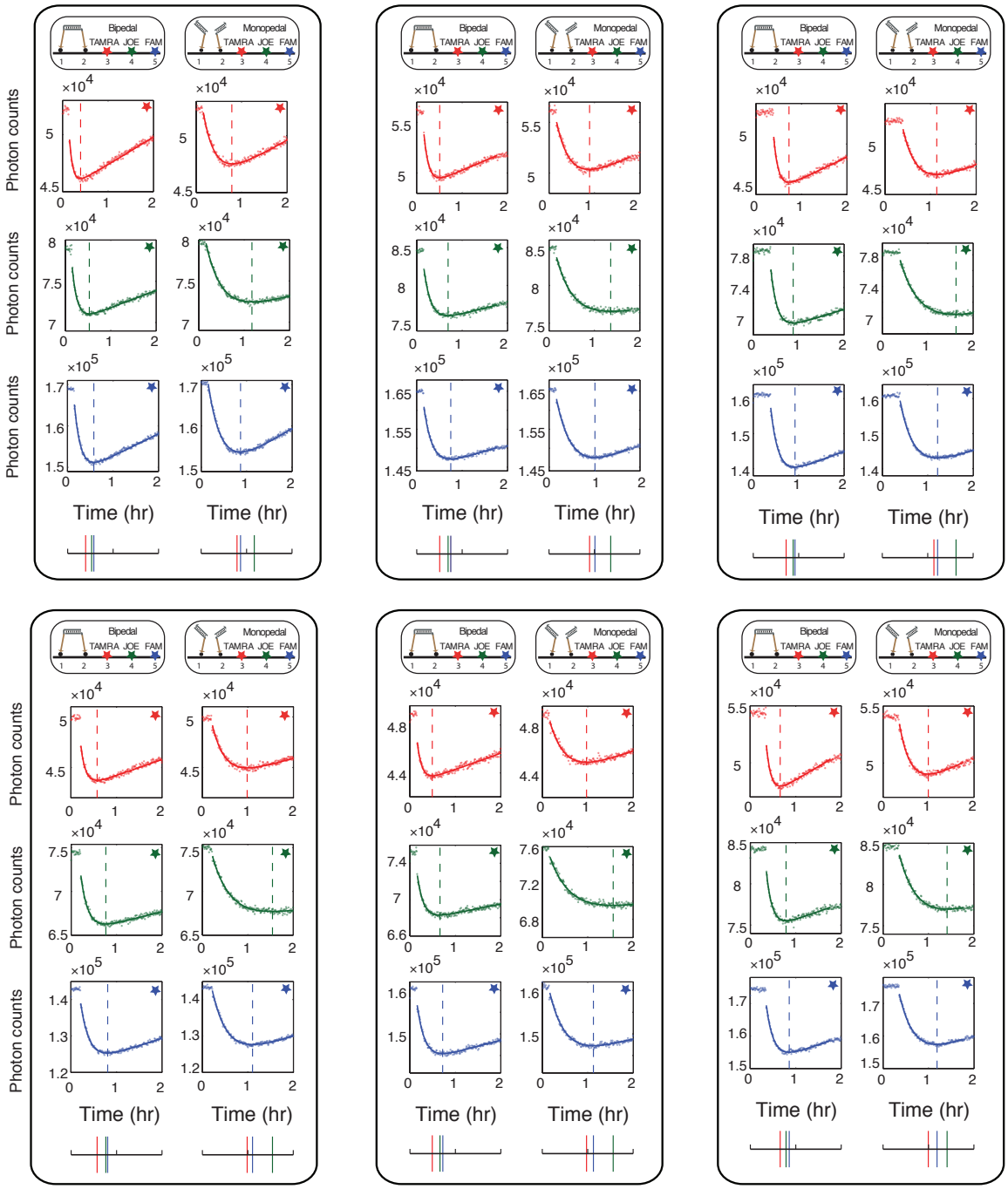

Figure C.9: Fluorescence data for track with fluorophores TAMRA → JOE → FAM.

C.5.4 Statistical Analysis

For the bipedal walker experiment of Figure C.6c, the fluorophore ordering along the track is JOE → TAMRA → FAM. We wish to assess the statistical significance of the observation that the time differences between consecutive minima in the three quenching curves are positive (i.e., that $t_{\min}^{\mathrm{TAMRA}} - t_{\min}^{\mathrm{JOE}} > 0$ and $t_{\min}^{\mathrm{FAM}} - t_{\min}^{\mathrm{TAMRA}} > 0$). For the monopedal walker experiments of Figure C.6d with the same ordering of fluorophores along the track, we wish to test the statistical significance of the observations $t_{\min}^{\mathrm{JOE}} - t_{\min}^{\mathrm{FAM}} > 0$ and $t_{\min}^{\mathrm{TAMRA}} - t_{\min}^{\mathrm{JOE}} > 0$. Analogous questions apply to the bipedal and monopedal experiments where the fluorophores are instead ordered TAMRA → JOE → FAM along the track (Figure C.6f).

For each time gap, we obtain six measurements ($x_1, x_2, \ldots, x_6$; sample size $n = 6$) from independent experiments (Tables C.2 and C.3). To avoid making the assumption that the underlying distribution is normal, we employ the distribution-free sign test, which applies to any continuous distribution [9]. Our null hypothesis is that the median of these measurements is zero ($H_0 : \tilde{\mu} = 0$); our alternative hypothesis is that the median is positive ($H_\mathrm{a} : \tilde{\mu} > 0$). The test statistic, y, is the number of x_i's that exceed 0; for all time gaps in Tables C.2 and C.3, $y = 6$ because all measured time differences are positive. Using a one-tailed sign test, the P-value is 0.0156 for all tests. Hence, the null hypothesis can be rejected for each time gap at significance level $\alpha = 0.0156$.

The above sign test analysis is preferred to the more familiar t-test analysis which requires the (unjustified) assumption of an underlying normal distribution. For purposes of comparison, we nonetheless include a t-test analysis (demonstrating that even smaller P-values are achieved under the assumption that the measurements are sampled from a normal distribution). In this case, the null hypothesis is that the mean of these measurements is zero ($H_0 : \mu = 0$); the alternative hypothesis is that the mean is positive ($H_\mathrm{a} : \mu > 0$). The test statistic is $t = \mu/(s/\sqrt{n})$, where s is the computed standard deviation of the measurements [9]. For a one-tailed t-test (with five degrees of freedom; $n - 1 = 5$), the P-values for all time gaps are shown in Tables C.2 and C.3. In each case, the P-value is smaller than the one for the corresponding sign test. Hence, the null hypotheses can be rejected with an even more stringent significance level α using the t-test.

Bipedal	x_1	x_2	x_3	x_4	x_5	x_6
JOE → TMR (sec)	515.5	588.3	621.8	590.1	669.2	658.5
TMR → FAM (sec)	143.0	211.5	135.2	103.3	66.0	287.1

Bipedal	Median ($\tilde{\mu}$)	Sign stat (y)	P-value	Mean (μ)	Std Dev (s)	t-stat	P-value
JOE → TMR (sec)	606.0	6	0.0156	607.2	56.1	26.5	0.0000
TMR → FAM (sec)	139.1	6	0.0156	157.7	79.7	4.8	0.0024

Monopedal	x_1	x_2	x_3	x_4	x_5	x_6
FAM → JOE (sec)	696.8	730.6	659.1	957.9	636.0	656.4
JOE → TMR (sec)	144.6	337.0	184.8	74.3	443.6	3.4

Monopedal	Median ($\tilde{\mu}$)	Sign stat (y)	P-value	Mean (μ)	Std Dev (s)	t-stat	P-value
FAM → JOE (sec)	678.0	6	0.0156	722.8	120.0	14.8	0.0000
JOE → TMR (sec)	164.7	6	0.0156	198.0	164.8	2.9	0.0169

Table C.2: Measured time differences between minima and statistical analysis for six experiments with bipedal or monopedal walkers on the track with fluorophore ordering: JOE → TAMRA → FAM. For raw data see Figure C.8.

Bipedal	x_1	x_2	x_3	x_4	x_5	x_6
TMR → JOE (sec)	471.3	658.9	553.5	691.7	615.6	462.6
JOE → FAM (sec)	178.1	216.2	144.0	143.1	215.8	245.6

Bipedal	Median ($\tilde{\mu}$)	Sign stat (y)	P-value	Mean (μ)	Std Dev (s)	t-stat	P-value
TMR → JOE (sec)	584.6	6	0.0156	575.6	96.1	14.7	0.0000
JOE → FAM (sec)	197.0	6	0.0156	190.5	42.2	11.1	0.0001

Monopedal	x_1	x_2	x_3	x_4	x_5	x_6
TMR → FAM (sec)	286.4	427.5	284.1	428.0	542.0	692.2
FAM → JOE (sec)	1092.4	1250.6	1430.4	1573.8	1575.1	799.0

Monopedal	Median ($\tilde{\mu}$)	Sign stat (y)	P-value	Mean (μ)	Std Dev (s)	t-stat	P-value
TMR → FAM (sec)	427.8	6	0.0156	443.4	156.3	6.9	0.0005
FAM → JOE (sec)	1340.5	6	0.0156	1286.9	304.4	10.4	0.0001

Table C.3: Measured time differences between minima and statistical analysis for six experiments with bipedal or monopedal walkers on the track with fluorophore ordering: TAMRA → JOE → FAM. For raw data see Figure C.9.

C.5.5 Comparison of Walker Time Scales

Figures C.10 and C.11 overlay the fitted curves from the six independent bipedal and monopedal walker experiments of Figures C.8 and C.9. To enable comparison in a single plot, all data are normalized: unity corresponds to the last baseline fluorescence value before adding hairpin B and zero corresponds to the minimum of the fitted curve. The time axis is translated so that $t = 0$ corresponds to the time of the last baseline data point before adding hairpin B. An upper bound on the variability in the time required to add hairpin B and mix the sample in each experiment is approximately 30 seconds. This represents the uncertainty in comparing the curve fits between different experiments along the same time axis.

The variability among the traces for each fluorophore is higher in Figure C.11 (TAMRA $\rightarrow$ JOE $\rightarrow$ FAM) than in Figure C.10 (JOE $\rightarrow$ TAMRA $\rightarrow$ FAM) because the six independent experiments in the prior case were performed over a period of several months. The wearing of the UV lamp over this time period may result in higher variability among the traces. The same conclusion is drawn from this data: the time scale to visit any one site with the monopedal walker is longer than the time scale to visit all three sites with the bipedal walker follows from either data set.

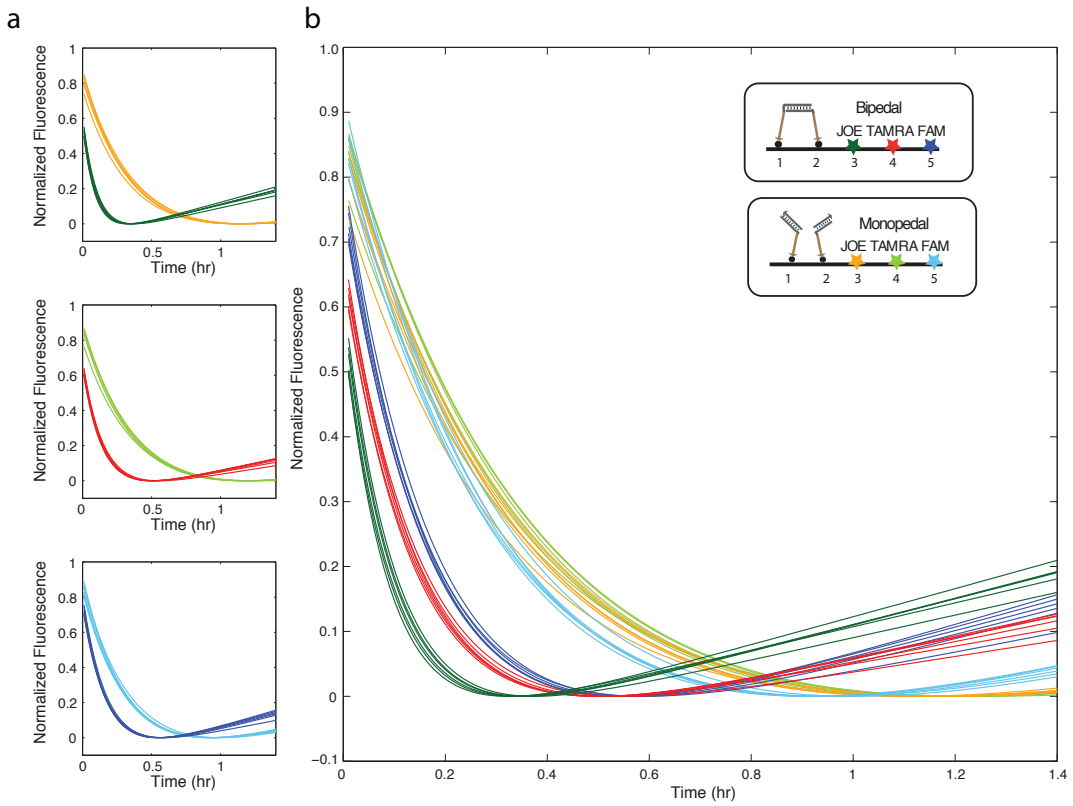

Figure C.10: Comparison of time scales for bipedal and monopedal walkers using normalized fitted curves from the raw fluorescence data of Figure C.8 with track labeled JOE → TAMRA → FAM. (a) For each fluorophore, 12 traces (six for each walker type) are plotted together, demonstrating that the bipedal walker visits each anchorage on a faster time scale than the monopedal walker. (b) All 36 traces (18 per walker type) are plotted together to demonstrate that the time scale for the monopedal walker to visit any one of the three anchorages is longer than the time scale of the bipedal walker to visit all three anchorages.

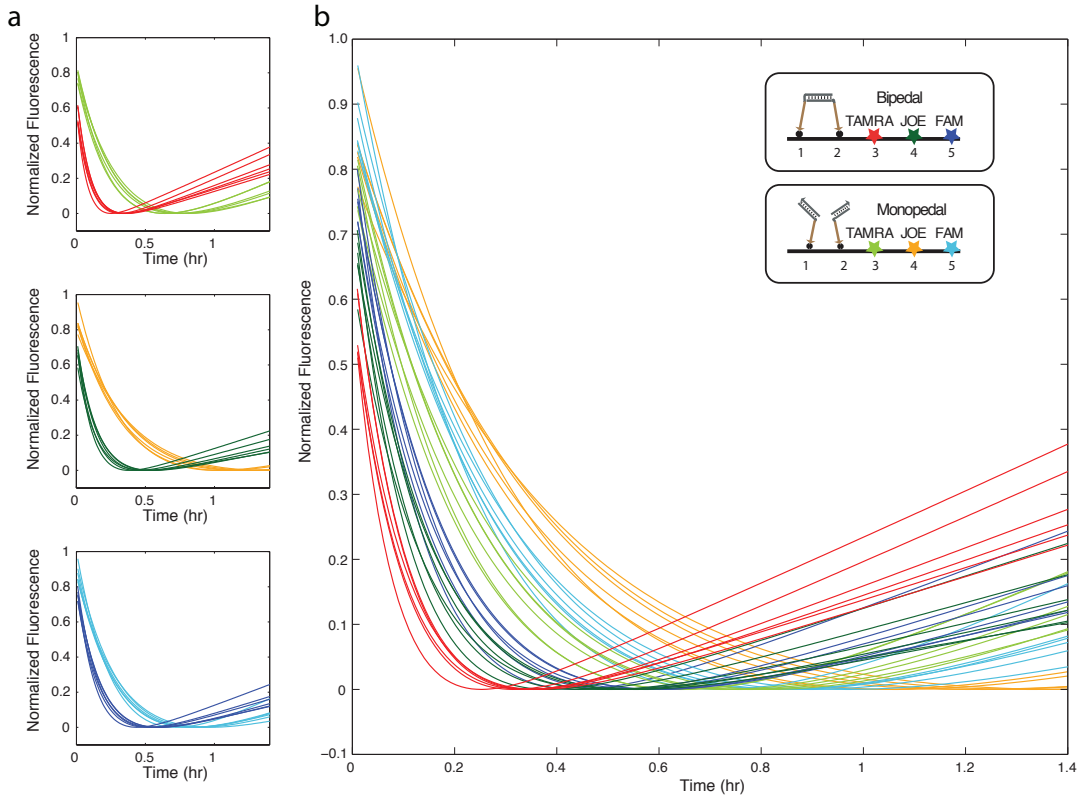

Figure C.11: Comparison of time scales for bipedal and monopedal walkers using normalized fitted curves from the raw fluorescence data of Figure C.9 with track labeled TAMRA → JOE → FAM. (a) For each fluorophore, 12 traces (six for each walker type) are plotted together, demonstrating that the bipedal walker visits each anchorage on a faster time scale than the monopedal walker. (b) All 36 traces (18 per walker type) are plotted together to demonstrate that the time scale for the monopedal walker to visit any one of the three anchorages is longer than the time scale of the bipedal walker to visit all three anchorages.

C.5.6 Control for Walker Landing Effects

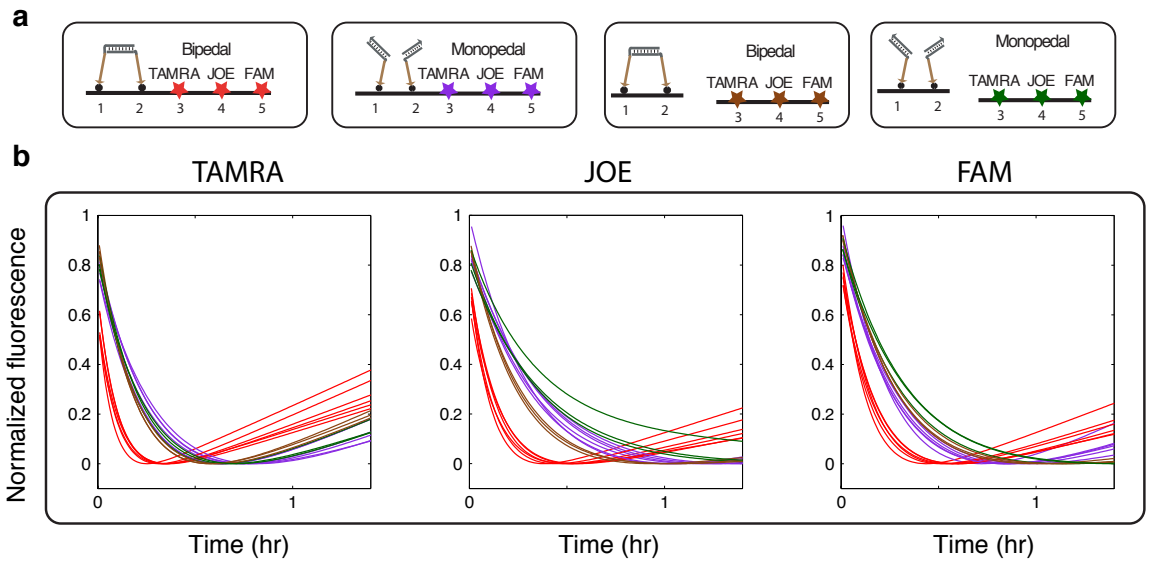

Figure C.12: Comparison of time scales for bipedal and monopedal walkers on the full track and on a disjoint track that requires both walker types to diffuse through solution to land on the track (labeled TAMRA→JOE→FAM). (a) These four types of experimental data are depicted with different colors. Red: Bipedal walker on the full track; purple: monopedal walker on the full track; brown: bipedal walker on the disjoint track; green: monopedal walker on the disjoint track. (b) For each of the three sites (3, 4, 5), the time scale for the bipedal disjoint track walker (brown traces) is similar to those for the the monopedal full track walker (purple traces) and the monopedal disjoint track walker (green traces), and slower than the time scale for the bipedal walker on the full track (red traces). See Figure C.13 for the raw data of bipedal and monopedal walkers on the disjoint track.

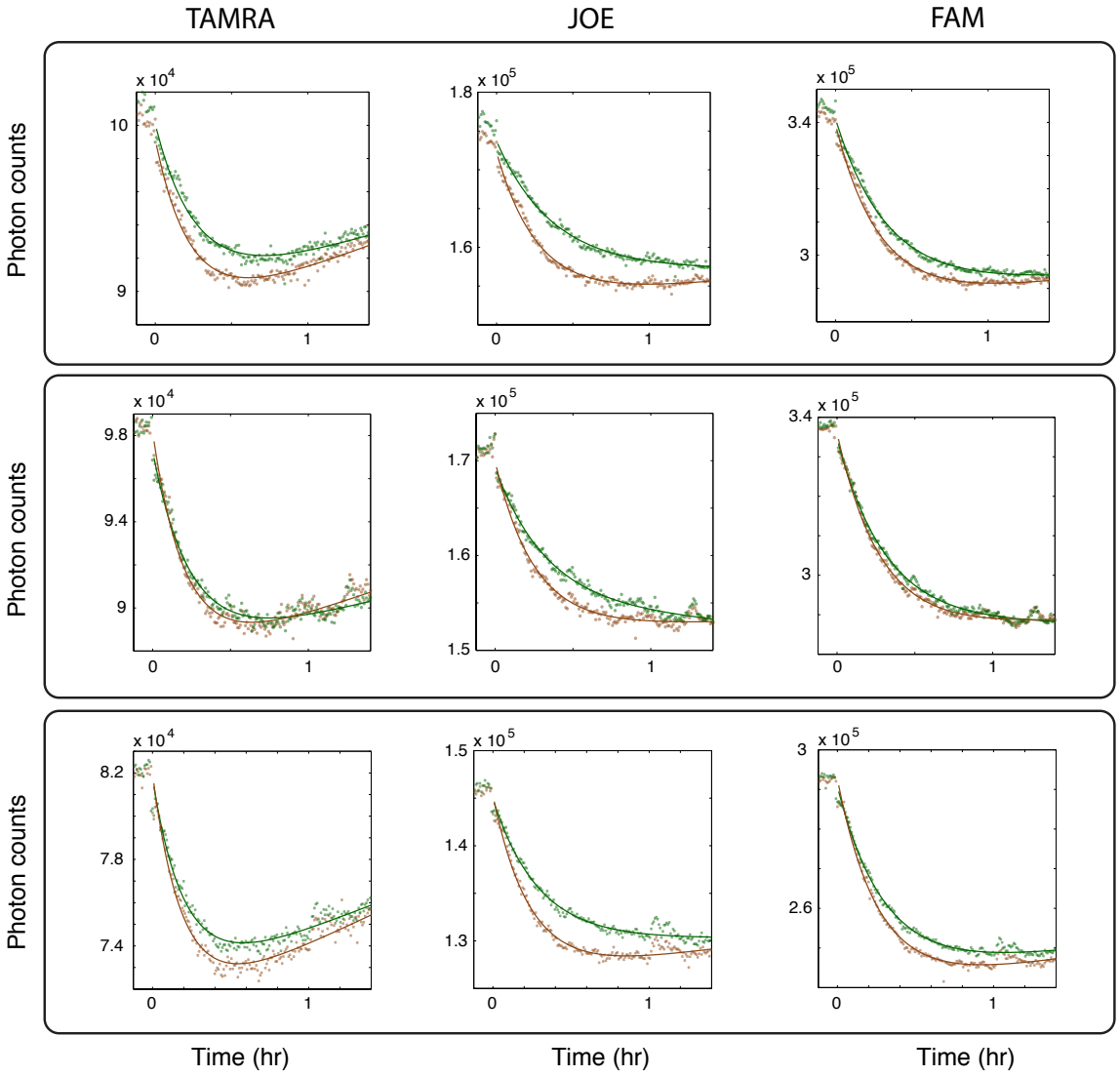

Figure C.13: Raw fluorescence data and curve fits for the three pairs of bipedal (brown) and monopedal (green) walker experiments on the disjoint track. The protocol for these landing experiments was the same as for the other walker fluorescence quenching experiments, with the exception that a disjoint track was pre-assembled as described in Section C.5.2.

C.5.7 DNA Sequences of the Walker System

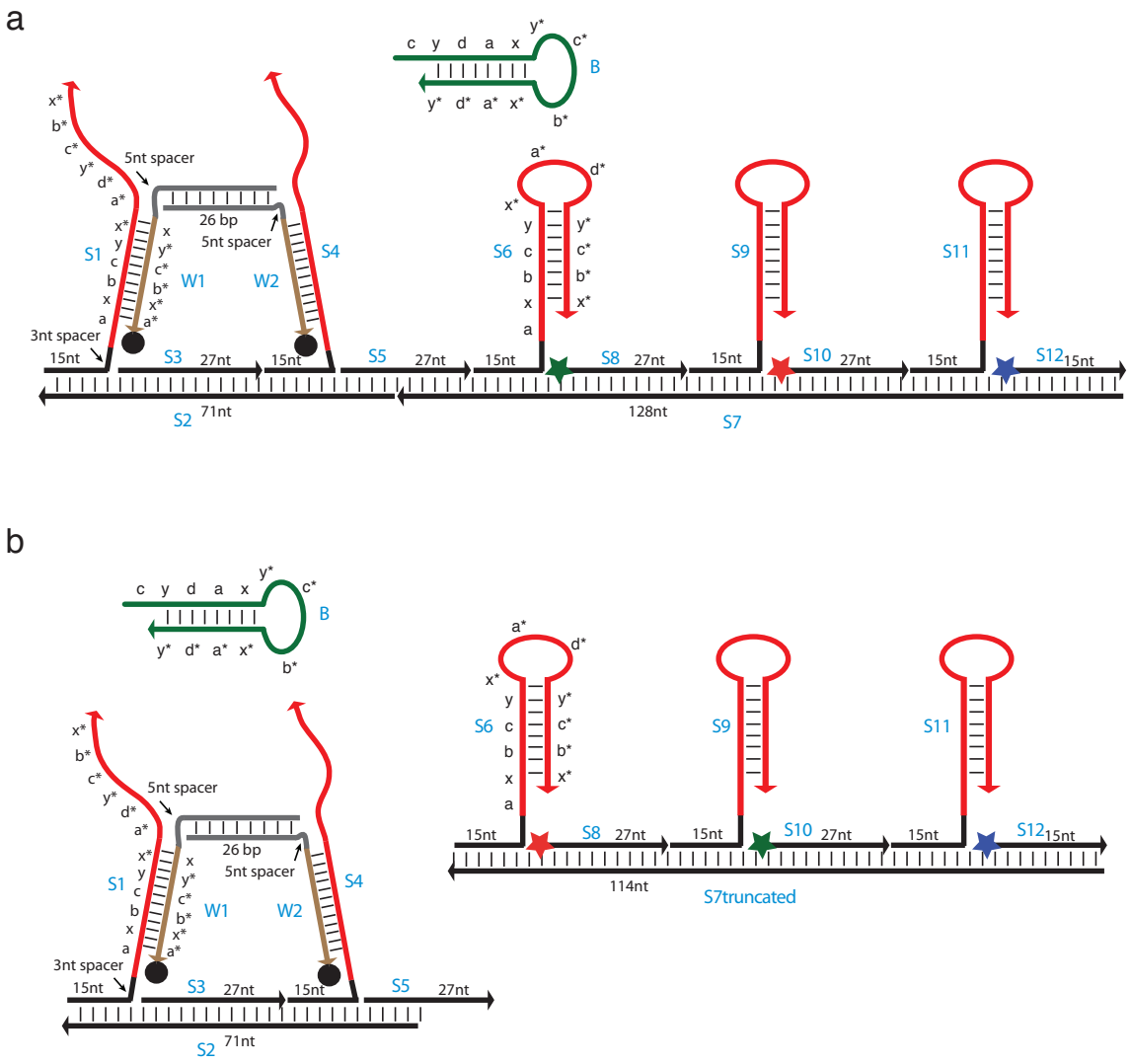

Figure C.14: Secondary structure schematics for the walker system. (a) Full track. (b) Disjoint track for landing control experiments (Figure C.13). Blue letters indicate sequence names used in the definitions below. The lengths of segments a, b, c, and d are are 7 nt; the lengths of segments x and y are 2 nt. Stars, fluorophores; black dots, quenchers.

Walker track sequences

For each hairpin sequence X, the two segments that are ligated to produce X are indicated as Xa and Xb. For the walker leg, W1s is the splint strand used for ligating strands W1a and W1b to produce W1. The same applies for W2s splint. Strand modifications are indicated as follows:

/5Phos/:	5′ phosphorylation
/36FAM/:	3′ 6-carboxyfluorescein
/5JOEN/:	5′ 6-carboxy-4′,5′-dichloro-2′,7′-dimethoxyfluorescein (NHS Ester)
/5TMRN/:	5′ carboxytetramethylrhodamine (NHS Ester)
/3BHQ_1/:	3′ black hole quencher-1

Strand	Sequence
S1	GGTAGTTCTAGGCAGCTGAAGTAGTGATTGAGCGTGATGAATGTCACTAC-TTCAACTCGCATTCATCACGCTCAATC
S1a	GGTAGTTCTAGGCAGCTGAAGTAGTGATTGAGCGT
S1b	/5Phos/GATGAATGTCACTACTTCAACTCGCATTCATCACGCTCAATC
S2	TCATAGGCACCGTCAGACAGGATAGAGCAGTGCATAGATAGTCATAGCCTT-GGACCTGCCTAGAACTACC
S3	GTCCAAGGCTATGACTATCTATGCACT
S4	GCTCTATCCTGTCTGCTGAAGTAGTGATTGAGCGTGATGAATGTCACTAC-TTCAACTCGCATTCATCACGCTCAATC
S4a	GCTCTATCCTGTCTGCTGAAGTAGTGATTGAGCGT
S4b	/5Phos/GATGAATGTCACTACTTCAACTCGCATTCATCACGCTCAATC
S5	ACGGTGCCTATGACATGGTACTCAGCT
S6	GCTCGTATCTGGTCGCTGAAGTAGTGATTGAGCGTGATGAATGTCACTAC-TTCAACTCGCATTCATCACGCTCAATC
S6a	GCTCGTATCTGGTCGCTGAAGTAGTGATTGAGCGT
S6b	/5Phos/GATGAATGTCACTACTTCAACTCGCATTCATCACGCTCAATC
S7	CGTAAGTCGCAGAGTATGCCATTGCCTCATCAGCGTAGCATCGAGATCTA-AGTTAGTAACTCTGGCAGCCTGGTAGAGCGAGCCTATCGTCCTGATGTAC-GACCAGATACGAGCAGCTGAGTACCATG
S7truncated	CGTAAGTCGCAGAGTATGCCATTGCCTCATCAGCGTAGCATCGAGATCTA-AGTTAGTAACTCTGGCAGCCTGGTAGAGCGAGCCTATCGTCCTGATGTAC-GACCAGATACGAGC
S8-TMR	/5TMRN/TACATCAGGACGATAGGCTCGCTCTAC
S8-JOE	/5JOEN/TACATCAGGACGATAGGCTCGCTCTAC
S9	CAGGCTGCCAGAGTTCTGAAGTAGTGATTGAGCGTGATGAATGTCACTA-CTTCAACTCGCATTCATCACGCTCAATC
S9a	CAGGCTGCCAGAGTTCTGAAGTAGTGATTGAGCGT
S9b	/5Phos/GATGAATGTCACTACTTCAACTCGCATTCATCACGCTCAATC
S10-TMR	/5TMRN/ACTAACTTAGATCTCGATGCTACGCTG
S10-JOE	/5JOEN/ACTAACTTAGATCTCGATGCTACGCTG
S11	ATGAGGCAATGGCATTAGAAGTAGTGATTGAGCGTGATGAATGTCACTA-CTTCAACTCGCATTCATCACGCTCAATC
S11a	ATGAGGCAATGGCATTAGAAGTAGTGATTGAGCGT
S12-FAM	/56FAM/ACTCTGCGACTTACG

Strand	**Sequence**
W1	TTGCCTCGTATCCTAACCGAACGGACTCCAGGACATTCATCACGCTCAAT-CACTACTT
W1a	TTGCCTCGTATCCTAACCGAACGGACTCC
W1b	AGGACATTCATCACGCTCAATCACTACTT /BHQ-1/
W1s	CGTGATGAATGTCCTGGAGTCCGTTCGGTT
W2	GTCCGTTCGGTTAGGATACGAGGCAATCCAGGACATTCATCACGCTCAAT-CACTACTT
W2a	GTCCGTTCGGTTAGGATACGAGGCAATCC
W2b	AGGACATTCATCACGCTCAATCACTACTT /BHQ-1/
W2s	CGTGATGAATGTCCTGGATTGCCTCGTATC
Hairpin B	TGATGAATGCGAGTTGAAGTAGTGACATTCATCACGCTCAATCACTACTTC-AACTCGCA

References

[1] P. Yin, H. Yan, X. G. Daniell, A. J. Turberfield and J. H. Reif. A unidirectional DNA walker that moves autonomously along a track. *Angewandte Chemie-International Edition* **43**, 4906–4911 (2004).

[2] Y. Tian, Y. He, Y. Chen, P. Yin and C. D. Mao. A DNAzyme that walks processively and autonomously along a one-dimensional track. *Angewandte Chemie-International Edition* **44**, 4355–4358 (2005).

[3] J. Bath, S. J. Green and A. J. Turberfield. A free-running DNA motor powered by a nicking enzyme. *Angewandte Chemie-International Edition* **44**, 4358–4361 (2005).

[4] R. Pei *et al.* Behavior of polycatalytic assemblies in a substrate-displaying matrix. *Journal of the American Chemical Society* **128**, 12693–12699 (2006).

[5] S. Venkataraman, R. M. Dirks, P. W. K. Rothemund, E. Winfree and N. A. Pierce. An autonomous polymerization motor powered by DNA hybridization. *Nature Nanotechnology* **2**, 490–494 (2007).

[6] C. L. Asbury. Kinesin: world's tiniest biped. *Current Opinion in Cell Biology* **17**, 89–97 (2005).

[7] Y. Chen, M. S. Wang and C. D. Mao. An autonomous DNA nanomotor powered by a DNA enzyme. *Angewandte Chemie-International Edition* **43**, 3554–3557 (2004).

[8] M. Behlke, L. Huang, L. Bogh, S. Rose and E. Devor. Fluorescence and fluorescence applications (2005).

[9] J. Devore. *Probability and Statistics for Engineering and the Sciences* (Brooks/Cole, 1991).